INVESTIGATIONS OF COMPLEX SYSTEMS: FROM GRANULAR TO COGNITIVE SYSTEMS

THESIS SUBMITTED FOR THE DEGREE OF

DOCTOR OF PHILOSOPHY (SCIENCE)

IN

PHYSICS (THEORETICAL)

BY

DATTATRAY PANDURANG SHINDE

DEPARTMENT OF PHYSICS

UNIVERSITY OF CALCUTTA

Dedicated to My Family

Acknowledgements

First, I would like to express sincere gratitude to my supervisor Prof. Anita Mehta for the continuous support and motivation. She introduced me to the topic of granular and cognitive complex systems. Her encouragement gave me strength to overcome my weaknesses. She taught me simple ways of quality research and skills of good presentations.

There are so many people who helped, supported and believed me during this entire journey. Their constant encouragement kept me on the research track after facing some setbacks in the past. It is for them that I owe my deepest gratitude.

My sincere thanks go to Prof. G. C. Barker, Institute of Food Research, United Kingdom, for his computational helps during this work. It was always a pleasure to discuss with him about the details of algorithms. He patiently gave answers to all my queries.

I would like to thank Dr. R. K. Mishra, Centre for Behavioral and Cognitive Sciences, University of Allahabad, for experimental data of eye movements. I visited his laboratory and learnt details about the eye tracking paradigm and linguistics.

I always feel that true friendship is important. "A friend in need is a friend indeed", I have an excellent company of Ravi Jaralikar, Shivprasad Poddar, Rekha Naik, Abhay Sagade, Rohini Kitture, Prasad Kulkarni, Ramhari Maske, Dattatray Patil, Suryakant Patil, Amar Musale, and Dattaguru. My special thanks go to Ravi, Rekha, Shivprasad (S. P.), Abhay and Dattaguru for their support throughout this work.

My sincere thanks go to my teachers, Prof. S. T. Navare, Prof. Y. D. Kolekar, Prof. H. D. Dhaygude, Prof. M. V. Takle, Prof. Kulkarni, and Prof. S. A. Gangawane, who introduced me to the world of physics.

I am grateful to my friends Dr. Madhav, Dr. B. G. Patel, Dr. Parth Chauhan, Anil Yadav, Harishankar Sahoo, Himavanthkumar, Shishir Purohit, Arvinder Singh, and Arvind Rajpurohit for their encouragement and support.

I have experienced the most enjoyable moments of Ph.D. life at S. N. Bose Centre. I am grateful to have company of Sumit Ghosh, Thaneshwar Kaloni, Soumi Roychawdhury, Santu Baidya, Ashutosh Yadav, Ranajay Saha, Debabrato Sinha, and Urbashi, with them I shared my happiness and disappointments. Special thanks to Sumit, Soumi, Ashutosh, Ranajay and Saintu who always help with me at every stage.

My heartfelt thanks to T. P. Sreeraj and Chauba, with them I discussed various topics. They introduced me to the game of Badminton which gave me pleasure and relief from stress. Also, they always react calmly towards my arguments. I would like to thank my friends, Bivas Rana, Shemanti Pal, Sushmita Saha, Kallol Mukherjee, Suman Aich, Suman Dutta, Soumyakanti Bose, Arindam Lala, Subhajit Sarkar, Shirsendu Dey, Biplab, Arghya Das, Subhasish Chakrabarty, Debashish Das Mahanta, Rajkumar Sadhu, Rakesh Das, Jagbandhu kumar, Souvanik, Samiran, Kaushik, Sourav, Subhodh, Sudhanshu and Shivraj. Special thanks to Suman Dutta, with whom I discussed different topics of nonequilibrium phenomena.

I am thankful to the Director, Dean (Academic), Registrar and Deputy Registrar (Academic) of S. N. Bose National Centre for Basic Sciences. I am also thankful to peoples from library, computer and reception sections. Special thanks to security staff for their help and kindness.

I would like to thank members of 'Statistical physics journal club' for healthy discussions on various topics. I would like to thank to CSIR, India and S.N.B.N.C.B.S for financial support.

I have no words to express my feelings about my parents, Mr. Pandurang Shinde and Mrs. Aanandi Shinde. Their love, support, and blessings are always with me. They teach me the values of life. My sister, Vaishali and brother, Prashant have given me their unequivocal support which keeps me mentally fit, for which I am grateful.

Dattatray Pandurang Shinde
S. N. Bose National Centre for Basic Sciences,
JD Block, Sector- III, Salt Lake
Kolkata, West Bengal, India.

Date:

Abstract

We examine the emergent dynamics of granular and cognitive complex systems. We use a hybrid Monte Carlo algorithm to simulate the shaking of granular spheres at different vibrational amplitudes. Several spontaneous crystallizing transitions are typically observed, leading to end states which can be fully or partially ordered, depending on the shaking amplitude, which we investigate using metrics of global and local orders. The crystallization is incomplete at low amplitudes, at least for our times of observation. For amplitude ranges where crystallization is complete, there is typically a competition between hexagonal close packed (hcp) and face-centered cubic (fcc) ordering. It is seen that fcc ordering typically predominates; in fact for an optimal range of amplitudes, spontaneous crystallization into a pure fcc state is observed. An interesting feature is the breakdown of global order when there is juxtaposition of fully developed hcp and fcc order locally: we suggest that this is due to the interfaces between the different domains of order, which plays the same role as dislocations. We perform the Delaunay tessellations of granular packings at various packing densities. The volumes of Delaunay simplices follow a gamma distribution; the volume fluctuations and entropy have shown drastic change at packing densities 0.62, 0.64 and 0.68. The minima's of length measures and distributions of dihedral angle of simplices provide basis for distinguishing regularity of simplices. Human eye movements involve in semantic search subjected to visual and aural inputs in a cognitive task. The probability distributions of saccades and fixations are obtained and analyzed. Scale-invariance is observed in the saccadic distributions, while the fixation distributions reveal the presence of a characteristic time scale for literate participants. A detailed analysis of Euclidean distance time series suggests that saccadic eye motions are an example of Levy, rather than Brownian, dynamics. We calculate the log-likelihood and Akaike weights to select the best fitting model for the saccade times. Power-law distribution has higher log-likelihood and Akaike weights against other probability models. We perform simulation of two-dimensional Levy random walks. The results of this model suggest the superdiffusive dynamics of Levy walker, which further find analogous to that of saccadic motion.

Contents

List of Figures

List of Tables

List of Abbreviations and Notations

PDF	**P**robability **D**ensity **F**unction
VWP	**V**isual **W**orld **P**aradim
MSD	**M**ean **S**quare **D**isplacement
SDA	**S**tandard **D**eviation **A**nalysis
DEA	**D**iffusion **E**ntropy **A**nalysis
MLE	**M**aximum **L**ikelihood **E**stimation
AIC	**A**kaike **I**nformation **C**riterion
ϕ	Packing density of spheres
$\overline{z}, z_c$	Mean and critical values of coordination number
$\rho(t)$	Time dependent packing density in experiments
A	Shaking amplitude
ξ_x & ξ_y	Gaussian random numbers
e	Random vector
d	Neighbourhood of spheres
N	Number of shakes
ϕ_{max}	Maximum packing density of spheres
$g(r)$	Radial distribution function
ϱ	Number density
$Q_{l,global}$ & $Q_{l,local}$	Global and local bond orientational order parameters.
$Y_l^m(\Theta(\vec{r}), \Phi(\vec{r}))$	Spherical Harmonics
Θ_{ji} and Φ_{ji}	Polar angles of spheres
N_s	Number of nearest neighbors
N_{fcc}, N_{hcp}	Number of fcc and hcp sphere-clusters

V_v	Voronoi region
χ	Compactivity
β_{gr}	Granular temperature
V	Volume of tetrahedron
$P(.)$	Probability distribution function
k	Shape Parameter of Gamma distribution
σ^2	Variance
S	Entropy of volume
$\overline{V}, V_{min}$	Average and Minimum attainable volume
η	Length criterion for regular tetrahedra
l	Length of tetrahedron
T, Q	Tetrahedricity and Quartoctahedricity of Delaunay simplexes
$B_H(.), L_H(.)$	Fractional Brownian and Levy motions
$subjects$	Participants
β	Exponent of power-law distribution of saccade times
$ds(t)$	Time series of Euclidean distances of saccade
$Z_i(n)$	Subtrajectory of time series of saccades spanning a time duration n
$S(n)$	Shannon entropies of subtrajectories of saccades
$D(n)$	Standard deviation of subtrajectories of length n
H	Hurst Exponent
δ	Diffusion Exponent
$P_s(f)$	Power Spectral Density
α	Exponent of Fourier power spectral density
κ	Exponent of power-law distribution of Euclidean distances of saccades
$\mathcal{L}(.)$	Likelihood function
D_i	Differences of Akaike information criterion
$E_h(.)$	Statistical expectation
$I(.)$	Information loss
ω_i	Akaike weight of i^{th} probability model for saccade times
μ	Levy index

Chapter 1

Introduction

1.1 Complex Systems

Most of the real systems in nature are complex. The interactions between large number of constituents introduce complexity to the system. The complexity may emerge in the form of simple or complex structures and patterns over different spatio-temporal scale. Examples of complexity can be found in a range of systems such as brain and cognition [1], foraging [2], complex materials [3], share market [5], complex network [4], chaos and turbulence [6], and so on. The emergent behavior is categorized into two groups: emergent simplicity and emergent complexity [7]. An emergent simplicity is observed when complex elements behave, as a whole, in a simple way [7]. For example, neuron, a complex cell in brain, makes simple view of real world. In particular, the collective behavior of neurons is strongly responsible for the mental processes [8]. On the other hand, an emergent complexity arises when simple elements interact, as a whole, in complex way [7]. For instance, granular materials such as beads, discs, spheres and powders exhibit complex static and dynamic properties [9]. These simple elements collectively form complex structures and patterns subjected to external perturbations [9]. Altogether, it is essential to understand not only the behavior of constituents but also their collective behavior as a whole.

Many experimental, theoretical and computational protocols explain the statics and dynamics of complex systems [10]. Specifically, the emergent behavior can be described using linear or nonlinear differential and integral equations, and computer algorithms

[11]. In addition, stochastic models discern the randomness of an emergent behavior [12]. Modern statistical methods construct probability models for the data and illustrate the best approximating model [13]. For example, the application of stochastic and information theoretic methods to time series data of linguistic study remarkably improve the inferences [14]. In case of granular materials, the computational techniques fill the gap between experiments and analytical frameworks. In particular, Molecular dynamics [15] and Monte Carlo [16] algorithms are used to examine the complexity of granular packings and their dynamics. Also, in the first place, the random packings of monodisperse, hard spheres with different densities are constructed and then, their dynamical aspects are examined. Nevertheless, a challenging task is to develop the theoretical framework for granular and cognitive complex systems.

1.1.1 Granular Systems

Granular materials have number of distinct characteristics. They exhibit behavior that is neither solid-like nor liquid-like. Moreover, the complexity in these materials emerges because of nonlinear and hysteric behavior of grains [16]. Besides, they show a unique property of dilatancy which is the ability to sustain different degrees of packings [17]. The inter-grain forces are repulsive; dissipation occurs due to static friction and inelastic collisions [18]. Granular media are athermal and noncohesive systems [18]. The ordinary temperature plays no role in granular systems so that each metastable state will exist indefinitely [18]. External mechanical perturbations such as shaking, vibration, stirring and shear alter the state of granular materials [18]. Therefore, the external forces play an important role in understanding the complex dynamics of granular grains.

The computational methods model either sequential [19, 20] or nonsequential [21, 22] processes of granular material. The sequential algorithms follow predefined rules of deposition. On the contrary, the nonsequential algorithms incorporate the cooperative rearrangement of particles. Further, the sequential algorithms neglect the stability of particles whereas nonsequential algorithms construct the stability of particles which in turn establish stable cluster. Besides, computer algorithms consider either hard sphere or soft sphere interaction between granular grains. The hard sphere models are used for the investigations of properties of thermal systems such as liquids [23] and colloids [24]. However, in an athermal system, lower and upper random packing limits have been set up for loose and close packings of spheres, corresponding to densities of 0.55

[25] and 0.64 [26] respectively. Significantly, these random packings illustrate the static properties of spheres. Nevertheless, both the random packing limits are ill-defined [27] and densities above 0.64 are achieved in shaken spheres [28]. At the other end of the spectrum, there is a conjecture by Kepler that the maximum density of sphere packings is that of fcc structures, corresponding to a value of 0.74 [29].

Granular systems show emergent behavior subjected to external perturbations. For instance, the sheared granular spheres [30] exhibit phase transitions where crystalline structures evolve spontaneously from disordered structures. In particular, the emergence of fcc and hcp structures is seen in sheared spheres [30] and horizontally shaken beads [31]. Likewise, the evolution of crystalline transitions are found similar to those of sheared colloids [32]. Next, the cluster analysis of sheared spheres [30] reveals that fcc structures are preferable than hcp structures. Altogether, it is important to address some issues: the emergence of crystalline structures subjected to shear or shaking, and functional relationship between driving forces and displacements of particles.

Our aim is to investigate the spontaneous crystallization of granular spheres. Importantly, we focus our attention on the role of shaking in the development of crystalline structures at different stages. To achieve the goal, we have performed computer simulation of hard spheres subjected to shaking. We have used Monte Carlo algorithms [21, 33] for the packing and shaking of spheres. In particular, the packing algorithm builds sequential deposition of monodisperse, hard spheres. The shaking algorithm includes nonsequential step which gives a clear understanding of the cooperative movements of spheres. It also establishes the stability of spheres in an aggregate. To assess the development at local as well as global level, it is important to use characterization methods that distinguish different crystalline phases. We have characterized the crystalline structures using the metrical and geometrical methods. Our analysis divided into two categories. First, we have analyzed the packings using metrical order parameters such as radial distribution function and bond orientational order parameters. Secondly, we have used Delaunay tessellations to explore the geometrical aspects of sphere packings at various densities. Further, we have calculated the volumes of Delaunay simplices, volume fluctuations and configurational entropies. At last, we are able to compute the angular and length measures of simplices at different densities.

1.1.2 Cognitive Systems

Cognitive science explores mental processes such as perception, thinking, knowledge and memory, attention, and feelings [34]. Usually, these processes are broadly classified and studied in psychology and physiology. Psychologists [35, 36, 37] study the human behavior during cognitive tasks. In particular, the linguistic psychologists [38, 39] study the language mediated patterns that describe the attentional behavior of people during linguistic tasks. On the other hand, neural or physiological cognition [8] mainly focuses on the brain and its activities.

The diversions of eyes on different locations of an image disclose inner cognitive processes [40, 41]. Attention is the key to these diversions. In particular, visual attention is used to focus mental capabilities on the stimuli so that the brain can process the information of area of interest. This addresses the issues of attraction of attention towards image features, the role of visual stimuli for making voluntary eye movements, and the link between attention and eye movements [40, 41]. The role of eye movements is crucial to understand the emergent human behavior during visual search. In general, eye movements are broadly classified into three categories: fixation, saccade and smooth pursuits [42]. In fact, saccades and fixations correspond to states of attention in a dynamical system, so that a realistic quantitative approach would examine each one, as well as how each one affects the other [43]. Many different approaches have been proposed to understand causes and clues of diversions of eyes [43]. For example, visual world paradigm [38], an experimental method, examines the emergence of human behavior in a simple language mediated task. Specifically, this paradigm deals with the interaction of cognitive systems to linguistic inputs. In experiments based on this paradigm, the eye movements of the participants time-locked between speech signals [38, 39]. These sequences of time locking, in response to aural inputs with visual analogue, show the emergent behavior of eyes. However, the characteristics of the spatio-temporal dynamics of eye movements have not been dealt in current research.

Our aim is to study the spatio-temporal dynamics of eye movements during simple language comprehension tasks. We examine the effect of literacy on our observations, since literacy may have a direct influence on attentional mechanisms affecting eye movements [44]. We underline that no previous study has measured eye movements in literate and

illiterate participants, with a view to examining their attentional responses. For our purposes, since we are interested in quantifying frequencies of saccades and fixations during a language mediated visual search, we assume that fixations indicate zones of attentional stability, while saccades involve random, relatively inattentive, search. Participants are under no instructional control, and carefully unaware that they are performing a set task. Another issue involves the selection of a comprehensive sample, with varying literacy levels; for this, one needs to construct a task which relies as little as possible on formal education.

We have divided the study into two categories: empirical analysis of the experimental data of eye movements and a numerical model for visual search. First, we have performed the temporal analysis of both saccade and fixation. To support the validity of probability model for saccades, the likelihood and information theoretical techniques have been applied to saccade times. Further, we have constructed the time series of Euclidean distances of saccades and then applied the scaling methods of standard deviation and diffusion entropy to the time series. The aim of these analyses is to identify the nature of spatial diffusion of saccades. Secondly, we have carried out simulation of two-dimensional Levy random walk. This numerical random walk model has been chosen for the comparison between the diffusive properties of both Levy walks and the motion of saccades.

1.2 Outline of the Thesis

We provide the basics of theoretical methods or empirical analysis at the beginning of each chapter.

Chapter 2 gives the review on the statics and dynamics of granular material and the human cognition.

In chapter 3, we present the first part of thesis, study of the spontaneous crystallization of granular spheres. The sections 3.1 and 3.2 provide some details of random packings and the role of external perturbations. The method of simulation, hybrid Monte Carlo algorithm is explained in section 3.3. In section 3.4, transient regimes of spheres for nine shaking amplitudes are shown. Some spontaneous crystalline transitions of spheres, subjected to nine shaking amplitudes, are explained in section 3.5. It is necessary to characterize the spatial orders of sphere packings at various densities so that section 3.6.1

focuses on the global order analysis of packings. In section 3.6.2., we have provided a detailed analysis of development of fcc and hcp sphere-clusters at different packing densities. Section 3.7 concludes the study of spontaneous crystallization of granular spheres.

Delaunay tessellations of granular packings are presented in chapter 4. In section 4.1, we give the basics of Voronoi-Delaunay tessellations and the statistical mechanical approach to volumes of Delaunay simplices. Section 4.2 starts with Delaunay tessellations of sphere packings. The subsection 4.2.1 contains statistical analysis of volumes of tetrahedra. The percentages quasiregular tetrahedra at various packing densities are shown in subsection 4.2.2. Section 4.2.3 explains the findings of angular and length measures of Delaunay tetrahedra. In section 4.3, we conclude our findings on Delaunay tessellation of packings.

Chapter 5 focuses on the second part of thesis, human cognition through eye movements. The visual attention mechanism, types and detection of eye movements, and the experimental paradigm are explained in section 5.1. Section 5.2 provides an overview of theoretical method of analyses. We present temporal analysis of saccade and fixation eye movements in section 5.3.2. Section 5.3.3 gives the details of anomalous diffusion in eye movements. We provide the conclusions on eye movement study in section 5.4.

The model selection for saccade times and the outcomes of numerical Levy walk model are explained in chapter 6. Section 6.1 entirely addresses the basics of statistics of model selection based on likelihood and information theory. The analytical description of likelihood functions for four candidate probability models and Akaike information criteria are presented in section 6.1.2. In section 6.2, we have shown the results of maximum likelihood estimation and Akaike information of four candidate models. The results of simulation of the two-dimensional Levy random walks are shown in section 6.3. Section 6.4 gives the conclusions.

Finally, in chapter 7, we summarize our results on studies of spontaneous crystallization of spheres and eye movements, and provide future perspectives.

Bibliography

[1] B. J. Baars and N. M. Gage, *Cognition, Brain, and Consciousness* (Academic Press), 2010.

[2] G. M. Viswanathan, M. G. E. da Luz, E. P. Raposo and H. E. Stanley, *The Physics of Foraging: An Introduction to Random Searches and Biological Encounters*, (Cambridge University Press), 2011.

[3] T. Aste, T. Di Matteo and A. Tordesillas (Editors), *Granular and Complex Materials* (World Scientific), 2007.

[4] A. Barrat, M. Barthélemy, A. Vespignani, *Dynamical Processes on Complex Networks* (Cambridge University Press), 2008.

[5] N. F. Johnson, P. Jefferies and P. M. Hui, *Financial Market Complexity: What Physics Can Tell Us About Market Behaviour* (Oxford University Press), 2003.

[6] M. Paul, *Instabilities, Chaos and Turbulence* (Imperial College Press), 2010.

[7] Y. Bar-Yam, *Dynamics of Complex Systems* (Westview Press, Colorado), 1997.

[8] R. J. Leigh and D. S. Zee, *The Neurology of Eye Movements* (Oxford University Press), 2006.

[9] P. G. de Gennes, *Rev. Mod. Phys.* **71**, S374(1999).

[10] M. Mitchell, *Complexity: A Guided Tour* (Oxford University Press), 2011.

[11] H. J. Jensen, *Self-Organized Criticality: Emergent Complex Behavior in Physical and Biological Systems* (Cambridge University Press), 1998.

[12] O. E. Barndorff-Nielsen, C. Kluppelberg (Editors), *Complex Stochastic Systems* (Chapman and Hall/CRC), 2000.

[13] K. P. Burnham and D. R. Anderson, *Model Selection and Multimodel Inference* (Springer-Verlag, New York), 2002.

[14] R. Clary, in*Language Acquisition and Learnability* edited by S. Bertolo, (Cambridge University Press), 2001.

[15] H. Hinrichsen, D. E. Wolf (Editors), *The Physics of Granular Media* (Wiley-VCH), 2004.

[16] A. Mehta, *Granular Physics* (Cambridge University Press), 2007.

[17] D. Weaire and T. Aste, *The Pursuit of Perfect Packing* (Taylor and Francis), 2000.

[18] H. M. Jaeger and S. R. Nagel, *Rev. Mod. Phys.* **68**, 1259(1996).

[19] M. Eden, *Proc. of the Fourth Berkeley Symposium on Mathematical Statistics and Probability* **4**, 223(1961).

[20] C. H. Benett, *J. Appl. Phys.* **43**, 2727(1972).

[21] A. Mehta and G. C. Barker, *Phys. Rev. Lett.* **67**, 394(1991).

[22] G. T. Nolan and P. E. Kawavanagh, *Powder Techn.* **72**, 149(1992).

[23] J. P. Hansen and I. R. McDonald, *Theory of Simple Liquids* (Academic Press, New York), 1986.

[24] T. Kawasaki and H. Tanaka, *Proc. Natl. Acad. Sci. U.S.A.* **107**, 14036(2010).

[25] G. Y. Onoda and E. G. Liniger, *Phys. Rev. Lett.* **64**, 2727(1990).

[26] J. D. Bernal, *Nature* **183**, 141(1959).

[27] S. Torquato, T. M. Truskett and P. G. Debenedetti, *Phys. Rev. Lett.* **84**, 2064(2000).

[28] A. Mehta and G. C. Barker, *J. Phys.: Condens. Matter* **12**, 6619(2000).

[29] T. C. Hales, *Ann. of Math.* **162**, 1065(2005).

[30] A. Panaitescu, K. A. Reddy and A. Kudrolli, *Phys. Rev. Lett.* **108**, 108001(2012).

[31] O. Pouliquen, M. Nicolas and P. D. Weidman, *Phys. Rev. Lett.* **79**, 3640(1997).

[32] U. Gasser *et al.*, *Science* **292**, 258(2001).

[33] G. C. Barker and M. J. Grimson, *J. Phys.: Condens. Matter* **1**, 2779(1989).

[34] D. Reisberg, *Cognition* (W. W. Norton and Company, New York), 2009.

[35] M. I. Posner, *Quart. J. Exp. Psychol.* **32**, 3(1980).

[36] R. M. Cooper, *Cog. Psychol.* **6(1)**, 84(1974).

[37] K. Rayner, *Psychol. Bull.* **124**, 372(1998).

[38] M. K. Tanenhaus *et al.*, *Science* **268**, 1632(1995).

[39] F. Huettig, N. Singh and R. Ramesh, *Fron. in Psychol.* **2**, 28(2011).

[40] G. T. Buswell, *How People Look at Pictures* (University of Chicago Press), 1935.

[41] R. H. S. Carpenter, *Movements of the Eyes*(Pion Ltd, London), 1988.

[42] E. Kowler, *Vis. Res.* **51**, 1457(2011).

[43] M. Carrasco, *Vis. Res.* **51**, 1484(2011).

[44] F. Huettig, R. K. Mishra, and C. N. Olivers, *Fron. in Psychol.*, **2**, 394(2012).

Chapter 2

Review of the Literature

Statics and dynamics of complex systems have been studied in interdisciplinary sciences [1, 2]. The dynamics of individual constituents and their collective behavior exhibit complex spatio-temporal structures. The emergent behavior of granular and cognitive systems depends on the applied protocols.

2.1 Statics and Dynamics of Granular Materials

The packings of different geometrical objects reveals their static properties. Specifically, the study of hard sphere packings in athermal systems received a boost when this became the centre-point of models of dry granular media [3, 4, 5]. However, the emergence of collective structures and dynamics of hard spheres were mostly ignored [6]. Bernal, [7, 8], Mason [9], and Scott [10, 11] provided a basis for random packing experiments of hard spheres. In these experiments, the monosize hard spheres packed to a compact and disordered configuration of density 0.64. They also examined the effect of friction on the properties of packings and also computed the coordination numbers of spheres. Onoda and Liniger [12] established the random loose packing of uniform spheres at the limit of zero gravitational force. This random configuration of spheres was stable, corresponding to packing density of 0.55 [12]. The computer simulations of hard spheres [13, 14, 15, 16, 17, 18] reproduced these two empirical limits of random packings. However, no mathematical framework has been established for random packing limits [19].

The methods of construction and the nature of randomness determine the characteristics of packings. The value of packing density and particle's coordination number depend

on the history of construction [6]. The influential factors such as history dependence, friction and stability between the particles, have been incorporated in computational models [20]. These models are broadly classified into two categories: nonsequential [21, 22, 23] and sequential [24, 25]. Moreover, in reality, shaking, pouring, tapping, and stirring processes reflect the collective restructuring of particles. In these processes, particles interact with each other so that their trajectories are nonsequential [21, 22].

In nonsequential algorithms [21, 23], particles cooperatively reorganise at the same time of their deposition. Therefore, the nonsequential algorithms present the realistic view of granular dynamics, in contrast to sequential algorithms [24, 25]. Computational studies [18] expanded the sequential and perturbative ordered configurations to nonsequential organizations. Mehta and Barker [21] developed a hybrid algorithm which comprises a hard sphere Monte Carlo method and a nonsequential step. Importantly, inclusion of nonsequential step assigned stability to particle in a cluster. Their algorithm [21, 22] successfully generated stable sphere packings with densities in the range of 0.55 to 0.60 and the mean coordination number in the range of 4.5 to 6. A nonsequential algorithm of Nolan and Kavanagh [23], based on gas compression method, constructed random packings of densities between 0.509 and 0.638. Also, Nolan and Kavanagh computed the mean coordination numbers of particles between 4.4 and 5.9 [23]. Soppe [26] did not consider the stability of particle in his Monte Carlo scheme. His algorithm generated a packing of spheres with density 0.60 [26]. Jodrey and Tory [27] included isotropic and deterministic compression methods in their nonsequential algorithm. Their packing contained non-contacting particles which further cause increased density with decreasing compression at final steps. Further, their algorithm generated a packing of density 0.64 [27].

Sequential algorithms consider on site search and deposition of particle. Eden [24] and Bennett [25] gave sequential models where particle's sites were continuously updated and chosen according to predefined rules. Specifically, in former model, particle occupied a site with equal a priori probability, whereas latter model constructed packings in central force fields. In sequential algorithms, particles are noninteracting and follow ballistic trajectories until a potential minimum is achieved [24, 25]. Eden and Bennett models packed particles to densities 0.57 and 0.60 respectively [24, 25]. In addition, these deposition models established packings where the mean coordination number of particle

was 6 in three dimensions [24, 25]. No collective reorganisations and history dependence were considered in sequential algorithms.

The bulk properties of granular materials gradually change due to the effect of external driving forces. Knight *et al.*, [28, 29, 30] carried out experiments which were focused on the evolution of packing density and the relaxation dynamics of spherical glass beads, subjected to vibration. They found that the density relaxation follows inverse-logarithmic law [28]. They also suggested multiple time scales for the density relaxation of beads. However, Mehta and Barker [21, 22] proposed two time scales: one for single particle relaxation and other for the cluster relaxation. In this model, the time dependence of packing density was fitted to sum of two exponential terms [21, 22]. In other compaction experiments [31], the density relaxation showed a stretched exponential behavior, in contrast to inverse-logarithmic law.

Recent experiments [32, 33, 34, 35] have examined the crystalline transitions of granular particles subjected to external perturbations. In particular, spontaneous transitions to crystallinity have been observed in horizontally shaken glass beads [31] and sheared granular spheres [35]. Kudroli *et al.*, [35] have studied the development of ordered phases of frictional glass beads by imposing shear. They [35] have also studied the non-spherical shapes and orientations of nucleating clusters. In addition, they calculate the correlation length and the fractions of fcc and hcp clusters. Computer simulations [36] of shaken spheres were first reported crystalline transitions for an optimal range of shaking amplitudes. Also, other simulation studies [37, 38] have shown the developments of different crystalline phases. It has been suggested that fcc structure dominates over hcp structure in sheared colloids [39, 40, 41]. However, none of the study determines the functional relationship between the driving force and packing density of crystalline states.

Various methods are found useful for the characterisation of the structural properties of liquids [42] and glasses [43, 44]. The bond orientational correlation functions [43] and the traditional methods of translational orders [45] identified the spatial ordering in the system. A radial distribution function is the simplest method to distinguish order from disorder [45]. Steinhardt *et al.*, [43] developed the bond orientational order parameters for the detection of ordered structures. These order parameters were used for the local and global analysis of thermal [43, 44] and athermal [46] systems. Torquato

et al., [47] computed the numerical values of bond orientational order parameters for different crystalline structures. Klumov *et al.*, [48] applied bond order metrics to hard sphere packings that were generated using Jodrey-Tory [49] and Lubashevsky-Stillinger [50] algorithms.

Anikeenko *et al.*, [51, 52] performed Voronoi-Delaunay tessellations of granular packings for the geometrical analysis. Their method established different length measures of regular and quasiregular Delaunay simplices. The minima's of length measure's have used for the separation of fcc from hcp structures [53]. Aste *et al.*, [54] have established a statistical mechanical approach for sphere packings via Voronoi-Delaunay tessellations. In addition, they have studied volume distributions of Delaunay simplices and their fluctuations, and configurational entropies [55]. This approach is based on Edwards's measure [56, 57] of granular matter. Also, the Voronoi-Delaunay techniques have been applied to jammed [58, 59], and crystallised granular packings [60].

2.2 The Human Cognition

Our eyes confront with an overwhelming amount of information about the visual world. Eyes capture selective information of an image or an object and ignore other [61]. This may disclose the attentional behavior of a person. The visual attention and perception are inner cognitive processes [62, 63, 64]. Moreover, the visual attention classified into three groups: spatial [65], feature-based [66] and object-based [67]. The spatial attention is divided into two types: overt or covert. In overt case, an attention deploy on relevant location accompanying with eye movements [65]. On the other hand, covert attention focuses on more than one location simultaneously, without coinciding with the movements of eyes [65]. However, the link between attention and eye movements has long been debated [68, 69, 70, 71]. Many attempts [72, 73] have been made to understand the missing link between attention and eye movements. Neurological studies [74, 75] have claimed that various areas of brain involve in visual attention and information processing. Behavioral studies [76, 77, 78] have shown that the attention deploy over large range of scene or image and also during reading.

The visual mechanisms are broadly classified into saccade, fixation and smooth pursuit [79, 80]. S. Martinez-Conde *et al.* [81] have given a review on the studies of fixational eye movements and the visual perception encoded by brain. Itti and Koch [82] have provided

a detailed procedure for the computational modelling of eye movements and attentional mechanisms. Various algorithms, based on velocity [83, 84], dispersion [85], and area of interest [86], are developed and used in eye tracking experiments. Specifically, velocity based algorithms consider thresholds to detect saccade and fixation. Various studies [87, 88, 89, 90] have provided insights into the cognitive dynamics through saccade and fixational eye movements. The change of eye gaze positions in response to linguistic inputs are examined in language mediated visual search [91, 92]. Saccades and fixations, during this natural search, are influenced by both the emerging visual and linguistic representations, and their interactions [91]. The experimental paradigm [92] of eye tracking contains a simple display of objects and neutral aural inputs. The eye movements time-lock between the linguistic inputs during cognitive tasks [92]. Further, linguistic studies [93, 94] have revealed that effect of formal literacy influences the behavior of a person during a simple look and listen task. Huetting and Mishra *et al* [95]., have extensively performed linguistic studies on high and low literate peoples. They have examined the influence of phonological and semantic competitors on identifying the target words [95]. This study suggests that the low literates use only phonological information whereas high literates use both semantic and phonological informations [95].

Humans continuously move their eyes during visual search. The emergent behavior of human cognition through eyes evolves over different spatio-temporal scales [96, 97]. Linguistic studies [98, 99, 100, 101] have shown that the changeability of human behavior during cognitive task understands in terms of diffusion phenomena. Scafetta *et al.*, [102] have developed a scaling method which transforms time series into diffusion processes. Their scaling method, diffusion entropy analysis (DEA), compute entropies of normal and Levy diffusion processes [102]. In general, scaling methods and exponents characterize the diffusive properties of time series [103]. The finite variance methods, standard deviation [104] and detrended fluctuation analyses (DFA) [105] detect the scaling functions of long range correlations of DNA sequences [106]. Stefan *et al.*, [107] have applied both SDA and DEA on the time series of eye movements. They observe that eye movements exhibit Levy like superdiffusion. Further, they have used likelihood and information theoretical methods in support of Levy's power-law distribution. In contrast, Shelhamer [108] claimed the fractional Brownian motions of the latencies of saccades. The anomalous diffusive behavior of eye movements are found similar to those described by Vishwanathan *et al.* In case of animal foraging dynamics, Vishwanathan

et al., [109, 110] have showed the scale free behavior of step lengths. This scale free behavior also exhibits power-law of Levy like distribution [109, 110]. Moreover, Kello *et al.*, [111] have given a comprehensive review on various forms of scaling laws that are observed in cognitive science. Prokett *et al.*, [112] have observed the scale invariance in dynamics of spontaneous behaviors of animals and humans. Reynolds [113] has suggested that fractional cases of Brownian and Levy motions are also useful in random search scenarios of animal foraging. The candidate probability models of animal foraging data further revised using likelihood, Akaike, and Bayesian information methods [114]. These modern statistical methods select the best approximate model for the empirical data [115, 116, 117].

Gaussian processes have finite mean and variance, whereas Levy processes do not [118]. Levy flights and random walks are the efficient ways of modelling anomalous diffusion [119, 120, 121, 122, 123]. The Levy and Brownian diffusive dynamics were studied in finance [124] and in fractal processes [125, 126]. Mandelbrot [127] further generalised the ordinary diffusion to fractional cases. In case of visual research, Mergenthaler and Engbert [128] have demonstrated the delay random walk model for the fixational eye movements. They have investigated transitions of fixational eye movements from persistent to anti-persistent behavior.

Bibliography

[1] Y. Bar-Yam, *Dynamics of Complex Systems* (Westview Press, Colorado), 1997.

[2] P. Bak, *How Nature Works: the science of self-organized criticality* (Copernicus), 1999.

[3] H. M. Jaeger, and S. R. Nagel, *Rev. Mod. Phys.* **68**, 1259(1996).

[4] P. G. de Gennes, *Rev. Mod. Phys.* **71**, S374(1999).

[5] D. Weaire, and T. Aste, *The Pursuit of Perfect Packing* (Taylor and Francis), 2000.

[6] A. Mehta, *Granular Physics* (Cambridge University Press), 2007.

[7] J. D. Bernal, *Nature (London)* **183**, 141(1959).

[8] J. D. Bernal, *Proc. Roy. Soc. London A* **280**, 299(1964).

[9] G. Mason, *Nature (London)* , **217**, 733(1968).

[10] G. D. Scott, *Nature (London)* **188**, 908(1960).

[11] G. D. Scott, and D. M. Kilgour, *Br. J. Phys. D* **2**, 863(1969).

[12] G. Y. Onoda, and E. G. Liniger, *Phys. Rev. Lett.* **64**, 2727(1990).

[13] J. L. Finney, *Proc. R. Soc. London, Ser. A* **319**, 479(1970).

[14] W. M. Visscher, and M. Bolsterli, *Nature (London)* **239**, 504(1972).

[15] E. M. Tory *et al.*, *Can. J. Chem. Eng.* **51**, 484(1973).

[16] W. S. Jodrey and E. M. Tori, *Powder Technol.* **30**, 111(1981).

[17] A. S. Clarke, and H. Jonsson, *Phys. Rev. E* **47**, 3975(1993).

[18] P. Meakin, and R. Jullien, *J. de Physique* **48**, 1651(1987).

[19] S. Torquato, T. M. Truskett, and P. G. Debenedetti, *Phys. Rev. Lett.* **84**, 2064(2000).

[20] T. Pöschel, and T. Schwager, *Computational Granular Dynamics: Models and Algorithms* (Springer, Berlin), 2005.

[21] A. Mehta, and G. C. Barker, *Phys. Rev. Lett.* **67**, 394(1991).

[22] G. C. Barker, and A. Mehta, *Phys. Rev. A.* **45**, 3435(1992).

[23] G. T. Nolan, and P. E. Kawavanagh, *Powder Techn.* **72**, 149(1992).

[24] M. Eden, *Proc. of the Fourth Berkeley Symposium on Mathematical Statistics and Probability* **4** , 223(1961).

[25] C. H. Benett, *J. Appl. Phys.* **43**, 2727(1972).

[26] W. Soppe, *Powder Tech.* **62**, 189(1990).

[27] W. S. Jodrey, and E. M. Tori, *Phys. Rev. A* **32**, 2347(1985).

[28] J. B. Knight *et al.*, *Phys. Rev. E* **51(5)**, 3957(1995).

[29] J. B. Knight *et al.*, *Phys. Rev. E* **57)**, 1971(1998).

[30] E. Ben-Naim, J. B. Knight, E. R. Nowak, H. M. Jaeger, and S. R. Nagel, *physica D* **123**, 380(1998).

[31] P. Phillippe, and D. Bideau, *Europhys. Lett.* **60(5)**, 677(2002).

[32] O. Pouliquen, M. Nicolas, and P. D. Weidman, *Phys. Rev. Lett.* **79**, 3640(1997).

[33] J. -C. Tsai and G. A. Voth and J. P. Gollub, *Phys. Rev. Lett.* **91**, 064301(2003).

[34] K. E. Daniels and R. P. Behringer, *Phys. Rev. Lett.* **94**, 168001(2005).

[35] A. Panaitescu, K. A. Reddy, and A. Kudrolli, *Phys. Rev. Lett.* **108**, 108001(2012).

[36] A. Mehta, and G. C. Barker, *J. Phys. : Condens. Matter* **12**, 6619(2000).

[37] V. Luchnikov, A. Gervois, P. Richard, L. Oger, and J. P. Troadec, *J. Mol. Liq.* **96**–**97**, 185 (2002).

[38] Y. Jin, and H. A. Makse, *Physica* **389A**, 5362(2010).

[39] L. V. Woodcock, *Nature (London)* **385**, 141(1997).

[40] U. Gasser *et al.*, *Science* **292**, 258(2001).

[41] S. Auer and D. Frenkel, *Nature (London)* **385**, 321(1997).

[42] J. P. Hansen, and I. R. McDonald, *Theory of Simple Liquids* (Academic Press, New York), 1986.

[43] P. J. Steinhardt, D. R. Nelson, and M. Ronchetti, *Phys. Rev. B* **28**, 784(1983).

[44] T. Kawasaki, and H. Tanaka, *Proc. Natl. Acad. Sci. U.S.A.* **107**, 14036(2010).

[45] M. P. Allen, and D. J. Tildesley, *Computer Simulation of Liquids* (Clarendon Press), 1989.

[46] W. Lechner, and C. Dellago, *J. Chem. Phys.* **129**, 114707(2008).

[47] M. D. Rintoul, and S. Torquato, *J. Chem. Phys.* **105**, 9258(1996).

[48] B. A. Klumov, S. A. Khrapak, and G. E. Morfill, *Phys. Rev. B* **83**, 184105(2011).

[49] W. S. Jodrey, and E. M. Tory, *Powder Tech* **30**, 111(1981).

[50] F. H. Stillinger ,and B. D. Lubachevsky, *J. Stat. Phys.* **73**, 497(1993).

[51] A. V. Anikeenko, and N. N. Medvedev, *Phys. Rev. Lett.* **98**, 235504(2007).

[52] A. V. Anikeenko, N. N. Medvedev, and T. Aste, *Phys. Rev. E* **77**, 031101(2008).

[53] A. V. Anikeenko, M. L. Gavrilova, N. N. Medvedev, in *Computational Science and Its Applications – ICCSA 2005*(Springer, Berlin), 2005.

[54] T. Aste, *Phys. Rev. Lett.* **96**, 018002(2006).

[55] T. Aste *et al.*, *Euro. Phys. Lett.* **79**, 24003(2007).

[56] S. F. Edwards, and D. V. Grinev, *Phys. Rev. Lett.* **82**, 5397(1999).

[57] S. F. Edwards, in *Granular Physics, A Mehta (Editor)* (Cambridge University Press), 2007.

[58] C. Briscoe, C. Song, P. Wang and H. A. Makse, *Phys. Rev. Lett.* **101**, 188001(2008).

[59] F. Lechenault, O. Dauchot, and E. Bertin, *J. Stat. Mech.* P07009(2006).

[60] N. Francois, M. Saadatfar, R. Cruikshank and A. Sheppard *Phys. Rev. Lett.* **111**, 148001(2014).

[61] G. T. Buswell, *How People Look at Pictures* (University of Chicago Press), 1935.

[62] D. Reisberg, *Cognition* (W. W. Norton and Company, New York), 2009.

[63] K. Nakayama, and P. Martini, *Vis. Res.* **51 (13)**, 1526(2011).

[64] P. Cavanagh (2011). *Vis. Res.* **51 (13)**, 1538(2011).

[65] M. Carrasco, *Vis. Res.* **51**, 1484(2011).

[66] C. R. Olson, *Curr. Opin. in Neurobio.* **11(2)**, 171(2001).

[67] B. J. Scholl, *Cognition* **80(1–2)**, 1(2001).

[68] R. M. Cooper, *Cog. Psychol.* **6(1)**, 84(1974).

[69] M. I. Posner, *Quart. J. Exp. Psychol.* **32**, 3(1980).

[70] K. Rayner, *Psychol. Bull.* **124**, 372(1998).

[71] J. M. Henderson, *Trends. Cogn. Sci.* **7(11)**, 498(2003).

[72] K. Rayner, *Quart. J. Exp. Psychol.* **62(8)**, 1457(2009).

[73] J. M. Henderson, *Curr. Dir. Psychol. Sci.* **16(4)**, 498(2007).

[74] M. I. Posner, and S. E. Petersen, *Ann,. Rev. Neurosci.* **13**, 25(1990).

[75] J. W. Bisley, and M. E. Goldberg, *Ann,. Rev. Neurosci.* **33** 1(2010).

[76] M. I. Posner and M. K. Rothbart, *Ann,. Rev. Psychol.* , 1(2007).

[77] M. M. Chun, J. D. Golomb, and N. B. Turk-Browne, *Ann,. Rev. Psychol.* **62**, 73(2011).

[78] H. Pashler, and J. C. Johnston, *Attentional limitations in dual-task performance* (Psychology Press/Erlbaum (UK) Taylor Francis), 1998.

[79] E. Kowler, *Vis. Res.* **51**, 1457(2011).

[80] A. T. Duchowski, *Eye Tracking Technology* (Springer, New York), 2007.

[81] S. Martinez-Conde, S. L. Macknik, and D. H. Hubel, *Nature Reviews Neuroscience* **5**, 229(2004).

[82] L. Itti and C. Koch, *Nature Rev. Neurosci.* **2**, 194(2001).

[83] D. D. Salvucci and J. H. Goldberg, *Proc. of Eye Tracking Research and Application Symposium* , 71(2000).

[84] T. Sen and T. Megaw, in *Theoretical and Applied Aspects of Eye Movement Research* (Elsevier, Amsterdam), 1984.

[85] H. Widdel, in *Theoretical and Applied aspects of Eye Movement Research* (Elsevier, New York), 1984.

[86] C. L. Erkelens and I. M. L. C. Vogels, in *Eye Movement Research : Mechanisms, Processes, and Applications*(Elsevier, New York, 1995.

[87] R. H. S. Carpenter, *Movements of the Eyes*(Pion Ltd, London), 1988.

[88] W. L. Shebilske and D. F. Fisher, in *Eye Movements and Psychological Functions : International Views* (Hillsdale, NJ: Lawrence Erlbaum, 1983.

[89] D. E. Irwin, in *Eye movements and visual cognition : Scene perception and reading* (Springer-Verlag, New York, 1992.

[90] L. Stark and S. R. Ellis, in *Eye Movements : Cognition and Visual Perception* (Hillsdale, NJ: Lawrence Erlbaum, 1981.

[91] Gonzalez-Marquez *et al.*, *Methods in Cognitive Linguistics*(John Benjamins Publishing Company, Amsterdam), 2006.

[92] M. K. Tanenhaus *et al.*, *Science* **268**, 1632(1995).

[93] F. Huettig, N. Singh and R. Ramesh, *Fron. in Psycho.* **2**, 28(2011).

[94] R. K. Mishra, N. Singh, A. Pandey, and F. Huettig, *J. Eye. Mov. Res.* **5(1): 3**, 1(2012).

[95] F. Huettig, R. K. Mishra, and C. N. Olivers, *Fron. in Psychol.* **2**, 394(2012).

[96] A. L. Yarbus, *Eye Movements and Vision* (Plenum Press, New York), 1967.

[97] T. S. Horowitz and J. M. Wolfe, *Nature (London)* **394**, 575(1998).

[98] R. Ratcliff, *Psychol. Rev.* **85**, 59(1978).

[99] J. Palmer, P. Verghese, and M. Pavel, V̂ision Res. **40**, 1227(2000).

[100] A. Voss and J. Voss, *J. Math. Psychol.*, **52**, 1(2008).

[101] D. J. Aks, G. J. Zelinsky, and J. C. Sprott, *Nonlin., Dyn. Psychol. Life Sci.* **6**, 1(2002).

[102] N. Scafetta and P. Grigolini, *Phys. Rev. E.* **66**, 036130(2002).

[103] N. Scafetta, V. Latora, and P. Grigolini, *Phys. Rev. E.* **66**, 031906(2002).

[104] P. Allegrini *et al.*, *Phys. Rev. E* **52**, 5281(1995).

[105] S. V. Buldyrev *et al.*, *Phys. Rev. E.* **47**, 4514(1993).

[106] C. -K. Peng *et al.*, *Phys. Rev. E.* **49**, 4514(1994).

[107] D. G. Stephen *et al.*, *Phys. Rev. E* **79**, 056114(2009).

[108] M. Shelhamer, *Biol. Cybern.* **93(1)**, 43(2005).

[109] G. M. Viswanathan *et al.*, *Nature (London)* **381**, 413-5(1996).

[110] G. M. Viswanathan *et al.*, *Nature (London)* **401**, 911-4(1999).

[111] C. T. Kello and G. G. Anderson and J. G. Holden and G. C. Van Orden, *Cogn. Sci.* **32**, 1217(2008).

[112] A. Prokett *et al.*, *Proc. Natl. Acad. Sci.* **109**,10564(2012)

[113] A. M. Reynolds, *J. Phys. A: Math. Theor.* **42**, 434006(2009).

[114] E. M. Edwards *et al.*, *Nature (London)* **449**, 1044-8(2007).

[115] K. P. Burnham, and D. R. Anderson, *Model Selection and Multimodel Inference* (Springer-Verlag New York), 2002.

[116] C. M. Hurvich, and C-L. Tsai, *Biometrika* **76**, 297(1989).

[117] H. Akaike, *IEEE Transactions on Automatic Control AC* **19**, 716(1974).

[118] D. H. Zanette, *Phys. Rev. E* **55**, 6632(1997).

[119] M. F. Shlesinger, B. J. West, and J. Klafter, *Phys. Rev. Lett.* **58**, 1100(1987).

[120] M. F. Shlesinger and G. M. Zaslavsky and J. Klafter, *Nature (London)* **363**, 31(1993).

[121] S. Moshel *et al.*, *Ann. N. Y. Acad. Sci.* **1039**, (2005).

[122] S. Moshel *et al.*, *Eur. Phys. J. Spec. Top.* **161**, 207(2008).

[123] J. R. Liang *et al.*, *Phys. Rev. E.* **71**, 031909(2005).

[124] B. B. Mandelbrot, *The Fractal Geometry of Nature* (Times Books), 1982.

[125] M. F. Shlesinger, G. M. Zaslavsky, and U. Frisch, *Levy Flights and Related Topics in Physics*(Springer, Berlin), 1995.

[126] M. F. Shlesinger, G. M. Zaslavsky, and J. Klafter, *Nature* **363**, 31(1993).

[127] B. B. Mandelbrot and J. W. Van Ness, *SIAM, Review* **10**, 422(1968).

[128] K. Mergenthaler and R. Engbert, *Phys. Rev. Lett.* **98**, 138104(2007).

Chapter 3

Spontaneous Crystallization of Granular Spheres

In this chapter, we mention the basics of random packings and the role of external driving forces. The remaining sections are devoted to hybrid Monte Carlo simulation and characterization of spontaneous transitions of granular spheres.

3.1 Basics of Random Packings

Random packing is a large collection of solid objects of regular and/or irregular geometrical shapes in a given spatial dimensions. Moreover, how much volume or fraction of a container occupied by particles, is a key problem in mathematics [1] and physics [2]. The properties of random close packings depend on sample composition, method of preparation and the nature of contact between the particles [3]. Besides, the shapes and texture of particles strongly influences statics and dynamics of packings. Furthermore, static friction and the inelastic collisions between particles alter the bulk properties of the packings [2]. Packing fraction or density and mean coordination number of particles, the key parameters, are used for the description of distinctive features of disc [4, 5], sphere [6], rod [7, 8] and ellipsoid [9] packings. Some important terms [10, 11, 12] relevant to granular packings are defined as follows.

- **Packing fraction or density ϕ**:

  Packing fraction is the ratio of volume of the total number of particles to the

volume of the box occupied by the particles. Let us consider, v_p be the volume of a particle and V_{ocp} is the volume occupied by M particles in a container, then the simplest formula for packing density is $\phi \equiv \frac{Mv_p}{V_{ocp}}$.

- **Mean coordination number** $\overline{z}$: Mean coordination number of a particle is the number of particles in touch with it.
- **Compaction**: The compaction is defined as the change in packing fraction or density with respect to external mechanical perturbations.

Random packings of particles attain stable mechanical equilibrium. The number and nature of contacts, and interaction between particles affect the stability of packings [13, 14]. The stability of particles is a major concern in computational models of packings [3]. Other important parameters such as the angular separation and friction between particles are also modelled in cluster algorithms [15, 16]. These algorithms consider the stability of spheres and their clusters [17, 18]. To attain stability, each sphere in random packing needs at least four or at most twelve other spheres in contact [6]. It has been argued that sphere packings are either isostatic [19] or hypostatic [20, 21]. In former case, the mean coordination number $\overline{z}$ of particles is equal to twice the number of degrees of freedom. On the other hand, in latter case, $\overline{z}$ is less than number of degrees of freedom. In a stable mechanical equilibrium, the total force and the torque on each particle should vanish. Experimental study [22] has shown that in marginally rigid state, for mechanical balance, the mean coordination number reach above the critical value z_c. For convex shape grains: $z_c = 3$ and 4 in two and three dimension respectively [22, 23]. This study also suggested that z_c corresponds to 6 and 12 for random close sphere packings [22, 23].

Random packing of spheres can be obtained by dropping them randomly in a container. If the spheres put in the container very gently then the density or the volume of the container occupied by the spheres is called the random loose packing density ϕ_{rlp} [24]. Afterwords, if the spheres in the container are tapped so that they come as close as possible, but still persist disorder, then the density $\phi_{rcp} \sim 0.64$ corresponds to random close packing [25, 26]. The random loose packing depends on the gravitational force and the density of spheres [24]. Onoda and Liniger [24] gave the value of loose packing density ϕ_{rlp} for glass spheres. The glass spheres with specific gravity of 2.94 were immersed in a mixture of d-iodomethane and toluene. The spheres were allowed to settle in

liquid and then $\phi_{rlp} = 0.55$ was determined for the limit g (acceleration)$\rightarrow 0$ [24]. Moreover, experiments [25, 26] and simulations [27, 28, 29] have suggested that the random packings at density 0.64 comprise noncrystalline structures.

3.2 Role of External Perturbation in Granular Compaction

Granular materials are athermal systems so that the traditional Gibbs thermal ensemble method is not useful for the sampling [3, 13]. The dynamics of particles subjected to external driving forces is intricate. A major source of difficulty is to understand the functional relationship between the external driving force and the displacement of particles. Despite the limitations, computer simulation of shaken spheres [17, 18] explained the stability and relaxation dynamics of a single sphere and sphere- clusters. This computer simulation algorithm reinforces the role of driving force, complex trajectories of spheres and the stability of packings. Furthermore, linear and nonlinear trajectories of spheres under shaking and tapping were examined in other simulations [15, 16, 17, 18, 28].

A series of experiments [30, 31, 32] were carried out on the compaction of monodisperse glass beads by tapping them vertically. In these experiments, the glass beads were confined to a long tube and then tapped. The initial state was a loose packing of density 0.58. The time dependence of density was fitted to inverse-logarithmic law [30],

$$\rho(t) = \rho_f - \frac{\Delta\rho_\infty}{1 + B \ln\left[1 + \frac{t}{\tau}\right]}, \tag{3.1}$$

where τ is characteristic time and B is fitting parameter. These parameters are constant and depend only on tapping strength [30]. Importantly, these experiments suggested that two or more timescales may involve in density relaxation. On the contrary, in other compaction experiment [33], the density relaxation of glass beads, under vertical tapping, was fitted to stretched exponential of Kohlrausch-Williams-Watts law,

$$\rho(t) = \rho_\infty - e^{-(t/\tau)^\epsilon}(\rho_\infty - \rho_0), \tag{3.2}$$

where ρ_0 and ρ_∞ are steady state values of initial and final densities respectively. The τ and ϵ are relaxation time and stretching parameter of the exponential fit respectively.

Random packings can undergo spontaneous transitions from disordered to crystalline states when subjected to given energy inputs under specific protocols [3]. In these cases,

the density increased above the random close packing limit ϕ_{rcp}. The crystalline transitions are observed in sheared [34] and horizontally shaken [35] beads. The crystallinity of granular spheres can occur via fcc or hcp structures, or indeed a mixture of the two [34]. In addition, the cluster analysis of granular spheres [34] focused on the developments of hcp and fcc structures at each step of shear [34] and vibration [36]. The competitive behaviour between fcc and hcp was observed during the later stages of sheared colloids [37, 38, 39, 40].

3.3 Hybrid Monte Carlo Simulation

In this section, we describe method of simulation and the details of our simulation.

3.3.1 Packing and Shaking Algorithms

We use a three-dimensional hybrid Monte Carlo simulation to investigate the crystallization of granular spheres [17, 18]. Our computational method consists two steps: packing and shaking of spheres. First, we are able to pack spheres randomly using sequential procedure [41]. Secondly, the configurations of spheres are gradually shaken. In packing step, hard and frictionless monodisperse spheres are slowly deposited inside the box. The gravitational force acts on the sphere during deposition and therefore generates an irreversible ballistic sphere-cluster aggregate [41]. In this aggregate, spheres reduce their potential energies along a trajectory. These trajectories are computed by considering series of linear free fall and circular rotations [41]. This sequential process finally produces packing of density 0.58.

The shaking cycle contains three stages: vertical expansion, stochastic rearrangement and cooperative recompression. Moreover, the shaking cycle is a hybridization of low temperature Monte Carlo and a nonsequential (cooperative) step [17, 18]. Further, the shaking amplitude is parameterized in terms of sphere diameters. For example, $A = 0.10$ means that the shaken spheres are free to move longitudinally on an average 0.10 sphere diameter.

In the first stage, the sphere assembly is displaced vertically in proportion with the shaking amplitude A. This vertical expansion assigns new heights to spheres, i.e., the height of the sphere i changes from z_i to $z_i^{'} = (1 + A)z_i$, and accompanied by random lateral displacements, $x^{'} = x + \xi_x$ and $y^{'} = y + \xi_y$. Here, ξ_x and ξ_y are Gaussian random

variables with zero mean and the variance proportional to A^2. Importantly, the vertical expansion introduces a free volume of size A between the spheres. Spheres utilize the free volume in their cooperative rearrangements during second and third stages of shaking cycle. The packing density during the expansion stage of n^{th} shake cycle drops from ϕ_{n-1} to $\phi_{n-1}/(1+A)$.

In the second stage, the whole packing is compressed by a series of stochastic arrangements of the individual spheres. A low temperature hard sphere Monte Carlo algorithm is used for random selection and displacement of individual spheres. Spheres are randomly selected and displaced according to the transformation, $r_i = r_i + e * d$. The components e_x, e_y, e_z of a random vector e lies in the interval $[-1, 1]$. The Monte Carlo step length d defines the neighbourhood for spheres. All successful moves reduce the overall potential energy of the system.

The final stage of the shaking cycle is a cooperative step. In this stage, spheres are chosen with increasing height and, in turn are allowed to roll and fall into stable positions. In this part of the shake cycle, spheres may roll over, and rest on, any other sphere in the assembly. This includes those spheres which are still to be stabilized and which may, in turn, undergo further rolls and falls. This is a fully cooperative process, which is crucial for realistic simulations of granular media.

3.3.2 Details of Simulation

We use monodisperse, rigid, incompressible hard spheres of unit diameter. Our sequential algorithm generates a stable packing of spheres with density 0.58. The simulation cell is an open-topped box of size $10\times10\times10$, and contains 1273 spheres in total. The periodic boundary conditions are applied in the lateral directions. Spheres are shaken at *nine* amplitudes parameterized in units of sphere diameters: $A = 0.05, 0.08, 0.10, 0.15, 0.18, 0.20, 0.25, 0.28$ and 0.30. We make three categories of amplitudes: low ($A = 0.05, 0.08, 0.10$), intermediate ($A = 0.15, 0.18, 0.20, 0.25$) and high ($A = 0.28, 0.30$) shaking amplitudes. The whole assembly is repeatedly and cooperatively packed using nonsequential reorganizations which represent the effect of shaking. We carry out 10 sets of simulation and computes packing density as a function of shaking amplitudes over 10^5 cycles. Also, Cartesian coordinates (x, y, z) of spheres are collected over an interval of 100 shakes. In

next sections, we give a detailed analysis of crystalline transitions and explore in brief transient behaviors.

3.4 Transient Behavior

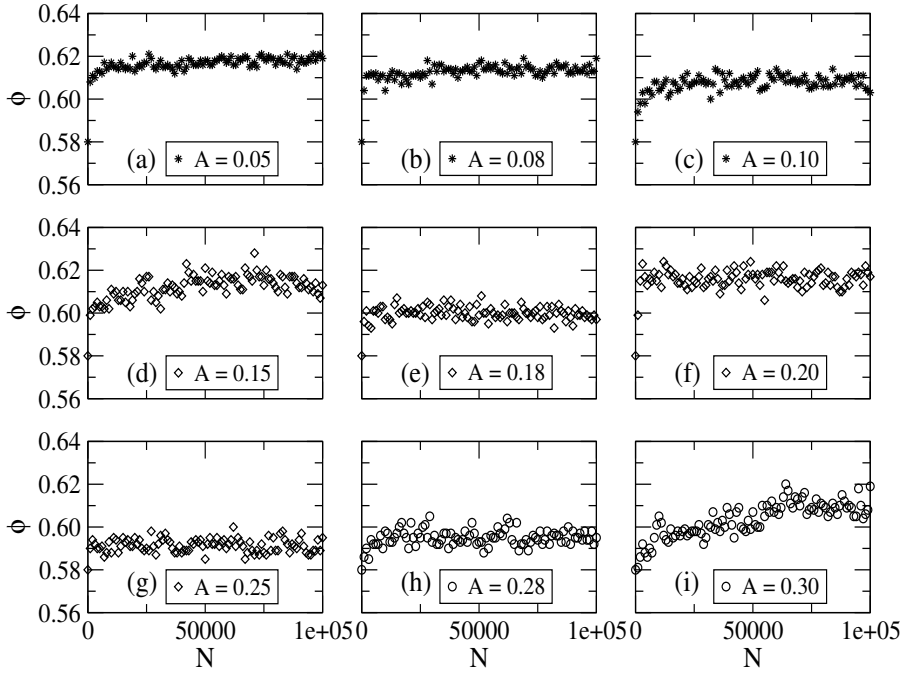

FIGURE 3.1: Packing density ϕ plotted against the number of shakes N for low [(a) to (c)](stars), intermediate [(d) to (g)] (diamonds) and high [(h) and (i)] (circles) shaking amplitudes. The initial state is sequential random close packing with packing density 0.58.

We briefly discuss the transient behavior of spheres. Figure 3.1 shows the variation of packing density ϕ against the number of shakes N. In all cases, the packing density ϕ increases slowly for $N < 5000$, and fluctuates around a steady state value between 0.60 to 0.62, at larger shaking times [Fig. 3.1]. This slow compaction towards vibrational steady state is due to nonsequential reorganizations [18]. In this state, the packings are insensitive to further shaking. A detailed analysis of transient behaviors is discussed by Barker and Mehta [18].

3.5 Spontaneous Transitions

We notice that within a range of excitation amplitudes there is a sharp increase in packing density well above the random close packing density 0.64. Moreover, the shaking process influences the sphere arrangements inside packing.

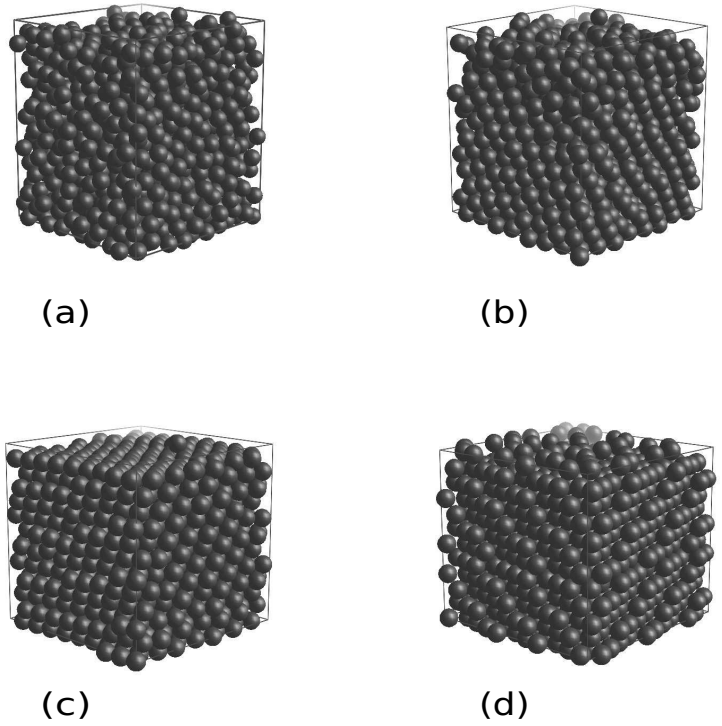

FIGURE 3.2: Different phases of sphere packings. (a) $\phi \sim 0.58$, (b) $\phi \sim 0.64$, (c) $\phi \sim 0.68$, (d) $\phi \sim 0.72$. The crystalline phase ($\phi \sim 0.72$.) emerges from initial disordered phase $\phi \sim 0.58$.

As the shaking time progresses, spheres move within the volume of size proportional to amplitude A. Further shaking for extended periods is seen to produce spontaneous jumps to denser and ordered packings. This has been called as "shaking-induced crystallization" [42]. Figure 3.2 displays different phases of sphere packings after 10^5 shakes, for four sample packing densities. The ordered-phase of spheres at maximum density of 0.72 [Fig. 3.2 (d)] evolves from a disordered-phase of spheres with density 0.58 [Fig. 3.2 (a)].

Figure 3.3 shows spontaneous crystalline transitions for different shaking amplitudes. In all cases, the packing density suddenly increases from low a value of 0.58 to maximum value, for $N > 5000$. Table 3.1 shows the values of maximum packing density ϕ_{max} with respect to all shaking amplitudes. We observed that the system of spheres attains lower packing density for low amplitudes than for higher amplitudes, at least in our simulation times. The situation at lower amplitudes can be changed for longer shaking times. The crystalline transitions which lead to end states comprise long-lasting partially ordered or fully ordered symmetries. Specifically, spheres may form crystalline structures of simple

cubic (sc), body-centered cubic (bcc), hexagonal close-packed (hcp), face-centered cubic (fcc) and icosahedral types.

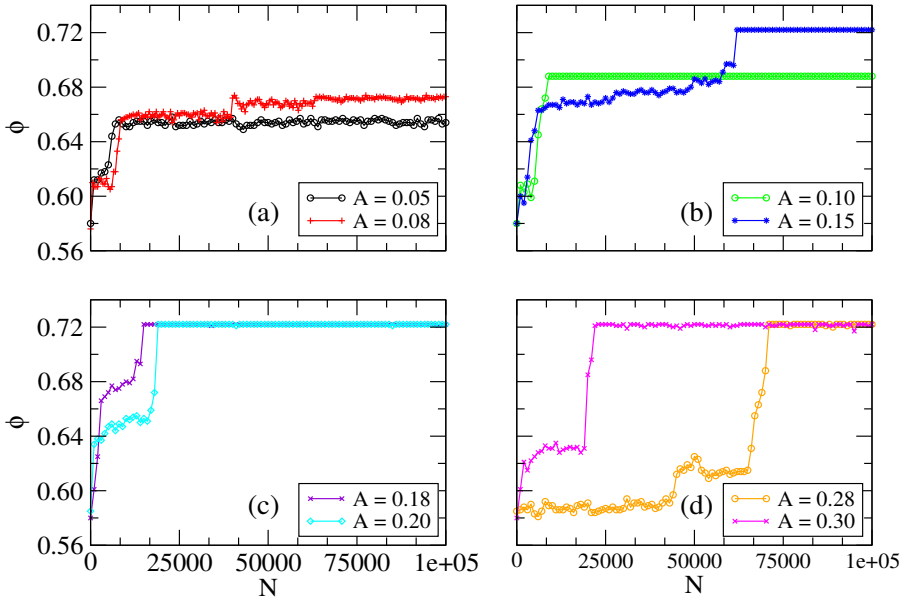

FIGURE 3.3: Plots of packing density ϕ vs. number of shakes N for low (a), intermediate ((b) and (c)), and high (d) shaking amplitudes. The maximum values of packing density ϕ_{max} with respect to amplitudes are displayed in Table 3.1. The lines serve as a guide for the eye.

TABLE 3.1: The maximum values of packing density ϕ_{max} for all shaking amplitudes.

Amplitude (A)	ϕ_{max}
0.05	0.66
0.08	0.69
0.10	0.70
0.15	0.72
0.18	0.72
0.20	0.72
0.25	0.72
0.28	0.72
0.30	0.72

3.6 Characterization of Spontaneous Transitions

In this section, we explain the methods of characterization for crystalline transitions. Next, we divide the analysis in two groups: global and local. The global analysis lays emphasis on the ordering in the system whereas the local order analysis demonstrates the development of fcc and hcp clusters.

3.6.1 Global Order Analysis

3.6.1.1 Radial Distribution Function

We define a radial distribution function (RDF) and show how it can be used to examine spatial structures. Radial distribution function gives the probability of finding a sphere from a distance r to $r+dr$ [43]. The histograms of sphere distances are constructed over number of bins. Each bin j has a width of dr and contains $n(j)$ pairs of spheres. The average number of spheres per bin is calculated as: $N_{av}(j) = \frac{n(j)}{N_s}$.

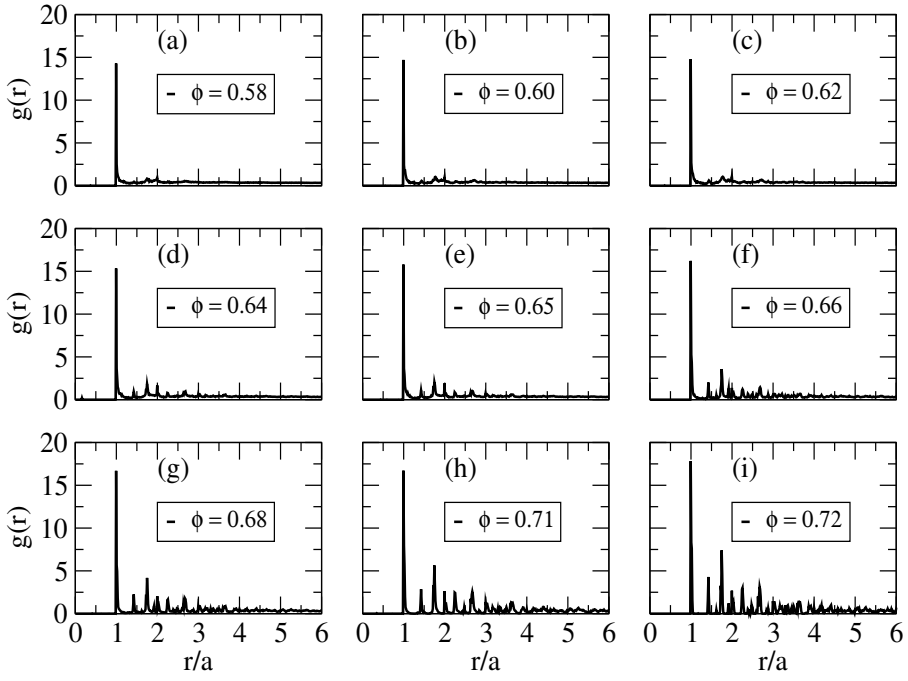

FIGURE 3.4: Plots of radial distribution functions $g(r)$ as a function of normalized distance r/a for various packing density ϕ. The number of peaks shows the development of spatial order from low ((a)) to high ((i)) density.

The radial distribution function $g(r)$ is computed using the formula,

$$g(r) = \frac{3N_{av}(j)}{4\pi\varrho((r+dr)^3 - r^3)}, \tag{3.3}$$

where $\varrho = N_{sp}/V$ is the density of the system and N_{sp} is the number of spheres in a volume V. In case of hard spheres with diameter a, $g(r) = 0$ for $r < a$.

Figure 3.4 shows the RDF $g(r)$ as a function of r for different packing densities, as generated by our simulations. Note that more and more peaks appear as the packing density increases. The appearance of peaks in the RDF confirms spatial order in the system via its indication that the spheres are at well-defined distances from each other. The fact that both fcc and hcp [see, for example, the peak at 1.91 in Fig. 3.4(g)] peaks are observed already indicates that, locally, both types of order are present.

3.6.1.2 Global Bond Orientational Order Parameter

In addition to radial distribution function, we utilize the global bond order orientational order parameters for more detailed analysis. Steinhardt *et al.*, [44] have developed the global bond order parameters as:

$$Q_{l,global} \equiv \left[\frac{4\pi}{2l+1} \sum_{m=-l}^{l} \left| \langle Y_l^m(\Theta(\vec{r}), \Phi(\vec{r})) \rangle \right|^2 \right]^{1/2}. \tag{3.4}$$

Here, $Y_l^m(\Theta, \Phi)$ are spherical harmonics defined with respect to an arbitrary coordinate system and l, m are integers. The spherical harmonics are computed with respect to a bond, i.e. a line joining a sphere with its neighbors. Furthermore, hcp cluster and cubic symmetry have nonzero averages for $l \geq 4$ and for even l, the spherical harmonics preserve the inversion symmetry [44]. The choice, $l = 6$ is sensitive to crystallization [44]. We first calculate the spherical harmonics,

$$Y_l^m(\Theta, \Phi) = (-1)^m \left[\frac{(2l+1)(l-m)\,!}{(4\pi)(l+m)\,!} \right]^{1/2} P_l^m(\cos\Theta) e^{im\Phi}, \tag{3.5}$$

where $P_l^m(\cos\Theta)$ are associated Legendre polynomials. The global bond orientation order parameter $Q_{6,global}$ is calculated using Eq. (3.4) for different packing densities. The averages in Eq. (3.4) are taken over all the bonds in the system for 100 configurations.

Figure 3.5 shows the variation of $Q_{6,global}$ against packing density ϕ. We mention here that the variation of $Q_{6,global}$ with shaking amplitude is implicit in the figures, since amplitude governs both the value of the final density max reached in a given time, as well as its rate of change. A universal feature is that after an initial increase, global order is seen to rise slightly at $\phi \sim 0.62$ and increase steadily after $\phi = 0.64$ until the final

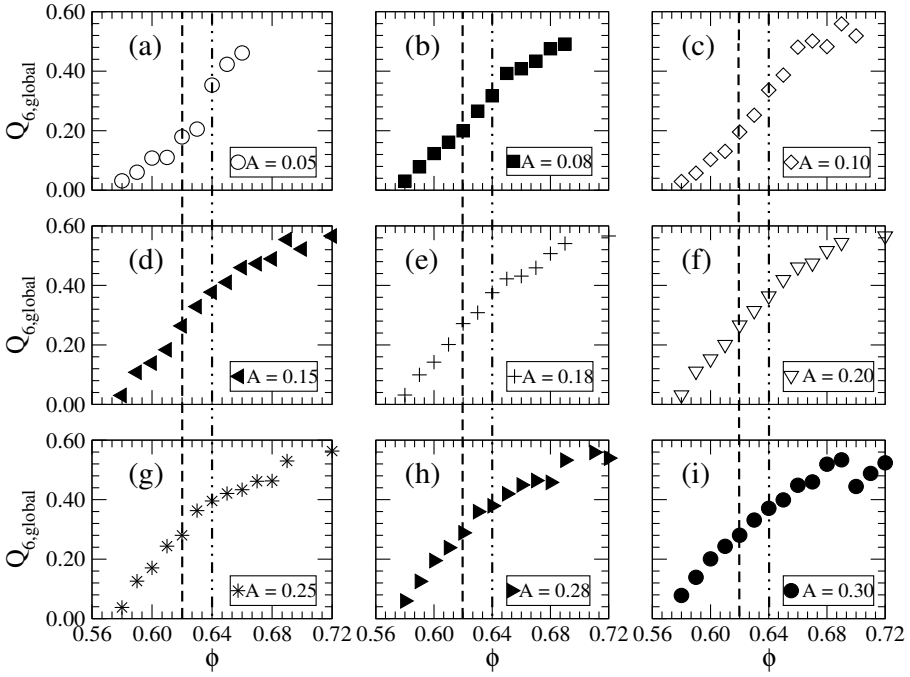

FIGURE 3.5: Variation of $Q_{6,global}$ against packing density ϕ. Note the slight jump (kink) at 0.62 and steady rise after 0.64. The global order shows breakdown at 0.69 [(c), (d), (g), (h) and (i)]. The vertical line markers at $\phi = 0.62$ (dotted line) and 0.64 (dot dashed line) serve as a guide to the eye.

density of ϕ_{max} is reached. This indicates that the shaking strength plays an important role in this protocol. Experiments on sheared granular spheres [34] show that $\phi \sim 0.62$ is the onset of ordering, where the ordering begins, which is suggested by our simulations as well. After $\phi \sim 0.64$, our results suggest a tendency towards ordered structures; this could be a critical state. This critical state is also suggested by other simulations of hard spheres [45, 46, 47]. We note that there appears to be a temporary 'breaking' of order around $\phi \sim 0.69$ in some cases before crystallinity is reached. Overall, the results of evaluating the $Q_{6,global}$ order parameter reveals that there are significant changes in the packings at densities $0.62, 0.64$ and 0.69. This global order parameter, however, does not distinguish hcp from fcc. Our observations of local orders confirm the phenomenon of spontaneous crystallization to fcc or hcp or mixtures of the two, which will be discussed in the next sections. Other symmetries are not observed, at least within our simulation times.

3.6.2 Local Order Analysis

The onset of global ordering must have local precursors; we investigate the ordering of local clusters in the rest of this chapter. We divide the local order analysis into two

group. First, we present the results of local orders for spheres with all coordination numbers. Secondly, we give the local order analysis for fcc and hcp sphere-clusters.

3.6.2.1 Local Bond Orientation Order Parameter

Steinhardt *et al.* [44] defined the local bond orientation order parameters as,

$$Q_{l,local}(i) \equiv \left[\frac{4\pi}{2l+1} \sum_{m=-l}^{l} \left| \sum_{j=1}^{N_s(i)} Y_{lm}(\Theta_{ji}, \Phi_{ji})/N_s(i) \right|^2 \right]^{1/2}, \tag{3.6}$$

where Y_{lm} are spherical harmonics, with l and m integers. The angles Θ_{ji} and Φ_{ji} are polar angles with respect to an arbitrary coordinate system, characterizing the bond vector $\vec{r}_{ij}$ from sphere j to sphere i and $N_s(i)$ is the number of neighbors of sphere i. The sum and averages in Eq. (3.6) are computed over all neighbors $N_s(i)$ of a sphere i. The numerical values [44, 45, 48] of $Q_{6,local}$ and $Q_{4,local}$ for different structures are given in the Table 3.2.

TABLE 3.2: Numerical values of local bond orientational order parameters $Q_{6,local}$ and $Q_{4,local}$ for different crystal structures.

Symmetry	$Q_{6,local}$	$Q_{4,local}$
Simple cubic	0.354	0.764
Face-centered cubic	0.575	0.191
Hexagonal close packed	0.485	0.097
Body-centered cubic	0.511	0.036
Icosahedral	0.663	0.000

3.6.2.2 Local Orders of Sphere Packings

In this section, we present local order analysis of spheres packings. We have calculated $Q_{6,local}$ and $Q_{4,local}$ using Eq. (3.6), for all spheres with their corresponding nearest neighbors, i.e., for all $N_s(i)$. Figure 3.6 shows the scatter plots of local order parameters at densities $\phi = 0.62$, 0.64 and ϕ_{max}, for low ($A = 0.05$), intermediate ($A = 0.15$) and high ($A = 0.30$) shaking amplitudes. At low packing densities 0.62 and 0.64, the plots of local order parameters show large scatter [Figs. 3.6 (a), (b), (d), (e), (d) and (h)].

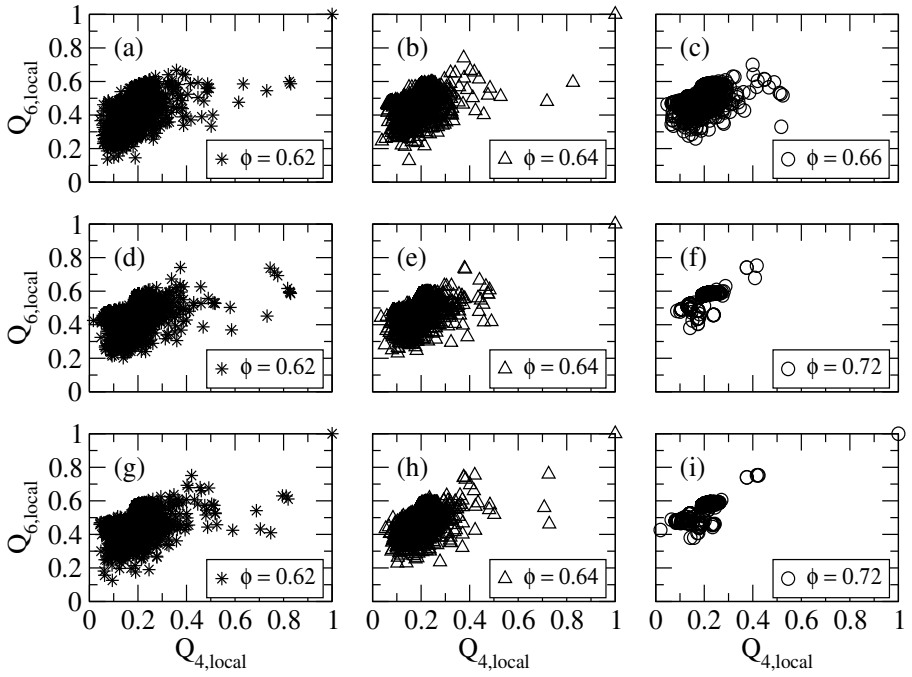

FIGURE 3.6: Plots of $Q_{6,local}$ vs. $Q_{4,local}$ for sphere packings of densities $\phi \sim 0.62$, 0.64 and ϕ_{max} for sample amplitudes $A = 0.05$ (low amplitude) [(a) to (c))], 0.15 (intermediate amplitude) [(d) to (f))] and 0.30 (high amplitude) [(g) to (i)].

On the other hand, at maximum density $\phi \sim 0.72$, Figs. 3.6(f) and 3.6 (i) depict tight clusters of $Q_{6,local}$ and $Q_{4,local}$ for intermediate and high amplitudes respectively. This indicates that spheres packings exhibit disorder at low packing densities of 0.62 and 0.64 and order at $\phi \sim 0.72$.

3.6.2.3 Detection of fcc and hcp Sphere-clusters

In a stable fcc and hcp lattice structures, a cluster of 12 spheres around a central sphere gives a maximum packing density of $\phi \sim 0.74$. We therefore considered an assembly of 13 spheres, which we will henceforth refer to as a sphere-cluster. This will be the basic unit of our investigations where we will use local measures to investigate the predominance of either form of crystalline structure.

The fcc and hcp structures differ in their stacking sequences. This difference of stacking is reflected in their values of the $Q_{4,local}$ and $Q_{6,local}$ through spherical harmonics. By choosing, $N_s(i) = 12$, we restrict ourselves to spheres which only have 12 neighbors, so that each data point gives a value of the local bond order parameter of a sphere-cluster as defined in Eq. (3.6). This is consistent with our main purpose, which is to check whether fcc or hcp symmetries predominate locally in sphere packings, as a function

of shaking amplitude. This choice is perfectly suitable for distinguishing hcp clusters from fcc clusters. However, this choice of local order parameters is not in general useful in distinguishing order from disorder of a system. It would lead to a strong bias, by leaving out the sphere-clusters which do not have exactly 12 neighbors. We note that the values of $Q_{6,local}$ and $Q_{4,local}$ for fcc and hcp sphere-clusters are $(0.575, 0.191)$ and $(0.485, 0.097)$ respectively [44, 45, 48].

We divide our local order analysis of fcc and hcp clusters into three temporal stages with respect to values of packing densities and shaking amplitudes. First, we discuss the disordered clusters corresponding to density ϕ from 0.61 to 0.65. Secondly, we emphasize the partially ordered clusters at $\phi \sim 0.68$ and 0.69. Finally, we discuss the clusters at highest density ϕ_{max} achieved. These results have been shown using scatter plots of $Q_{6,local}$ and $Q_{4,local}$ and non-parametric kernel density plots of $Q_{6,local}$.

3.6.2.3.1 Disordered Sphere-clusters at Low Densities

We have considered the nucleation of fcc and hcp sphere-clusters; other symmetries are not examined. Note that our simulation algorithm considers the parameterized amplitudes which introduces a free volume for rearrangements of spheres. As shaking progresses, spheres build coordination with their neighbors within available volume. Since such collective rearrangement is the catalyst which drives the nucleation of order in a packing, we would expect more rapid nucleation to occur for larger free volumes, i.e., the larger amplitudes in our set of nine. This nucleation process of spheres starts at the low densities for all amplitudes. We note that none of these is, of course, large enough to cause the assembly to be so fluidized that order never sets in.

Figure 3.7 shows the disordered states of sphere-clusters from $\phi \sim 0.61$ to $\phi \sim 0.63$ respectively. The scatter plots of $Q_{6,local}$ vs. $Q_{4,local}$ and probability density plots of $Q_{6,local}$ confirm that sphere packings in this range are largely disordered at a local level. Note that for $\phi \sim 0.62$ and 0.63, Fig. 3.8 displays the onset of double peaked distributions. Both peaks are, however, relatively broad, indicating that full crystallization has not occurred. This is consistent with our remark that $\phi \sim 0.62$ could possibly be thought of as the first hint of crystallization.

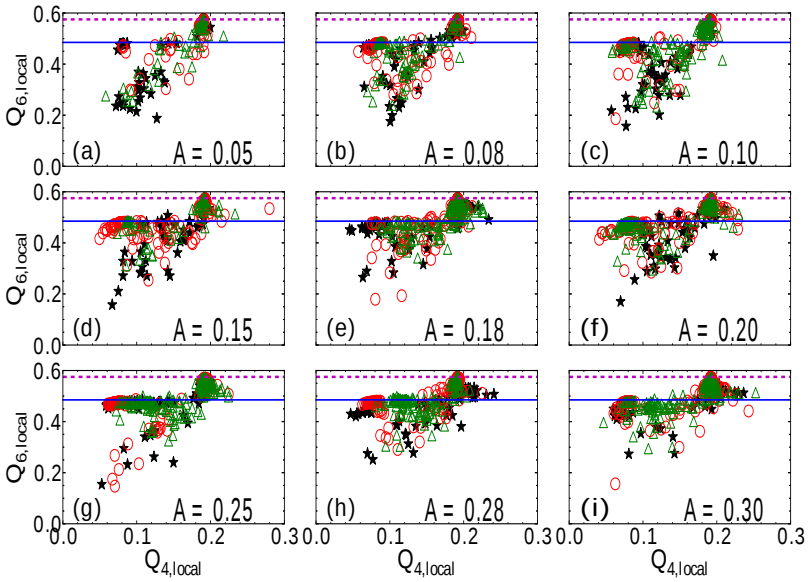

FIGURE 3.7: Plots of $Q_{6,local}$ vs. $Q_{4,local}$. The scattered values show disordered states of $\phi \sim 0.61$ (stars), $\phi \sim 0.62$ (open circles) and $\phi \sim 0.63$ (open triangles). The horizontal line markers at 0.485 (blue solid line for hcp) and 0.575 (magenta dashed line for fcc) serve as a guide for the eye.

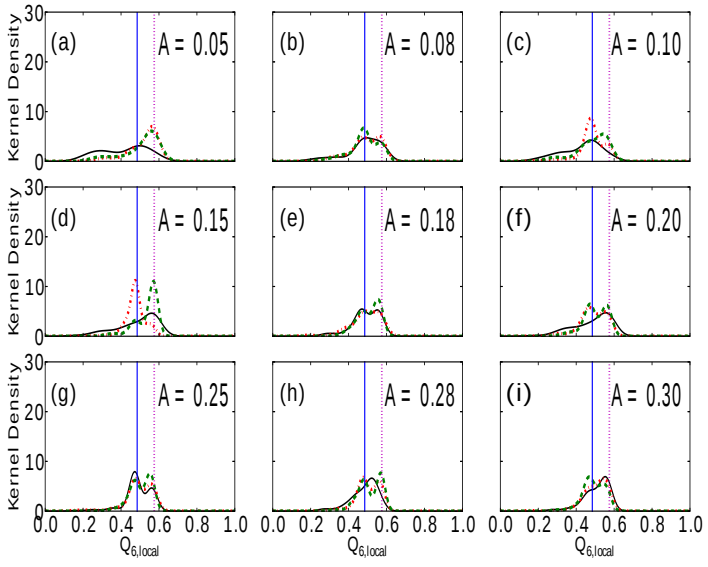

FIGURE 3.8: Probability density plots of a $Q_{6,local}$ for $\phi \sim 0.61$ (black solid line), 0.62 (red dash-dotted line) and 0.63 (green dashed line). The peaks are broad and robust. The vertical line markers at 0.485 (blue solid line for hcp) and 0.575 (magenta dashed line for fcc) serve as a guide for the eye.

Partially ordered sphere clusters begin to make their presence felt at $\phi \sim 0.64$ and 0.65 respectively. These are less disordered clusters than those at low densities [Fig. 3.9].

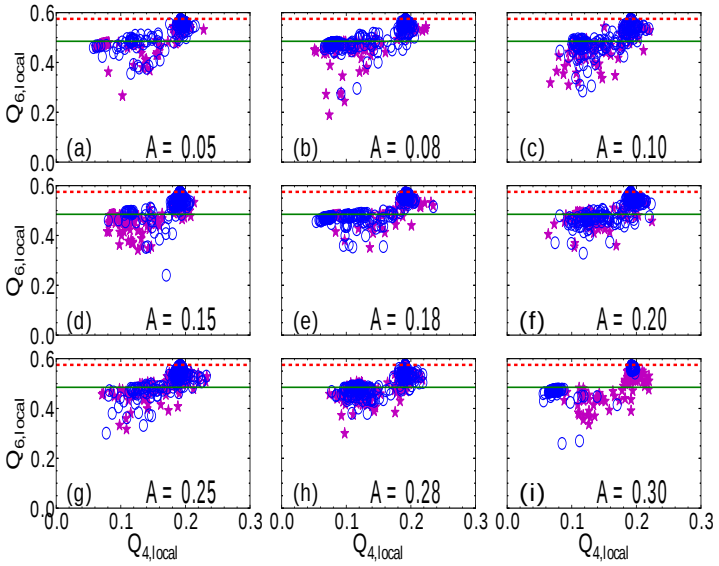

FIGURE 3.9: Plots of $Q_{6,local}$ vs. $Q_{4,local}$ for the densities $\phi \sim 0.64$ (stars) and 0.65 (open circles). Both the states are disordered. The $\phi \sim 0.65$ state has less scatter than 0.64. The horizontal line markers at 0.485 (green solid line for hcp) and 0.575 (red dashed line for fcc) serve as a guide for the eye.

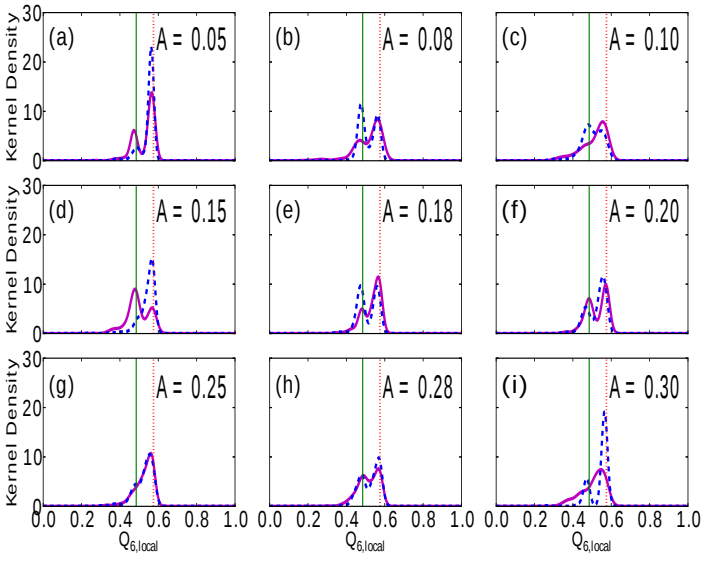

FIGURE 3.10: Probability density plots of a $Q_{6,local}$ for $\phi \sim 0.64$ (magenta solid line), 0.65 (blue dashed line). The distributions have sharper peaks than before with some predominance of the second peak. The vertical line markers at 0.485 (green solid line for hcp) and 0.575 (red dashed line for fcc) serve as a guide for the eye.

The number of nucleating sites increases more than that at lower densities, indicating that ordering has been facilitated by access to greater free volume. The peaks of probability density for fcc and hcp ordering [Fig. 3.10] are sharper than at lower densities, indicating a greater proportion of ordered sphere-clusters. In fact, we note that the second peak of $Q_{6,local}$ densities is more consistently observed than the first peak [See Fig. 3.10].

3.6.2.3.2 Partially Ordered Clusters : Competition between fcc and hcp

Our discussions so far have only called attention to disordered clusters. We now characterize the states of packing densities of $\phi \sim 0.68$ and 0.69 [Fig. 3.11]. The number of sphere-clusters as well as the degree of ordering of spheres within clusters increases. In this intra-cluster dynamics, shaking force is used in rearrangement of the spheres. Consequently, the important issue is the competition between hcp and fcc ordering (rather than the competition between order and disorder). We notice accordingly that there is now a tendency for the sphere clusters around the fcc and hcp values, a process which is much sharper for the higher of the two densities. The local order parameters are broadly divided into two groups at $\phi \sim 0.68$ [Fig. 3.11] for all shaking amplitudes.

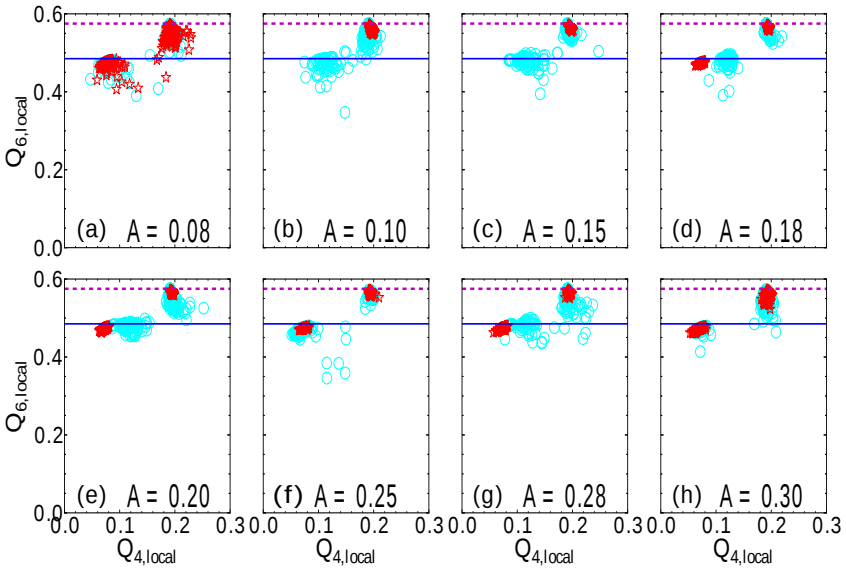

FIGURE 3.11: Plots of $Q_{6,local}$ vs. $Q_{4,local}$ for densities $\phi \sim 0.68$ (open circles) and 0.69 (stars). The state of $\phi \sim 0.68$ has more scatter than 0.69. Notice the sharp division into two distinct groups for $\phi \sim 0.69$. The special noticeable situations are for $A = 0.10$ ((b)) and 0.15 ((c)). The horizontal line markers at 0.485 (blue solid line for hcp) and 0.575 (magenta dashed line for fcc) serve as a guide for the eye.

The packing density $\phi \sim 0.69$ is the maximum density achieved for $A = 0.08$. The most interesting case is that of density of the $\phi \sim 0.69$ for $A = 0.10$ and 0.15, showing a single cluster. In contrast, two partially ordered clusters emerge for $A = 0.18, 0.20, 0.25$ and 0.30 [Fig. 3.11]. We speculate that the dearth of free volume at $A = 0.10$ and 0.15 could have led to the interruption of evolution into hcp ordering since this seems to set in for higher amplitudes.

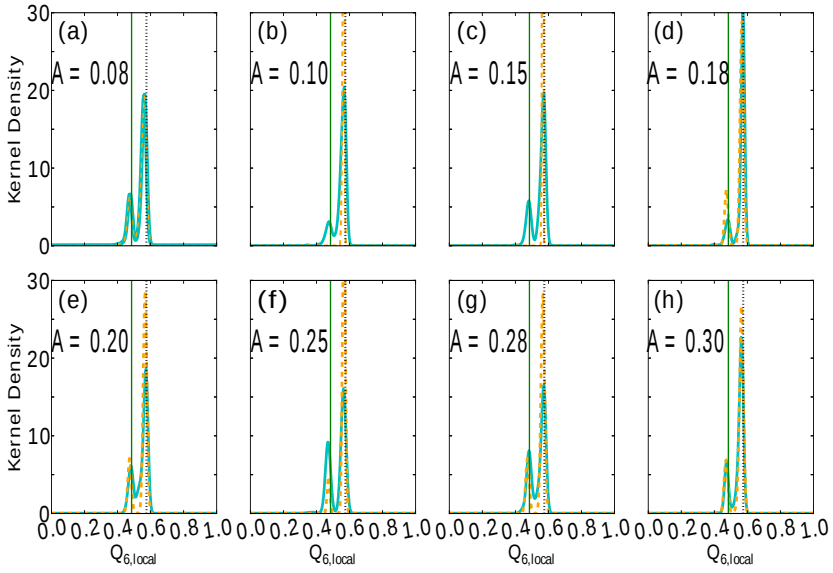

FIGURE 3.12: Probability density plots of $Q_{6,local}$ for $\phi \sim 0.68$ (cyan solid line), 0.69 (orange dashed line). The peaks of $\phi \sim 0.69$ are sharper than those of 0.68. For $\phi \sim 0.69$ at $A = 0.10$ and 0.15 only one sharp peak at $Q_{6,local} \sim 0.575$ is visible ((b) and (c)). The vertical line markers at 0.485 (green for hcp) and 0.575 (black for fcc) serve as a guide for the eye.

The kernel density plots [Fig. 3.12] support our claim as well. The distributions of $Q_{6,local}$ for $\phi \sim 0.69$ are sharper than those for 0.68. Note that, a breakdown of global ordering was observed at $\phi \sim 0.69$. Our local ordering analysis suggests that interfaces between crystallites of fcc and hcp might be responsible for this.

3.6.2.3.3 Sphere-clusters at Maximum Densities

This section focuses on the features of sphere-clusters at maximum densities ϕ_{max} achieved for each of the shaking amplitudes considered. We divide these features into three categories. First, we give the partial or incomplete evolution of clusters for low amplitudes. Secondly, we address the emergence of single fcc clusters for intermediate

amplitudes. Finally, we present the coexistence phase of fcc and hcp clusters for high amplitudes.

(A) Incomplete Sphere-clusters:

We begin with our analysis of ordering corresponding to maximal densities attained at low amplitudes $A = 0.05, 0.08$ and 0.10. For these amplitudes, the sphere-clusters are not able to achieve full crystallization, at least in our simulation times.

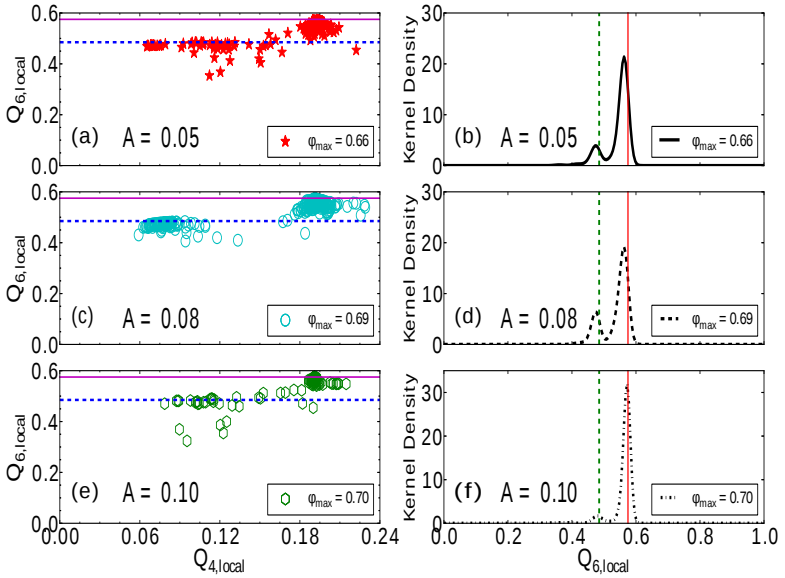

FIGURE 3.13: Plots of the maximum densities for $A = 0.05$, 0.08, and 0.10. Scatter plots of $Q_{6,local}$ vs. $Q_{4,local}$ are distributed into two groups. The probability density plots ((b), (d) and (f)) indicate a second peak which is sharper than the first. The horizontal and vertical lines at 0.485 (for hcp) and 0.575 (for fcc) serve as a guide for the eye.

Figure 3.13 shows the scattered plots of $Q_{6,local}$ vs. $Q_{4,local}$ and the probability density plots of $Q_{6,local}$. For each case, local order values indicate the enhancement of fcc ordering than hcp [Figs. 3.13(a), 3.13(c), and 3.13(e)]. Also, the sharpness of second peak of the probability density of $Q_{6,local}$ gives a clear indication of dominance of fcc [Figs. 3.13(b), 3.13(d), and 3.13(f)]. We cannot rule out a further evolution for longer shaking times, and in fact we would expect more complete ordering to emerge in that limit for the lowest shaking amplitudes.

(B) Single fcc Clusters :

For intermediate amplitudes ($A = 0.15, 0.18, 0.20$ and 0.25), a single fcc phase appears at asymptotic density $\phi_{max} \sim 0.72$ [Fig. 3.14]. This seems very robust, lending support to our arguments that an optimal range of amplitudes exist for spontaneous crystallization into single fcc state. The values of $Q_{6,local}$ and $Q_{4,local}$ fall into the intervals $(0.571, 0.575)$ and $(0.1905, 01925)$ respectively.

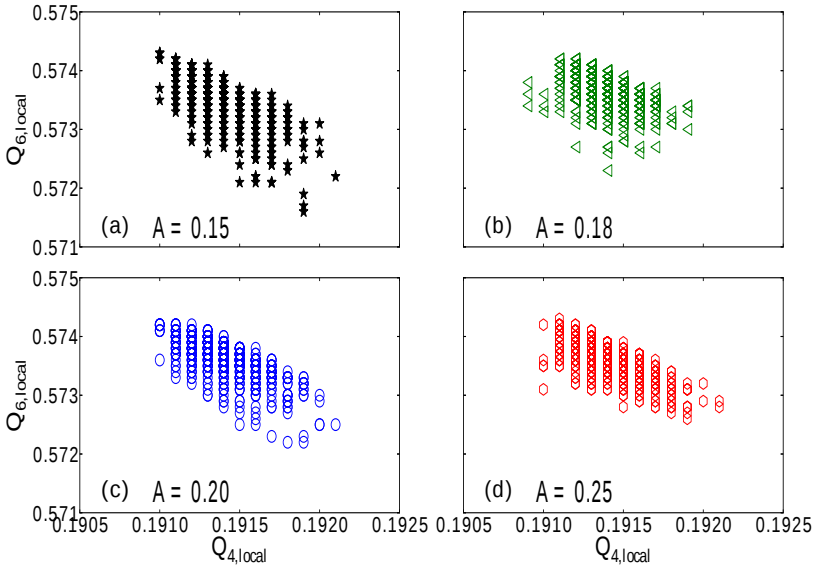

FIGURE 3.14: The scatter plots of $Q_{6,local}$ vs. $Q_{4,local}$ show a single fcc cluster for a maximum density of $\phi \sim 0.72$ for $A = 0.15$ 0.18, 0.20, and 0.25.

(C) Coexistence of fcc and hcp Clusters :

For higher amplitudes $A = 0.28$ and 0.30, we see a clear separation of two kinds of ordering at $\phi_{max} \sim 0.72$. Figure 3.15 shows the coexistence of fcc and hcp, centered on the lines corresponding to respective values both structures. This coexistence reinforces the conclusions of previous simulations [49, 50, 51]. However, fcc ordering is still predominates: the relative fraction of fcc sphere clusters, given by $N_{fcc}/(N_{fcc} + N_{hcp})$, is 0.78 for $A = 0.28$ and 0.77 for 0.30, where N_{fcc} and N_{hcp} are numbers of sphere-clusters for fcc and hcp structures, respectively.

We emphasize of course that these results are valid for the time of shaking we have considered, and so we cannot rule out further crossovers for longer periods. Although experimental studies have investigated the coexistence of these two cluster types in

colloids [37, 38, 39, 40] and granular materials as a function of shear rate [34], we believe that this is the first attempt to analyze crystalline clusters systematically by varying shaking amplitudes.

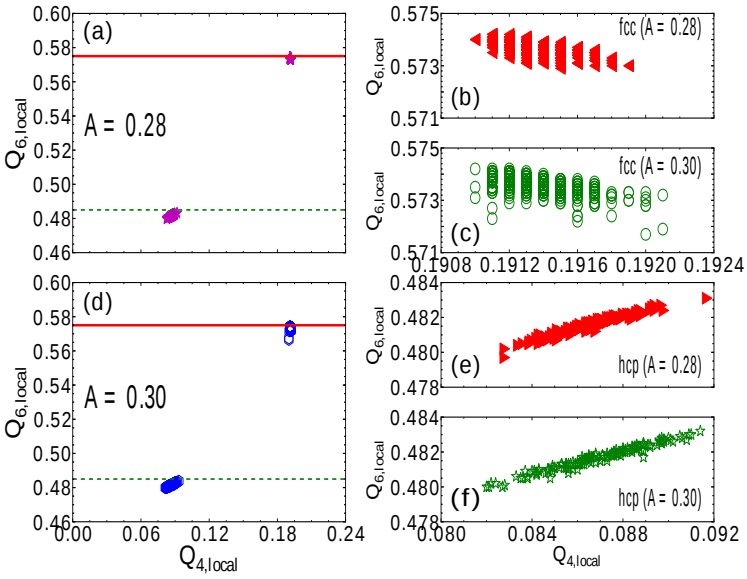

FIGURE 3.15: Graphs of $Q_{6,local}$ vs. $Q_{4,local}$ show the coexistence of two fcc and hcp sphere-clusters. The data of fcc and hcp cluster is again plotted in (c), (d) and (e), (f) for the respective amplitudes. The horizontal line markers at 0.485 (green for hcp) and 0.575 (red for fcc) in (a) and (b) serve as a guide for the eye.

3.7 Conclusions

We have carried out computer simulation of shaken granular packings over a range of amplitudes. Shaking plays a vital role in the development of crystalline orders. We have observed that spontaneous crystallization occurs in our chosen dynamical regime in the limit of long shaking times. Sphere packings shaken at low amplitudes need more time to manifest full crystallisation than those shaken at high amplitudes. The global order measurements of radial distribution function and bond orientation order parameter $Q_{6,global}$ confirm the spatial orders. Our observations of global bond orientational order parameter suggests that the density $\phi \sim 0.64$ is a critical density. Also, an apparent breakdown of global order is seen at $\phi \sim 0.69$ which our local order parameters suggest may be due to interfaces between crystallites of fcc and hcp. Our local order analysis confirms that spheres clusters are disordered at low packing densities for all shaking amplitudes. Also, we noted that at maximum packing densities, there may be an optimal

range of amplitudes where crystallization into a single fcc state occurs. Amplitudes even higher than this lead to a coexistence of hcp and fcc order, with the latter dominating.

Bibliography

[1] J. Conway and N. J. A. Sloane, *Sphere Packings, Lattices and Groups* (Springer), 1999.

[2] H. M. Jaeger and S. R. Nagel, *Science*, **255**, 1523(1992).

[3] A. Mehta, *Granular Physics* (Cambridge University Press, Cambridge), 2007.

[4] D. E. G. Williams, *Phys. Rev. E* **57**, 7344(1998).

[5] T. Unger, J. kertesz, and D. E. Wolf *Phys. Rev. Lett.*, **94**, 178001(2005).

[6] J. D. Bernal, *Nature* **183**, 141(1959).

[7] S. Alexander, *Phys. Rep.* **296**, 65(1998).

[8] A. V. Tkachenko and T. A. Witten, *Phys. Rev. E* **60**, 687(1999).

[9] A. Donev *et al.*, *Science* **303**, 990(2004).

[10] P. Richard *et al.*, *Nature Materials* **4**, 121(2005).

[11] D. Weaire and T. Aste, *The Pursuit of Perfect Packing* (Taylor and Francis), 2000.

[12] J. Blouwolff and S. Fraden, *Europhys. Lett.* **76(6)**, 1095(2006).

[13] H. M. Jaeger, S. R. Nagel, and R. P. Behringer, *Rev. Mod. Phys.* **68**, 1259(1996).

[14] Y. Jiao, F. H. Stillinger and S. Torquato, *Phys. Rev. E* **81**, 041304(2010).

[15] P. Meakin and R. Jullien, *J. de Physique* **48**, 1651(1987)

[16] G. T. Nolan and P. E. Kawavanagh, *Powder Techn.* **72**, 149(1992).

[17] A. Mehta and G. C. Barker, *Phys. Rev. Lett.* **67**, 394(1991).

[18] G. C. Barker and A. Mehta, *Phys. Rev. A.* **45**, 3435(1992).

[19] S. F. Edwards and D. V. Grinev, *Phys. Rev. Lett.* **82**, 5397(1999).

[20] C. S. O'Hern *et al.*, *Phys. Rev. E* **68**, 011306(2003).

[21] A. Donev, S. Torquato, and F. H. Stillinger, *Phys. Rev. E* **71**, 011105(2005).

[22] R. Blumenfeld, S. F. Edwards and R. C. Ball, *J. Phys.:Condens. Matter* **17**, S2481(2005).

[23] R. C. Ball, in *Structures and Dynamics of Materials in the Mesoscopic Domain, M. Lal et al (Editors)* (Imperial College Press), 1999.

[24] G. Y. Onoda, and E. G. Liniger, *Phys. Rev. Lett.* **64**, 2727(1990).

[25] G. Scott and D. M. Kilgour, *J. Phys. D* **2**, 863(1969).

[26] G. Mason, *Nature*, **217**, 733(1968).

[27] J. L. Finney, *Proc. R. Soc. London Ser. A*, **319**, 479(1970).

[28] W. S. Jodrey and E. M. Tory, *Phys. Rev. A* **32**, 2347(1985).

[29] A. S. Clarke and H. Jonsson, *Phys. Rev. E* **47**, 3975(1993).

[30] J. B. Knight *et al.*, *Phys. Rev. E* **51(5)**, 3957(1995).

[31] E. R. Nowak, *et al.*, *Powder Techn.* **94**, 79(1997).

[32] E. R. Nowak, *et al.*, *Phys. Rev. E* **57(2)**, 1971(1998).

[33] P. Phillippe and D. Bideau, *Europhys. Lett.* **60(5)**, 677(2002)

[34] A. Panaitescu, K. A. Reddy, and A. Kudrolli, *Phys. Rev. Lett.* **108**, 108001(2012).

[35] O. Pouliquen, M. Nicolas and P. D. Weidman, *Phys. Rev. Lett.* **79**, 3640(1997).

[36] J. -C. Tsai, G. A. Voth, and J. P. Gollub, *Phys. Rev. Lett.* **91**, 064301(2003).

[37] U. Gasser, E. R. Weeks, A. Schofield, P. N. Pusey, and D. A. Weitz, *Science* **292**, 258(2001).

[38] A. van Blaaderen, R. Ruel and P. Wiltzlus, *Nature* **409**, 1020(2001).

[39] A. van Blaaderen, P. Wiltzius, *Science* **270**, 1177(1995).

[40] S. Auer and D. Frenkel, *Nature* **385**, 321(1997).

[41] G. C. Barker and M. J. Grimson, *J. Phys.: Condens. Matter***1**, 2779(1989).

[42] A. Mehta and G. C. Barker, *J. Phys. : Condens. Matter* **12**, 6619(2000).

[43] M. P. Allen and D. J. Tildeley, *Computer simulation of liquids* (Oxford University Press), 1989.

[44] P. J. Steinhardt, D. R. Nelson, and M. Ronchetti, *Phys. Rev. B* **28**, 784(1983).

[45] M. D. Rintoul, and S. Torquato, *J. Chem. Phys.* **105**, 9258(1996).

[46] M. D. Rintoul and S. Torquato, *Phys. Rev. Lett.* **77**, 4198(1996).

[47] Y. Song, R. M. Stratt, and E. A. Mason, *J. Chem. Phys.* **88**, 1126(1988).

[48] W. Mickel, *et al.*, *J. Chem. Phys.* **138**,044501(2013).

[49] V. Luchnikov *et al.*, *J. Mol. Liq.* **96–97**, 185(2002).

[50] K. J. Dong *et al.*, *Europhys. Lett.* **86**, 46003(2009).

[51] Y. Jin and H. A. Makse, *Physica (Amsterdam)* **389A**, 5362(2010).

Chapter 4

Structural Insights to Granular Packings

4.1 Geometrical Method

Mathematical methods, based on partitioning the given space, identify the geometrical structures of atoms and molecules [1]. The term 'partitioning' relates to allocation of all points or objects in the given space with their closest neighbors. The resulting geometrical regions or partitions are called Voronoi cells. Moreover, dual partitions for Voronoi cells correspond to Delaunay diagrams [2, 3]. In this chapter, we have shown Delaunay tessellations of sphere packings.

4.1.1 Basics of Voronoi-Delaunay Tessellation

A Voronoi diagram can be constructed by assigning a closest point to every other point in the hyperplane [2]. For instance, consider a set of n points, $c_1, c_2..., c_n$ in two-dimensional Euclidean plane. For each point c_i with coordinates (x_i, y_i) in the set, we can draw a boundary enclosing all the intermediate points lying closer to c_i than to other points in the set. Let us illustrate this in simple mathematical terms. The Euclidean distance between the two points is calculated as: $ds(c_1, c_i) = \sqrt{(x_1 - x_{i1})^2 + (y_1 - y_{i1})^2}$. If c_i is the point nearest to c_1 than other point c_j then the region defined by the expression,

$$\begin{aligned} V_v(c_i) &= \{x | \|x - x_i\| \leq \|x - x_j\|, i \neq j\}, \\ &= \{x | \|ds(c_1, c_i\| \leq \|ds(c_1, c_j\|, i \neq j\}, \end{aligned} \tag{4.1}$$

is a Voronoi polygon associated with c_i [2].

Figure 4.1 depicts the Voronoi-Delaunay triangulation of points of uniform random distribution. The set of all Voronoi polygons for a given point set is called Voronoi diagram. First, Voronoi polygons (black lines) are generated and accordingly, the convex hull, i. e. the intersection of all convex sets constructs the Delaunay triangles (red lines) [Fig. 4.1]. An edge, the side of a Voronoi polygon, is shared by two polygons. Now, if we join generator points (blue stars) of all Voronoi polygons by line segments then the resulting digram correspond to Delaunay triangulation [2]. Triangulation in three-dimensional space is called 'Tetrahedralization' [2]. The shapes of Delaunay and Voronoi diagrams reveal the geometrical arrangement of points in a set [4].

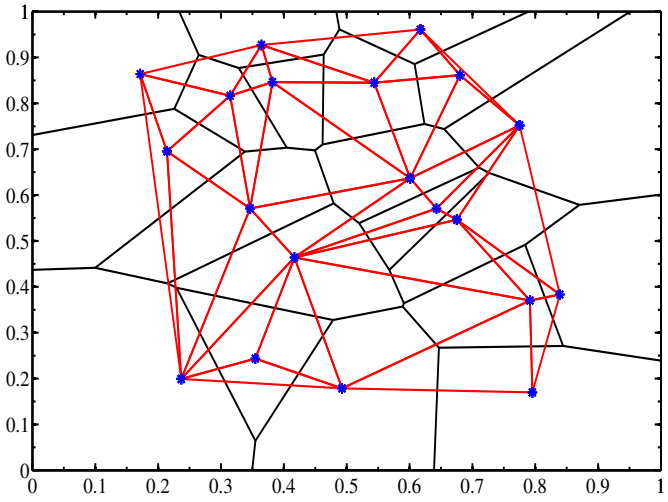

FIGURE 4.1: Two dimensional Voronoi-Delaunay Tessellation for points (blue stars) of uniform random distribution. The solid black lines are edges of Voronoi polygons. Delaunay triangles (solid red lines) have empty interiors.

In Fig. 4.1, the Delaunay triangles (red lines) have empty interior. The construction of triangles follows the Delaunay empty circle property [2, 5]. The basic unit of the tessellations is a 'simplex' in a given dimension; for example, a triangle in 2D and a tetrahedron in 3D [2, 5]. A tetrahedron is the basic unit of Delaunay tessellations that

are used for geometrical analysis of sphere packings [6]. The computer algorithms of tessellations construct tetrahedra from the coordinates of spheres [6]. The parameters of regular or quasiregular tetrahedron such as volume, length, and dihedral angles give geometrical insights of sphere packings [5, 6, 7]. In particular, clusters of regular or quasiregular tetrahedra represent crystalline structures of spheres [6, 8]. Also, the shapes of both Delaunay tetrahedron and its neighbors are used to identify the fcc and hcp structures [9].

4.1.2 Statistical Mechanics of Granular Packings

Edwards *et al.*, [10, 11] have developed a statistical mechanical framework for the dynamics of granular material. They assumed that the mechanically stable states of the system are equally probable and the averages can be taken over jammed states [10, 11]. The central quantity of this approach is the "compactivity". The compactivity [10, 11] is defined as, $\chi = \partial V/\partial S$ analogous to the thermodynamic temperature $T = \partial E/\partial S$. In this approach, the volume V and compactivity χ play the roles of energy E and the temperature T respectively. Other analogous quantities are explained in [12].

Aste *et al.*, [13, 14, 15] have used the Edwards statistical mechanical approach to describe equilibrium properties of granular packings. They have defined the configurational entropy,

$$S = -\sum_{V} P(V) \ln P(V) + \sum_{V} P(V) S(V), \tag{4.2}$$

where $P(V)$ and $S(V)$ are probability and entropy of state with volume V, respectively. It is assumed that the packings can be partitioned into k elementary Voronoi or Delaunay cells [13]. Therefore the cells with arbitrary volumes v, but greater than v_{min}, occupy total volume V in the phase space [13, 14, 15]. In this case, the volume of accessible phase space,

$$\Omega(V) = \frac{(V - k v_{min})^{k-1}}{\Lambda^{3k}(k-1)!}, \tag{4.3}$$

where Λ is a constant analogous to the Debye length. The probability distribution $P(V)$ [14, 15] of volume V is given as,

$$P(V) = \frac{k^k}{\Gamma(k)} \frac{(V - V_{min})^{k-1}}{(\overline{V} - V_{min})^k} \exp\left(\frac{-k(V - V_{min})}{\overline{V} - V_{min}}\right), \tag{4.4}$$

where $V_{min} = kv_{min}$. Equation 4.4 is a Gamma distribution in the variable $V - V_{min}$ with a 'shape parameter' k and a 'scale parameter' ($\frac{\overline{V}-V_{min}}{k}$). The variance of Gamma distribution of $P(V)$ is given as:

$$\sigma_v^2 = \frac{(\overline{V} - V_{min})^2}{k}, \tag{4.5}$$

where $\overline{V}$ is the average volume. Moreover, a granular temperature [14, 15] can be defined, following the analogy with the thermodynamic temperature $\beta = (1/k_B T) = \partial(entropy)/\partial(energy)$ as,

$$\beta_{gr} = \chi^{-1} = \partial(S)/\partial(\overline{V}). \tag{4.6}$$

Using Eq. 4.2 and Eq. 4.3,

$$\beta_{gr}^{-1} = \chi = \frac{\overline{V} - V_{min}}{k}. \tag{4.7}$$

Further, using Eq. 4.5 and Eq. 4.7, χ becomes,

$$\chi = \frac{\sigma_v^2}{\overline{V} - V_{min}}. \tag{4.8}$$

Equation 4.7 reveals that the compactivity χ is the average free volume per elementary cell [13, 14]. After substituting Eq. 4.4 into Eq. 4.2, the configurational entropy [14, 15] can be obtained as,

$$S = k\left[1 + \ln\left(\frac{\overline{V} - V_{min}}{k\Lambda^3}\right)\right], \tag{4.9}$$

where $\overline{V}$ is the average volume and $V_{min} = mv_{min}$ is the minimum attainable volume. The quantity v_{min} is the minimum volume of Voronoi cell and k is shape parameter of Gamma distribution. Aste *et al.*, [13, 14] have shown that the volumes of Voronoi or Delaunay simplices follow Gamma distribution. Also, the configurational entropy and the volume fluctuations are calculated for granular sphere packings [3].

4.2 Delaunay Tessellations of Sphere Packings.

We perform the Delaunay tessellations on the simulated data of sphere packings. Our algorithm is written in MATLAB which constructs the Delaunay partitions using the Cartesian coordinates (x, y, z) of spheres. This algorithm successfully generates the Delaunay tetrahedra (simplices) for all simulated packing densities. Typically, more than six thousand tetrahedra are generated for 1273 spheres.

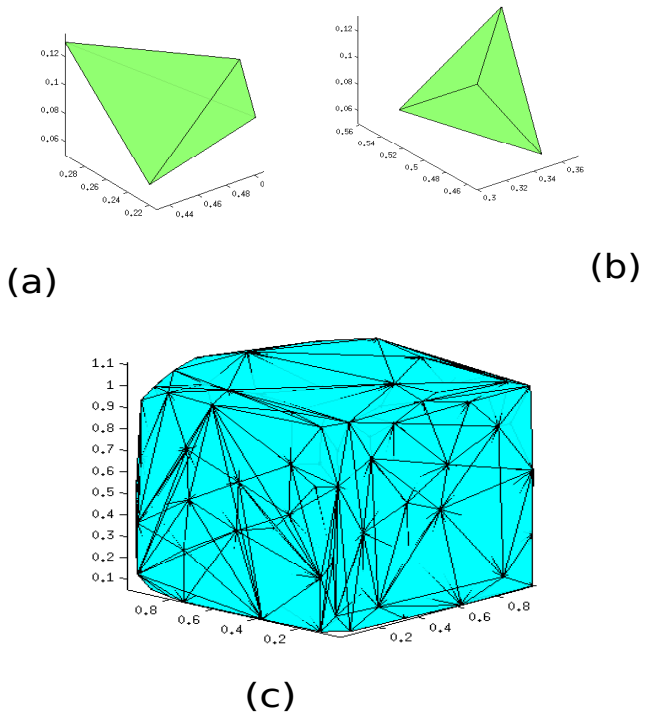

FIGURE 4.2: A typical irregular ((a)), and regular ((b)) tetrahedra and Delaunay tessellations ((c)) of spheres at packing density $\phi \sim 0.64$. The vertices of tetrahedra represent the centers of spheres.

The MATLAB program also supplies the sets of vertices and edges of Delaunay tetrahedra. These sets are further used for the computation of the volumes, dihedral angles and length of edges of tetrahedra. Figure 4.2 depicts the irregular, regular and Delaunay tessellations of spheres packing of density 0.64. Note that, the vertices of tetrahedra represent the centers of spheres. Therefore, the shapes of tetrahedra determine the arrangement of spheres. Consequently, the clusters of regular or quasiregular tetrahedra typify stable and closed sphere packings. We follow the goodness criteria of tetrahedron and choose good tetrahedra with dihedral angles lies between 14° to 154° [16, 17].

We divide the analysis into three categories. First, we present the statistics of volumes of tetrahedra. Secondly, we give the analysis of volume fluctuations and entropy. Finally, we provide detailed account of dihedral angles and length measure's of tetrahedra.

4.2.1 Statistics of Volumes of Tetrahedra

The volume of each tetrahedron is calculated using formula [18],

$$V = \frac{\Big|(\mathbf{a}-\mathbf{d}).((\mathbf{b}-\mathbf{d})\times(\mathbf{c}-\mathbf{d}))\Big|}{6}, \tag{4.10}$$

where, $\mathbf{a}, \mathbf{b}, \mathbf{c}$ and $\mathbf{d}$ are vectors representing the coordinates of the tetrahedral vertices.

4.2.1.1 Distribution of Volumes of Delaunay Tetrahedra

We first calculate the values of V_{min} and $\overline{V}$, and then use the scaling form, $\frac{V-V_{min}}{\overline{V}-V_{min}}$ [13, 14, 19]. Figure 4.3 shows the Gamma distributions of volumes of the tetrahedra for three representative shaking amplitudes: low ($A = 0.05$), intermediate ($A = 0.18$) and high ($A = 0.30$). For all cases, the distributions become narrower as density increases from 0.58 to 0.64 [Fig. 4.3 (i) to Fig. 4.3 (iii)]. After $\phi \sim 0.64$, the peak of distribution shift to a value 1 [Figs. 4.3 (iv) to 4.3 (vi)]. Interestingly, Gamma PDF manifests a sharp peak at $\phi \sim 0.68$ for high amplitude $A = 0.30$. Note that our global bond order analysis shows a breakdown at density $\phi \sim 0.69$.

TABLE 4.1: The values of the shape k, and scale b parameters of Gamma distribution of a variable $\frac{V-V_{min}}{\overline{V}-V_{min}}$ for three shaking amplitudes. The $\phi \sim 0.66$ is the maximum density achieved for $A = 0.05$.

ϕ	$A = 0.05$		$A = 0.18$		$A = 0.30$	
	k	b	k	b	k	b
0.58	13.9 ± 0.2	0.071 ± 0.001	13.9 ± 0.2	0.071 ± 0.001	13.9 ± 0.2	0.071 ± 0.001
0.61	12.2 ± 0.2	0.081 ± 0.001	12.6 ± 0.2	0.078 ± 0.001	11.1 ± 0.1	0.090 ± 0.002
0.62	13.2 ± 0.2	0.075 ± 0.001	14.7 ± 0.2	0.068 ± 0.001	22.3 ± 0.4	0.044 ± 0.001
0.63	32.0 ± 0.6	0.031 ± 0.001	26.6 ± 0.5	0.038 ± 0.001	26.9 ± 0.5	0.038 ± 0.001
0.64	15.7 ± 0.3	0.063 ± 0.001	26.8 ± 0.5	0.037 ± 0.001	18.1 ± 0.3	0.055 ± 0.001
0.65	22.4 ± 0.4	0.044 ± 0.001	25.5 ± 0.4	0.044 ± 0.001	16.6 ± 0.2	0.060 ± 0.001
0.66	26.8 ± 0.5	0.037 ± 0.001	20.5 ± 0.3	0.048 ± 0.001	24.4 ± 0.4	0.041 ± 0.001
0.67			29.1 ± 0.5	0.034 ± 0.001	25.7 ± 0.4	0.039 ± 0.001
0.68			21.6 ± 0.4	0.046 ± 0.001	130.6 ± 2.3	0.007 ± 0.0001
0.69			27.4 ± 0.5	0.036 ± 0.001	25.8 ± 0.4	0.037 ± 0.001
0.72			20.4 ± 0.3	0.046 ± 0.001	11.8 ± 0.2	0.081 ± 0.001

Table 4.1 displays the values of shape (k) and scale (b) parameters of Gamma distributions. We note a drastic change in the shape parameter k at densities 0.63 and 0.64 for low and high amplitudes (see Table 4.1). On the contrary, in the interval of

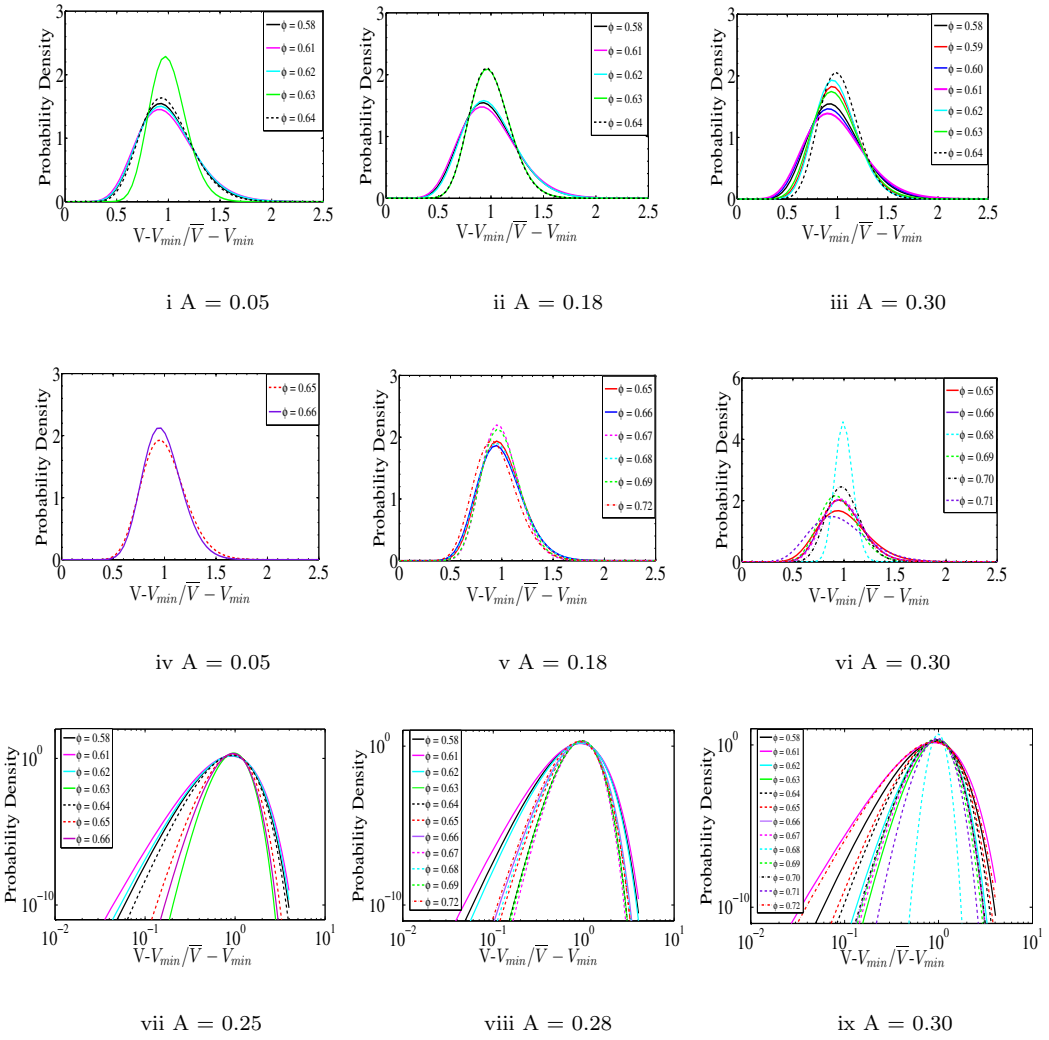

FIGURE 4.3: Gamma distributions of volumes for low ($A = 0.05$), intermediate ($A = 0.18$) and high ($A = 0.30$) amplitudes. (i) to (vi): Gamma PDF's at disordered and maximum packing densities. The peak of the distributions become narrow as density increases. (vii) to (ix): log-log plots of Gamma PDF's for three shaking amplitudes. The values of shape parameter k, scale parameter b, mean and variance are shown in Table 4.1 and Table 4.2.

$0.58 < \phi < 0.64$, k increases with density for intermediate amplitude $A = 0.18$. Surprisingly, k becomes very large at $\phi \sim 0.68$ for high amplitude $A = 0.30$. Other parameters, the mean 'kb' and the variance 'kb^2' of Gamma distributions are shown in Table 4.2. These values also suddenly alter at $\phi \sim 0.63$ for low and higher amplitudes. In addition, we observe another change in the variance at $\phi \sim 0.68$ for $A = 0.30$. Taken together, the parameters of Gamma distributions exhibit drastic changes at densities 0.63, 0.64, and 0.68. Furthermore, we have shown the log-log representations of Gamma PDF's [Figs. 4.3 (vii) to 4.3 (ix)]. This may suggests the hyperbolic type distributions [20], which deserves further investigation.

TABLE 4.2: The values of the mean and variance of Gamma distribution of a variable $\frac{V-V_{min}}{\overline{V}-V_{min}}$ for three shaking amplitudes. The $\phi \sim 0.66$ is the maximum density achieved for $A = 0.05$.

ϕ	$A = 0.05$		$A = 0.18$		$A = 0.30$	
	mean	variance	mean	variance	mean	variance
0.58	0.9922	0.0707	0.9922	0.0707	0.9922	0.0707
0.61	0.9940	0.0807	0.9910	0.0777	0.9928	0.0891
0.62	0.9970	0.0750	0.9980	0.0675	0.9946	0.0443
0.63	1.0000	0.0312	0.9994	0.0375	1.0222	0.0388
0.64	0.9931	0.0628	0.9967	0.0370	0.9939	0.0548
0.65	0.9966	0.0443	0.9961	0.0441	0.9988	0.0599
0.66	0.9844	0.0362	0.9898	0.0477	0.9911	0.0403
0.67			0.9922	0.0338	0.9983	0.0387
0.68			0.9920	0.0456	1.0003	0.0077
0.69			0.9972	0.0363	0.9535	0.0353
0.72			0.9472	0.0439	0.9578	0.0780

4.2.1.2 Volume Fluctuations

We compute the variance, $\sigma^2 = \overline{V^2} - \overline{V}^2$ of volumes of Delaunay tetrahedra using a nonscaled variable V.

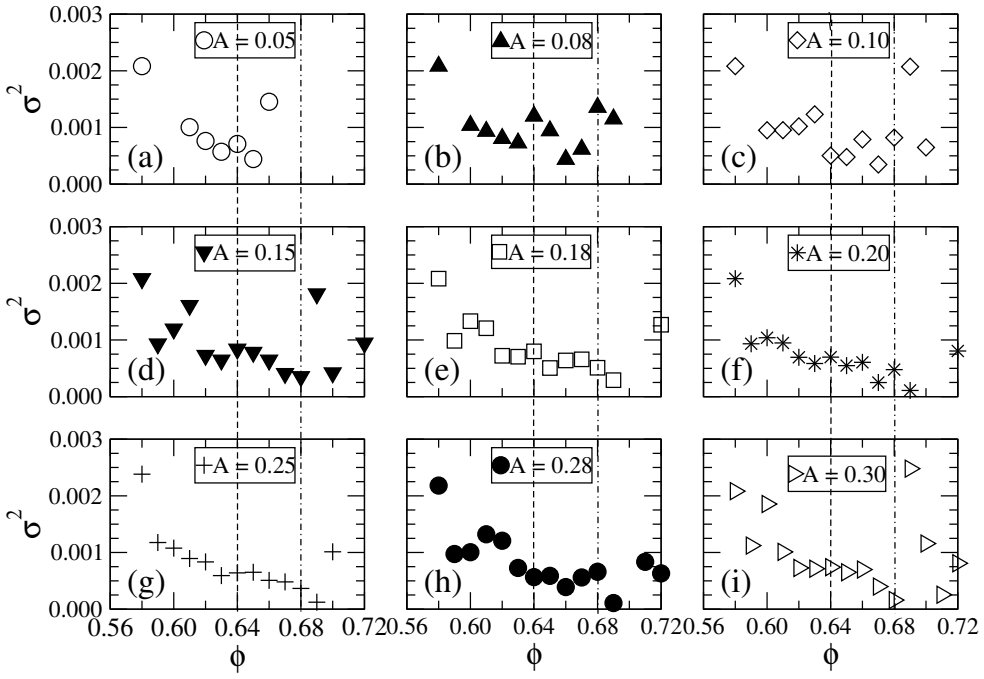

FIGURE 4.4: Plots of σ^2 vs. ϕ for low ((a) to (c)), intermediate ((d) to (g)) and high ((h) to (i)) shaking amplitudes. The variance σ^2 decreases in the region of density between 0.58 and 0.64. The vertical lines at 0.64 (dotted line) and 0.68 (dot dashed line) serve as a guide for the eye.

Figure 4.4 shows the variation of σ^2 against packing density for all shaking amplitudes. In all cases, the variance σ^2 decreases in the interval of density $0.58 < \phi < 0.64$. Further, it either increases or decreases in the range between 0.65 and 0.68 for all shaking amplitudes. Specifically, this change occurs at density $\phi \sim 0.66$. In addition, at density $\phi \sim 0.69$, the variance show sudden change for intermediate [Figs. 4.4 (d) to 4.4 (g)] and high shaking amplitudes [Figs. 4.4 (h) and 4.4 (i)]. We observe that the variance changes at packing densities 0.64 and 0.68. Note that our global and local order analysis identify the criticality and breakdown of orders at 0.64 and 0.68 respectively. Therefore, the correlation between the shaking process and the developments of orders of spheres may explain the drastic changes in the variance. Our results agree with the findings of other studies of jammed [21] and crystallized [22] granular packings.

4.2.1.3 Configurational Entropy of Volumes

We first substitute $1/\Lambda^3 = 50$ in Eq. 4.9 and then calculate the configurational entropy [13, 14]. The average volume $\overline{V}$ and the minimum attainable volume V_{min} are calculated for all cases. The value of shape parameter k is obtained from Gamma distribution.

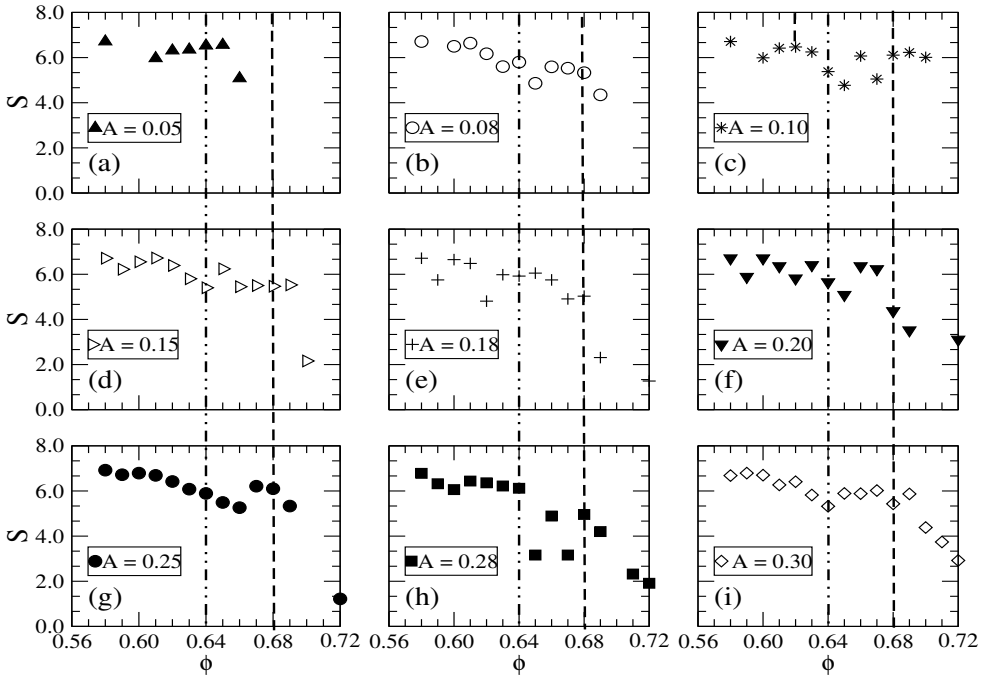

FIGURE 4.5: Plots of entropy S vs. ϕ for all shaking amplitudes. At maximum density $\phi \sim 0.72$, S attains minimum for intermediate ((d) to (g)) and high ((h) and (i)) amplitudes. The vertical lines at 0.64 (dot dashed line) and 0.68 (dotted line) serve as a guide for the eye.

We define three regions with respect to packing density: disordered region ($\phi \sim 0.58$ - 0.64), mixed region ($\phi \sim 0.65$ - 0.68) and ordered region ($\phi \sim 0.69$ - 0.72). Figure 4.5 shows the variation of entropy S against packing density ϕ. Over all, the entropy shows robust behaviour in the disordered region ($\phi \sim 0.58$ to 0.64) for all shaking amplitudes. Specifically, it either increases or decreases in the interval of packing density $0.65 < \phi < 0.68$ (mixed region) for intermediate [Figs. 4.5(d) to 4.5(g)] and high amplitudes [Figs. 4.5(h) and 4.5(i)]. In the ordered region, from $\phi \sim 0.69$ to 0.72, entropy decreases continuously and attains minimum at crystalline density $\phi \sim 0.72$ for intermediate [Figs. 4.5(d) to 4.5(g)] and high amplitudes [Figs. 4.5(h) and 4.5(i)]. The most important limitation for explanation of these results is due to lack of an adequate formalism of entropy for athermal system.

4.2.2 Percentage of Quasiregular Tetrahedra

In general, length [3] and volume [1, 4] measure's are useful in identification of regular or quasiregular tetrahedra. A quasiregular tetrahedron has volume between 0.118 and 0.130 [1, 4]. Instead, we use the length criteria [3, 5] $\eta = l_{max} - 1$ for the calculation of percentage of quasiregular tetrahedra. Here, l_{max} is the maximal length of an edge of a tetrahedron. A regular tetrahedron with equal unit edges has $\eta = 0$. We calculate l_{max} of Delaunay tetrahedron, and accordingly, pick the quasiregular tetrahedra with $\eta < 0.255$ from a set. Finally, we calculate the percentage of quasiregular tetrahedra. This percentage indicates the portion of space occupied by quasiregular tetrahedra inside packing; thus, discloses the degree of regularity of structures in packings.

Figure 4.6 shows the percentage of quasiregular tetrahedra for all shaking amplitudes. The percentage of quasiregular tetrahedra increases with packing density. In the range of density, $0.58 < \phi < 0.64$, the percentage increases rapidly to 25% for all amplitudes. Further, it increases steadily in the interval of density, $0.64 < \phi < 0.68$. Finally, the percentage reach to 31% at maximum density $\phi \sim 0.72$ for intermediate [Figs. 4.6(d) to 4.6(g)] and high [Figs. 4.6(h) and 4.6(i)] amplitudes. This infers that regular or quasiregular structures of spheres become apparent as density increases. We notice accordingly that the percentage changes at densities 0.64 and 0.68. However, other studies [3] have reported higher values of percentage of 33%.

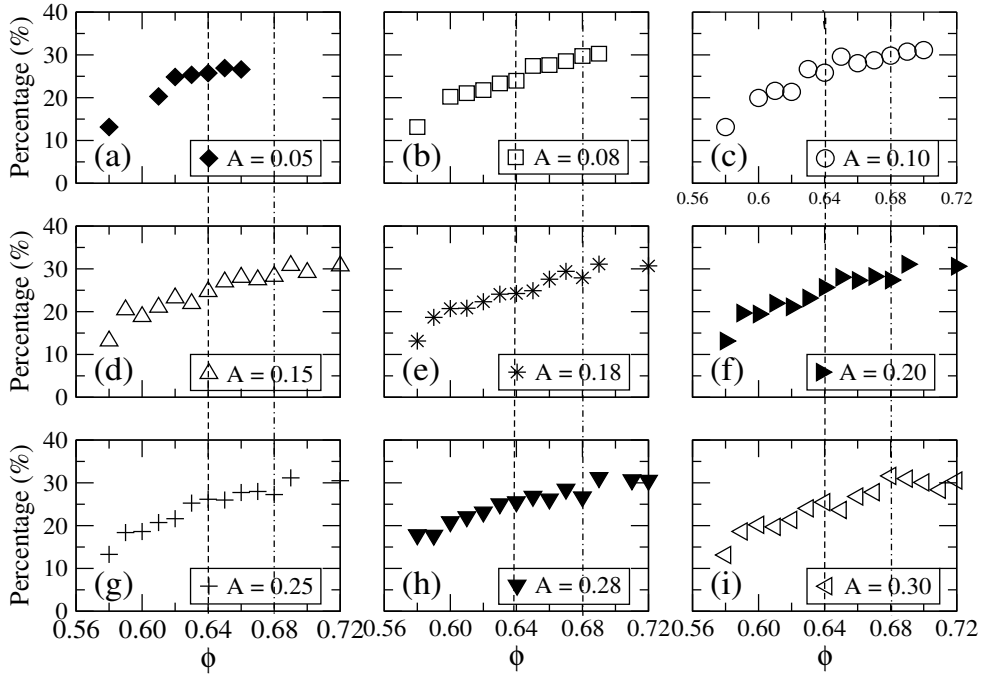

FIGURE 4.6: Percentage of quasiregular tetrahedra vs. packing density ϕ . It increases with packing density and reaches maximum 31% at crystalline density $\phi \sim 0.72$ for intermediate ((d) to (g)) and high ((h) and (i)) amplitudes. The vertical lines at 0.64 (dotted line) and 0.68 (dot dashed line) serve as a guide for the eye.

4.2.3 Angular and Length Measures of Tetrahedra

To do more detailed analysis, we focus on angular and length measures of Delaunay tetrahedra.

4.2.3.1 Dihedral Angle Distributions

The arrangement of common neighbors of a sphere provides a hint of local organization of packings. In particular, the dihedral angles of tetrahedra that formed by common neighbors of spheres give insight into regular or irregular structures. Moreover, four faces of a regular tetrahedron constitute six dihedral angles, corresponding to value 70.5° [2]. This value of dihedral angle represents the stable and compact structures of spheres [14]. We first select two triangular faces of tetrahedron from four faces, i.e., $\binom{4}{2}$ number of ways and then calculate dihedral angles [7, 23],

$$cos(\psi) = -\frac{(\mathbf{a}\times\mathbf{b}).(\mathbf{b}\times\mathbf{c})}{\Big|(\mathbf{a}\times\mathbf{b})\Big|\Big|(\mathbf{b}\times\mathbf{c})\Big|}, \tag{4.11}$$

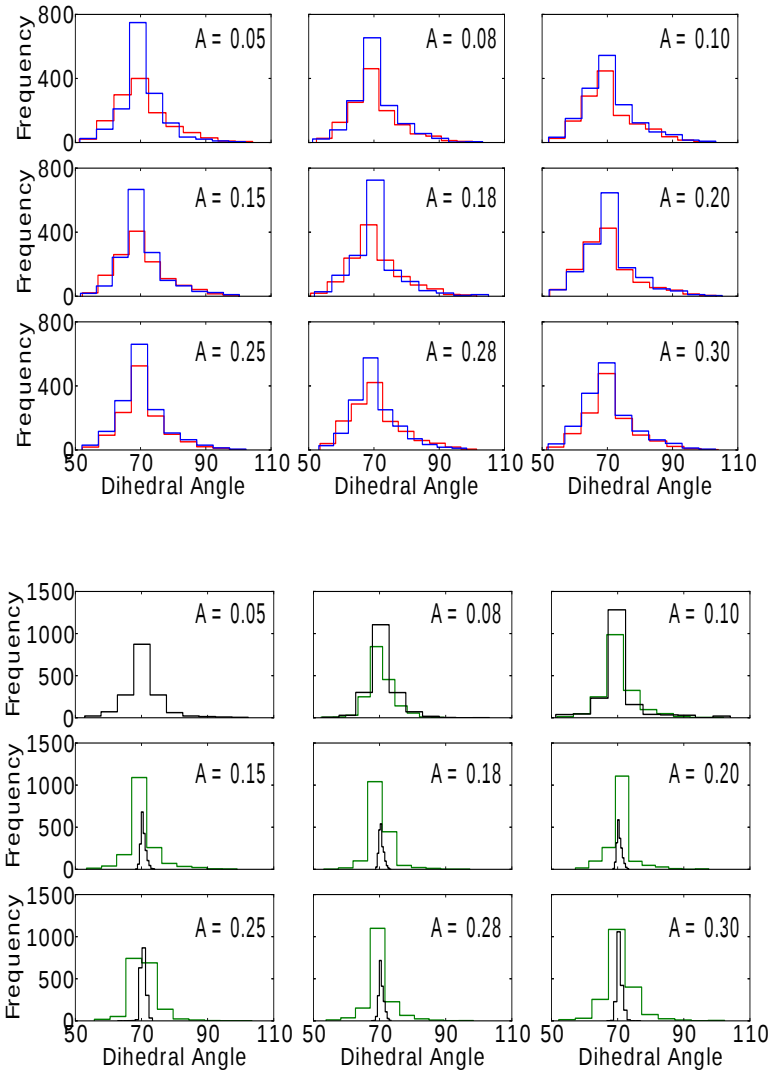

FIGURE 4.7: Histograms of dihedral angles of tetrahedra for all shaking amplitudes. (I): disordered packing densities $\phi \sim 0.62$ (red solid line) and $\phi \sim 0.64$ (blue solid line). (II): maximum packing densities ϕ_{max} (black solid line) and $\phi \sim 0.68$ (green solid line). The distributions become narrow as density increases from $\phi \sim 0.62$ to $\phi \sim 0.72$.

where, $\mathbf{a}, \mathbf{b}$ and $\mathbf{c}$ are vectors representing vertices of the triangular faces of the tetrahedron.

The distributions of dihedral angles of all tetrahedra are shown in Fig. 4.7 for four sample packing densities $\phi \sim 0.62, 0.64, 0.68$, and 0.72. The distributions appear broad for low densities $\phi \sim 0.62$ and 0.64, for all shaking amplitudes [Fig. 4.7I]. For intermediate ($A = 0.15, 0.18, 0.20, 0.25$) and high amplitudes ($A = 0.28, 0.30$), the distributions become narrow around a value 70° at $\phi_{max} \sim 0.72$ [Fig. 4.7II]. This peak of dihedral angle asserts

the presence of regular tetrahedra at maximum density $\phi_{max} \sim 0.72$. On the other hand, the dihedral angle manifests broad distributions for low amplitudes $A = 0.05, 0.08$ and 0.10 at maximum densities [Fig. 4.7II].

4.2.3.2 Length Measures : Tetrahedricity and Quartoctahedricity

Spheres can form tetrahedral or octahedral configurations inside the packings [24, 25]. In particular, fcc and hcp configurations generate clusters of regular or quasiregular tetrahedra and quartoctahedra [9]. A regular tetrahedron has six equal edges. On the other hand, a regular quartoctahedron has five equal edges and the sixth edge is $\sqrt{2}$ times longer than the other edges [5, 24]. Moreover, a regular quartoctahedron is a quarter of regular octahedron. Therefore, four congruent quartoctahedra forms a regular octahedron [24].

Anikeenko *et al.*, [6] have given a systematic method for the detection of regular simplices (tetrahedra or quartoctahedra) based on their lengths. They have defined two length measure's: tetrahedricity T and quartoctahedricity Q [9]. The equation for tetrahedricity is given as,

$$T = \frac{\sum\limits_{i \neq j} (l_i - l_j)^2}{15\bar{l}^2}. \tag{4.12}$$

For a regular tetrahedron $T = 0$.

Similarly, the equation for quartoctahedricity is given as,

$$Q = \frac{\sum\limits_{\substack{i<j \\ i,j \neq m}} (l_i - l_j)^2 + \sum\limits_{i \neq m} (l_i - (l_m/\sqrt{2}))^2}{15\bar{l}^2}, \tag{4.13}$$

where l_i, l_i and l_m are lengths of edges of the simplex, m is the index of the longest edge and $\bar{l}$ is the average length of tetrahedron. A regular quartoctahedron has $Q = 0$. It has been suggested that the minima's of T and Q distinguish the regular or quasiregular simplices [6]. These limits also distinguish the fcc and hcp structures [9].

We first compute the length of edges of all tetrahedra, and then calculation of T is carried out according to Eq. 4.12. For the calculation of Q, the longest edge l_m is found first and then Eq. 4.13 is used. Figures 4.8 and 4.9 illustrate the kernel density plots of T and Q respectively, at different packing densities.

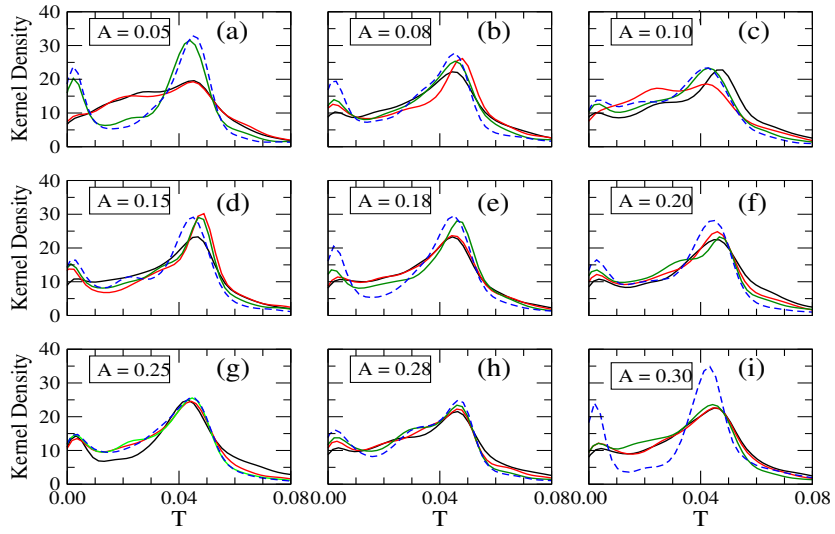

I

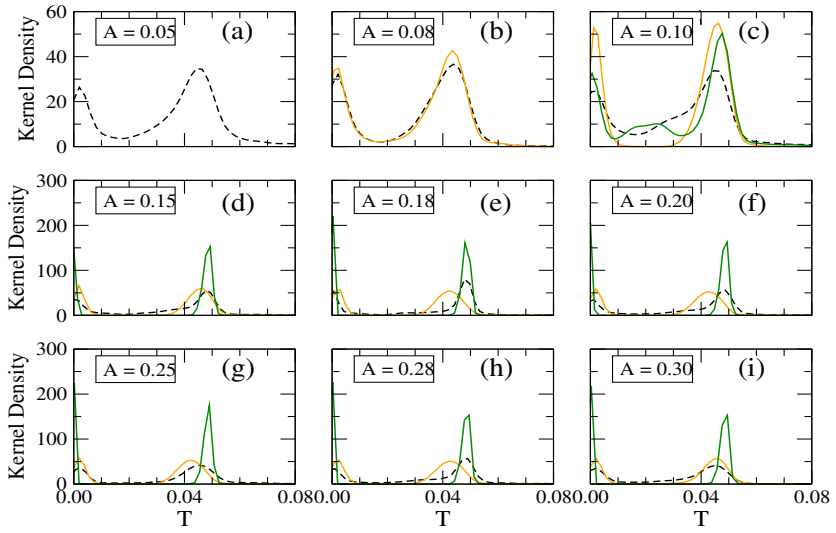

II

FIGURE 4.8: Kernel density of tetrahedricity T for all amplitudes at different densities. (I): The distributions of T have no sharp minima's at densities $\phi \sim 0.62$ (black solid line), 0.63 (red solid line), 0.64 (green solid line) and 0.65 (blue dotted line). (II): The distribution of tetrahedricity T has a sharp minimum at density $\phi \sim 0.72$ (orange solid line) for intermediate ((d) to (g)) and high ((h) and (i)) amplitudes.

No sharp minima's of T and Q are observed at low packing densities of $\phi \sim 0.62, 0.63, 0.64$, and 0.65 for all shaking amplitudes [Figs. 4.8I and 4.9I]. At maximum density $\phi_{max} \sim 0.72$, both distributions manifest the minima's at 0.018 and 0.013 respectively, for intermediate ($A = 0.15, 0.18, 0.20, 0.25$) [Figs. 4.8II (d) to (g) and Figs. 4.9II (d) to (g)] and high amplitudes ($A = 0.28, 0.30$) [Figs. 4.9II (d) to 4.9II (g) and Figs. 4.9II (h) to

4.9II (i)]. The emergence of these sharp minima's implies that the degree of regularity of simplices increases with packing density. These findings are are consistent with those of Medvedev's findings [9].

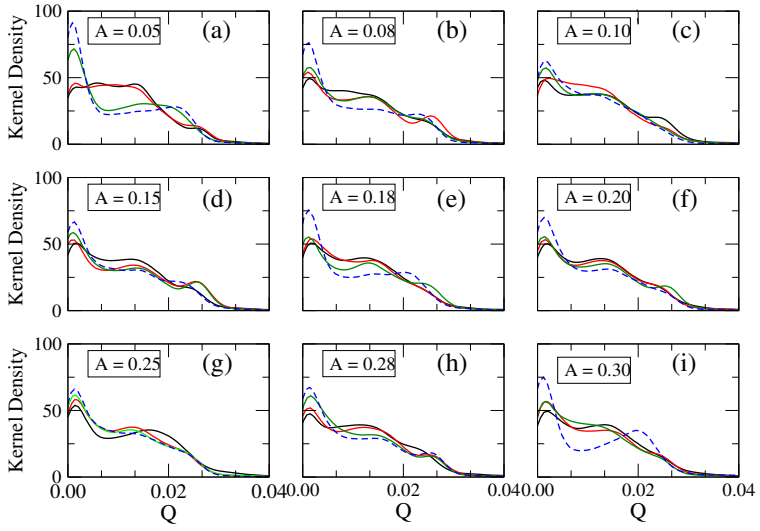

I

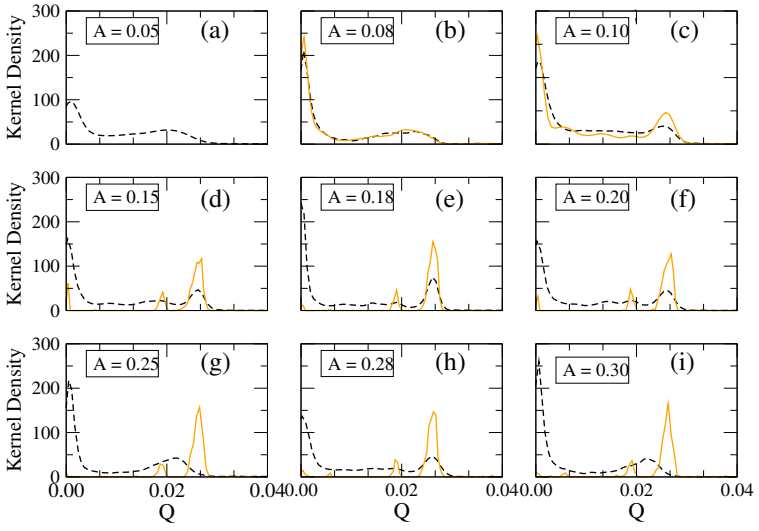

II

FIGURE 4.9: Kernel density of quartoctahedricity Q for all amplitudes at various packing densities. (I): The distributions of Q have no sharp minima's at low densities $\phi \sim 0.62$ (black solid line), 0.63 (red solid line),0.64 (green solid line) and 0.65 (blue dotted line). (II) At maximum density $\phi_{max} \sim 0.72$, Q has sharp minimum for intermediate ((d) to (g)) and high amplitudes ((h) and (i)).

4.3 Conclusions

This chapter has given the detailed study of Delaunay tessellations of sphere packings via packing densities. We have described the study of volumes of tetrahedra, their fluctuations and entropy. Two parameter Gamma distribution of volumes emerges at all packing densities. Our findings highlighted the fact that volume fluctuations and entropies show drastic changes at packing densities 0.62, 0.64 and 0.68. The benefit of this contribution lies in the establishment of an analogy with thermal systems. We observed that the percentage of regular tetrahedra increases with packing density and reaches 31% for intermediate and high amplitudes at crystalline density of 0.72. Additionally, we have provided considerable insights into packings through dihedral angles and length measure's of tetrahedron. The dihedral angle distribution manifests a peak around 70° at maximum density, which indicates the growth of regular tetrahedra. The benefit of length measures tetrahedricity T and quartoctahedricity Q lies in identifying the regular or quasiregular simplices. The minima's of the distributions of tetrahedricity and quartoctahedricity appear at 0.018 and 0.013 respectively, which may identify the crystalline structures.

Bibliography

[1] V. P. Voloshin, Y. I. Naberukhin and N. N. Medvedev, *Molecular Simulation*, **4**, 209(1989).

[2] A. Okabe, B. Boots, K. Sugihara, and S. N. Chiu, *Spatial Tessellation- Concepts and Applications of Voronoi Diagrams* (Wiley, New York), 2000.

[3] A. V. Anikeenko, N. N. Medvedev, and T. Aste, *Phys. Rev. E* **77**, 031101(2005).

[4] N. N. Medvedev, Y. I. Naberukhin, *J. of Noncrys. Sol.* **94**, 402(1987).

[5] T. C. Hales, *Ann. of Math.* **162**, 1065 (2005).

[6] A. V. Anikeenko, M. L. Gavrilova, and N. N. Medvedev, *in Computational Science and Its Applications – ICCSA 2005* (Springer,Berlin), 2005.

[7] W. F. Kern, and J. R. Bland, *Solid Mensuration with Proofs*, (Wiley, New York), 1948.

[8] J. P. Troadec, A. Gervois, and L. Oger, *Europhys. Lett.* **42 (2)**, 167(1998).

[9] A. V. Anikeenko, and N. N. Medvedev, *Phys. Rev. Lett.* **98**, 235504(2007).

[10] S. F. Edwards and D. V. Grinev, *Phys. Rev. Lett.* **82**, 5397(1999).

[11] S. F. Edwards, in *Granular Physics)* (Cambridge University Press), 2007.

[12] Anita Mehta, *Granular Physics* (Cambridge University Press), 2007.

[13] T. Aste, M. Saadatfar, T. J. Senden, *Phys. Rev. E* **71**, 061302(2005).

[14] T. Aste, *Phys. Rev. Lett.* **96**, 018002(2006).

[15] T. Aste and T. Di Matteo, *Phys. Rev. E* **77**, 021309(2008).

[16] J. R. Shewchuk *Computational Geometry: Theory and Applications*, **22(1–3)**, 21(2002).

[17] S. W. Cheng, T. K. Dey, and J. R. Shewchuk, *Delaunay Mesh Generation* (CRC Press, Boca Raton, Florida), 2012.

[18] R. K. Singh, A. Tropsha and I. I. Vaisman, *J. Comput. Biol.* **3(2)**, 213(1996.

[19] V. Senthil Kumar, and V. Kumaran, *J. Chem. Phys.* **123**, 114501(2005).

[20] O. Barndorff-Nielsen, *Proc. Roy. Soc. London, ser. A)* **353 (1674)**, 401(1977).

[21] C. Briscoe *et al.*, *Phys. Rev. Lett.* **101**, 188001(2008).

[22] N. Francois *et al.*, *Phys. Rev. Lett.* **111**, 148001(2013).

[23] W. Gellert *et al.*, *VNR Concise Encyclopedia of Mathematics* (Van Nostrand Reinhold, New York), 1989

[24] J. Illian, A. Penttinen, H. Stoyan, and D. Stoyan, *Statistical Analysis and Modelling of Spatial Point Patterns* (John Wiley and Sons, UK), 2008.

[25] M. L. Gavrilova, *Generalized Voronoi Diagram: A Geometry-Based Approach to Computational Intelligence* (Springer-Verlag, Berlin Heidelberg), 2008.

Chapter 5

Human Cognition through Eye Movements

In this chapter, we give a detailed account of the eye movement study. We discuss the methodology of an eye movements and visual world paradigm. We divide the experimental data analysis into temporal and spatial categories. We mention, in brief, the theoretical background of the analysis. Temporal analysis of saccade and fixation times has given for 32 literate and 36 illiterate subjects (participants). Our spatial analysis includes the construction, diffusive characteristics and Fourier analysis of time series of eye movements.

5.1 Methodology of Eye Movements

This section explains the visual attention, types and detection of eye movements.

5.1.1 Visual Attention

Cognitive scientists [1, 2] extensively study the mechanisms of cognition through eye movements. Eye movements serve as an archetype and provide the paths of attention and its causes. The dynamics of attentional states give clues about the perception during selection or ignorance of information relevant to ongoing behavior. In particular, our eyes respond to verbal influences by looking at an object of speech or by imagining its visual analogues [3]. Moreover, visual attention focuses either with or without accompanying the eye movements. However, whether eyes disclose the dynamics of attention is a long

standing question [3, 4]. Also, it is important to illustrate some questions: what drives the eyes from one location to another ?, and how does the process of visual perception occurs ? To address these questions, we must examine the properties of stimuli, response and roles of eye, and the brain.

Visual attention is an inner cognitive mechanism, mainly based on psychological [5] and neurological [6] viewpoints. Both these viewpoints examine the human behavior and neural mechanisms of learning, memory and attention. For example, psychologists [7, 8, 9] have carried out experiments on human eye movements during reading, visual search and scene perception. Their studies suggest that the participants continuously change their attentional states in response to aural and visual inputs [10, 11]. Also, both voluntary and involuntary components of attention involve during linguistic tasks [11]. Further, linguistic study [12] suggests that literacy has direct influence on attention mechanisms through eye movements. In addition, participants who are given an overt task to perform may respond differently from those who are tacking images through unconscious processing; the latter might yield insights that are more natural [13]. A challenging task is to find the link between components of attention and eye movements [14].

Neurologists [15, 16] examine the regions of brain and their functions. The human brain is complex neuronal hardware which processes visual inputs. When light enters to the eyes, cornea, lens and the retina produce a clear and stable image of visual world [15, 16]. Each time we move our eye on different locations of an image or an object. In fact, the diversions of the eyes are controlled by regions of the brain. These regions build a coherent representation of the visual and sensory inputs. Therefore, the brain plays a vital role in visual attention [15, 16].

5.1.2 Eye Movements : Types and Detection

Eye movements are broadly divided into three categories: saccade, fixation and small pursuits [14, 17, 18]. Here, we mention the characteristics of saccade and fixation. Saccades are rapid, voluntary movements that alter the fovea from one location to another in the visual scene [14]. On the other hand, fixations are stationary movements that stabilize the retina over an area of interest in an image or scene [17]. During a saccade, the visual system is involved in searching, and cognitive processing is minimal;

while when it is fixated on an object, searching is temporarily at an end, and cognitive processing is maximal [18]. It is now accepted that attention is not focused on any object during saccades, as the system searches for its next fixation. Nevertheless, the start and end of fixations are uncertain [18]. The durations of saccade and fixation movements depend on cognitive task [18]. It has been shown that durations of fixation lie between 150 ms to 600 ms [19] whereas those of saccades typically vary from 10 ms to 100 ms [20].

Different eye tracking techniques identify the attentive behavior of the participants. A few computer algorithms classify the spatial and temporal information of participant's eye movements [21]. To identify spatial characteristics, the algorithms are classified into three types: dispersion-based [22, 23], area-based [24] and velocity-based [25, 26]. The dispersion-based algorithms consider the dispersion, i.e. spread between successive fixation points, whereas area-based algorithms recognize the gaze points in area of interest. The velocity-based algorithms set up thresholds to detect fixation and saccade. In general, the velocity of a saccade has two thresholds [21, 25, 26]; the low threshold, $100°/sec$ for fixations and high threshold, $300°/sec$ for saccades. Moreover, the distance between the sampled gaze points gives the velocity of eye movement [25, 26]. A high resolution eye tracking camera records the coordinates (in pixels) and time durations of fixations and saccades. In addition, it also records the amplitude, velocity, and the acceleration of saccades.

5.1.3 Visual World Paradigm

Visual and linguistic information affect the mental processes in our daily life. Tanenhaus *et al.*, [10] have developed an experimental paradigm which imparts the dynamics of eyes and attention during spoken language tasks. This experimental paradigm is called "Visual World Paradigm" (VWP) which mimics the real world. Specifically, this paradigm is used in an experiment where subjects (participants) look at visual displays in response to auditory inputs [10]. The visual display contains everyday objects while the auditory inputs contain neutral sentences [10]. The subject's eye movements time-lock between the linguistic inputs during the task [10]. Mishra *et al.*, [27] have studied the effect of formal literacy on attention of literate and illiterate subjects. Both literate and illiterate subjects perform the language-mediated task.

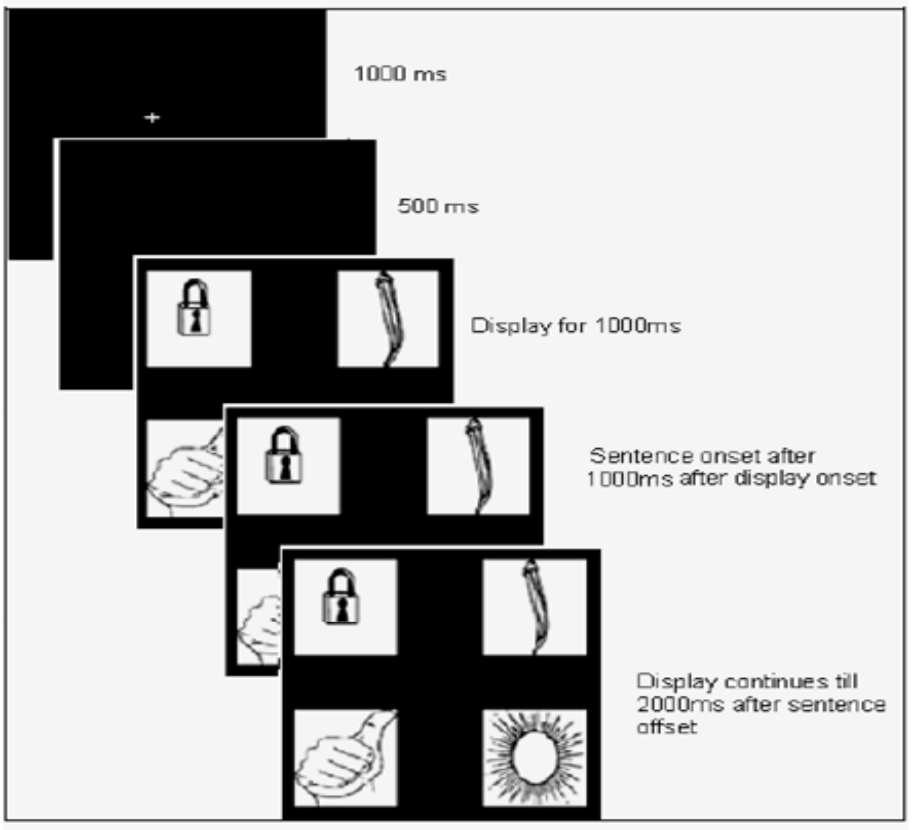

FIGURE 5.1: Experimental display of visual world paradigm. The auditory sentence "Usne aaj taara dekha", (He saw a star today), appeared after 1000 *ms* display onset. The phonological analogue to taara (star) is taala (lock), while the semantic analogue is the image of the sun. The other two images are distractors.

Figure 5.1 shows a typical trial sequence of VWP [27] which contains four black and white line drawings of common objects. In this display [Fig. 5.1], the auditory sentence is "Usne aaj taara dekha" (He saw a star today). The sample stimulus shows the phonological analogue "taala" of target word "taara", whereas the semantic analogue of "taara" is the image of sun. The other two objects are distractors. Moreover, in linguistics, phonology and semantic relate to sounds of speech and meaning of a word or symbol respectively. For example, the Hindi word 'magar' (crocodile in English) can have a phonological competitor 'matar' (peas in English) and, kachua, (turtle in English) as a semantic competitor [27]. These experiments have been suggested that formal literacy is a significant enhancer of language mediated visual search and gives an insight into the overt attentional mechanism [27]. During this visual search, saccades and fixations are influenced by both the emerging visual and the linguistic representations, and their interactions [27].

5.2 Theoretical Methods of Analysis

In this section, we mention in brief the theoretical background of the method of analyses.

5.2.1 Power-law and Scale Invariance

Scaling is the most powerful method for the characterization of physical [28] and biological systems [29]. For instance, the scaling analysis and universality classes are developed in statistical physics to understand the dynamics of phase transitions and critical phenomena [28]. Also, many empirical quantities in biological and economical processes are modelled using scale transformation [30]. In simple terms, the function $g(x)$ under scale transformation becomes,

$$g(cx) = c^{\gamma} g(x). \tag{5.1}$$

The form of the function remains $g(x)$ invariant after multiplied by the factor c. Further, the scaling exponent γ characterize the process [30].

A random variable manifests scale invariance property through its probability density function and correlation function [30]. The scale invariance of random processes is often expressed in terms of power-laws or inverse power-laws. Besides, a random process favors an inverse power-law that originates in the spectral analysis [31] and probability density models [30, 32]. In addition, the decay of autocovariance functions of long-range memory processes manifests power-law [33]. Furthermore, the inverse power-laws of probability density indicate that probabilities of random variables clump together across multiple scales. Let x be an outcome of an experiment. The frequency $P(x)$ of an event x can be written in terms of inverse power-law [30, 32],

$$P(x) = B\left(\frac{1}{x^{\xi}}\right), \tag{5.2}$$

where $x \geq x_{min}$ and B normalization factor. Equation 5.2 represents a straight line with slope ξ in log-log representation,

$$\log P = \log B - \xi \log x. \tag{5.3}$$

The appearance of inverse power-law is ubiquitous in many processes. For example, the inverse power-law of Pareto, Zipf, and Levy types emerged in the distribution of income

[34], occurrence of word in linguistic study [35], and scale free distributions in foraging [36], respectively. Also, cognitive scientists recognize the applications of scaling laws in their studies on human perception [37] and memory [38, 39, 40].

5.2.2 Diffusion Processes

Gaussian distribution describes the ordinary diffusive processes such as Brownian motion and ordinary random walks [41]. Importantly, the properties of Brownian motion and random walk obey the central limit theorem. In statistics, the mean and the variance are the simplest quantities to characterise nature of random variable or processes. For example, in case of Brownian motion, the mean and the variance are finite, and depend linearly on time: $\overline{x_t} = vt$, and $\overline{x_t^2} - \overline{x}_t^2 = 2Dt$ [42, 43, 44]. Here, v is the velocity of Brownian particle and D is the diffusion coefficient. The distribution function of position x of Brownian particle follows Gaussian [44],

$$P(x,t) = \frac{1}{\sqrt{2\pi\sigma^2 t}} \exp\left(-\frac{x^2}{2\sigma^2 t}\right). \tag{5.4}$$

Equation 5.4 is the solution of diffusion equation,

$$\frac{\partial P(x,t)}{\partial t} = \frac{\sigma^2}{2} \frac{\partial^2 P(x,t)}{\partial x^2}. \tag{5.5}$$

Some complex systems show anomalous diffusive behavior. The failure of the central limit theorem in anomalous diffusion indicates a radical departure from Gaussian statistics [42, 45]. Anomalous dynamics further classify into subdiffusive and superdiffusive categories [42, 45]. In general, the mean and the variance of the anomalous dynamics grow nonlinearly with respect to time [42, 45]. The mean square displacement (MSD) of a variable $z(t)$ vary with time, $< |z(t) - z(0)|^2 > \sim t^{2H}$ [30, 32]. For $H = 1/2$, the MSD is linearly proportional to time and corresponds to the Gaussian process. For anomalous cases, where $H \neq 1/2$, the MSD increases nonlinearly with time. Furthermore, the values of H divide the anomalous property into two cases: subdiffusive, $0 < H < 1/2$ and superdiffusive, $1/2 < H < 1$ [30, 32].

In case of anomalous processes, the distributions of random variables can be written in terms of Levy's stable probability laws. For instance, distribution of a random variable y show a Levy's inverse power-law distribution [45]: $P(y) = y^{-\mu}$, where $1 < \mu < 3$. The

exponent μ is called the Levy index. The probability density function $P(y)$ is not the solution of ordinary diffusion Eq. (5.5). Moreover, anomalous dynamics is described using fractional order differential equations [30, 32]. Similarly, numerical methods of fractional Brownian, and fractional Levy motions can model the anomalous property [46, 47]. The stochastic approximations [46, 47] for fractional Brownian $B_H(n)$ and fractional Levy $L_H(n)$ motions are given as:

$$B_H(n) = C_{1H}\left[\sum_{i=-J}^{n}(n-i)^{H-1/2}B(i) - \sum_{i=-J}^{0} i^{H-1/2}B(i)\right], \tag{5.6}$$

where $B(i)$ are Gaussian random variables with zero mean and unit variance. Here H is the Hurst parameter and the index n denotes time. The constant C_{1H} is so chosen that the increments, $B_H(j+1) - B_H(j)$ have unit variance [46, 47]. Similarly,

$$L_H(n) = C_{2H}\left[\sum_{i=-J}^{n}(n-i)^{H-1/2}L(i) - \sum_{i=-J}^{0} i^{H-1/2}L(i)\right], \tag{5.7}$$

where $L(i)$ are Levy random variables and constant C_{2H} is so chosen that the smallest increments, $L_H(j+1) - L_H(j)$ has unit size [46, 47].

5.2.3 Time Series Analysis

A time series is a set of observations, taken sequentially in time. Examples of time series are the measurements of heart beats [48], the data of weather forecasting [49] and rainfall [50], and so on. In time series data, adjacent observations are dependent on each other [51, 52]. The sequences of observations map the probability distribution function (PDF) of a random variable. Moreover, the length of these sequences and the accompanied PDF characterize the diffusive properties of time series.

5.2.3.1 Scaling of Time Series

Scaling of time series relies on the assumption that the diffusion process is stationary, i. e. the PDF is time invariant. Using the scaling methods, the scaling exponents of time series have been obtained for ordinary and anomalous diffusion [53]. A scale-invariant PDF of a random variable x satisfy,

$$ap(x,t) = p(a^{g_x}x, a^{g_t}t), \tag{5.8}$$

where a is constant. Put $a^{g_t}t = 1$ to eliminate the time dependence of $p(x,t)$,

$$p(x,t) = \frac{1}{t^{1/g_t}} p(t^{-g_x/g_t}x, 1) \equiv \frac{1}{t^{\delta}} F\left(\frac{x}{t^{\delta}}\right), \tag{5.9}$$

where $\delta = 1/g_t$ is scaling exponent and called diffusion exponent. If the function F in Eq. (5.9) has Gaussian form then the diffusion becomes ordinary (normal) with $\delta = 0.5$ [53].

In case of anomalous diffusion, particularly in Levy like diffusion, the diffusion exponent δ is computed using entropy of the processes. This method of analysis is called diffusion entropy analysis (DEA) [53]. The DEA analysis starts with the classical Shannon entropy functional,

$$S(t) = -\int_{-\infty}^{\infty} p(x,t)\ln(p(x,t))\,dx. \tag{5.10}$$

After substituting the probability density function from Eq. (5.9) in Eq. (5.10), $S(t)$ becomes,

$$S(t) = -\int_{-\infty}^{\infty} \frac{1}{t^{\delta}} F(\frac{x}{t^{\delta}}) \left[\ln F\left(\frac{x}{t^{\delta}}\right) - \delta \ln t\right]\, dx. \tag{5.11}$$

By changing the integration from x to $y = \frac{x}{t^{\delta}}$, finally we get,

$$S(t) = A_s + \delta \ln(t), \tag{5.12}$$

where $A_s \equiv \int_{-\infty}^{\infty} F(y)\ln[F(y)]dy$. The slope of resulting line [Eq. (5.12)] gives the diffusion exponent δ.

In general, the second moment of a random variable x vary with time,

$$\langle x^2(t)\rangle \propto t^{2\delta}. \tag{5.13}$$

It has been shown that the Eq. (5.13) fails to give correct value of δ for anomalous diffusion [53]. The modified form [53] of Eq. (5.13) is given as :

$$\langle x^2(t)\rangle \propto t^{2H}. \tag{5.14}$$

The symbol H is the Hurst exponent. The most common method, standard deviation analysis (SDA) [54] easily estimates the exponent H for ordinary and anomalous diffusion. Allegrini *et al.*, [54] have given the standard deviation analysis for times series of

$x(t)$ as:

$$D(t) = \sqrt{\frac{\sum_{i=1}^{M-t}[x_i(t) - \overline{x(t)}]^2}{M-t-1}}. \tag{5.15}$$

where $\overline{x(t)}$ is the average of sequences or trajectories of length t. In case of Gaussian diffusion, the two exponents satisfy the relation $\delta = H = 1/2$ [53, 54].

5.2.3.2 Spectral Analysis

Random time series constitute deterministic and random components. The deterministic component varies smoothly or periodically in time whereas the random part fluctuates rapidly with time [30]. In general, a time series [30] of a random variable $x(t)$ is written as,

$$x(t) = y(t) + \eta(t), \tag{5.16}$$

where y(t) and $\eta(t)$ are deterministic and random components respectively. Suppose that time series $x(t)$ is constructed at M points over total time T, then we can define M such that $T = M\Delta t$. The time window varies as: $t = j\Delta$, where $j = 0, 1, 2, ...M$. The discrete Fourier transform technique [30, 55] decomposes the time series, Eq. (5.16), into the sum of sinusoidal components,

$$x_j = \sum_{j=0}^{M-1} C_j e^{2\pi i j f_j} + \eta_j, \tag{5.17}$$

where η_j is white noise and f denotes the frequency. In general, the coefficients C_k are complex. In case of random time series, i.e., Eq. (5.17), C_k are random complex numbers. A power spectral density P_s or a periodogram of given time series x is obtained as,

$$P_s(f_j) = \frac{1}{M}|C_j|^2, \tag{5.18}$$

or it can be also written as,

$$P_s(f_j) = \frac{1}{M}\left|\sum_{j=0}^{M-1} x_j e^{2\pi i j \omega_j}\right|^2. \tag{5.19}$$

This is normalised power spectral density [30, 55]. Furthermore, power spectral density is written as a function of frequency f,

$$P_s(f) = \frac{1}{f^\alpha}, \tag{5.20}$$

where α lies between 0 and 3. In case of white noise, the power spectrum has constant value, i.e. $P_s(f) = constant$ and shows no correlation in time [30, 55]. Moreover, the observations of $1/f$ fluctuations in the system imply existence of self-organized criticality [31]. In addition, these fluctuations have been observed in physical [56, 57], biological [58, 59], and economical [60] processes.

5.3 Analysis of Eye Movements

In this section, we give the temporal and spatial analyses of the eye movement data.

5.3.1 Details of Data Collection

The experiments were carried on 36 illiterate and 32 literate subjects, selected from the Hindi-speaking population of Allahabad [12, 27]. The literate and illiterate categories were made using mean years of formal education of people. The mean years of formal education were 15 and 4 years for literate and illiterate peoples respectively. The spoken sentences were neutral, and the target word came after about 16 seconds on average from the sentence onset (see Fig. 5.1). The fixation and saccadic eye movement data were collected and recorded with an SMI High Speed eye tracker running at a sampling rate of 1250 Hz; this recovered the X and Y coordinates of a gaze with an accuracy of 0.01°, and the resulting data were binned using MATLAB. This was done for 35 trials per subject. Saccades were identified following a velocity-based algorithm [21] when the movement of the eye was greater than $30°/sec$ in any direction from its current position. Fixations were identified with the stationarity of eye motion in any location, for a minimum duration of 80 ms occurring between two saccades.

5.3.2 Temporal Analysis

Now, we give the detailed analysis of saccade and fixation times. We mainly consider eye gaze points of target, competitor, and distractors objects. For each of the subjects, the data is manually scanned, and probability distributions are computed to show the

frequencies of fixation and saccade durations. Figure's 5.2 and 5.3 show the distributions of fixation and saccade times for literate and illiterate subjects.

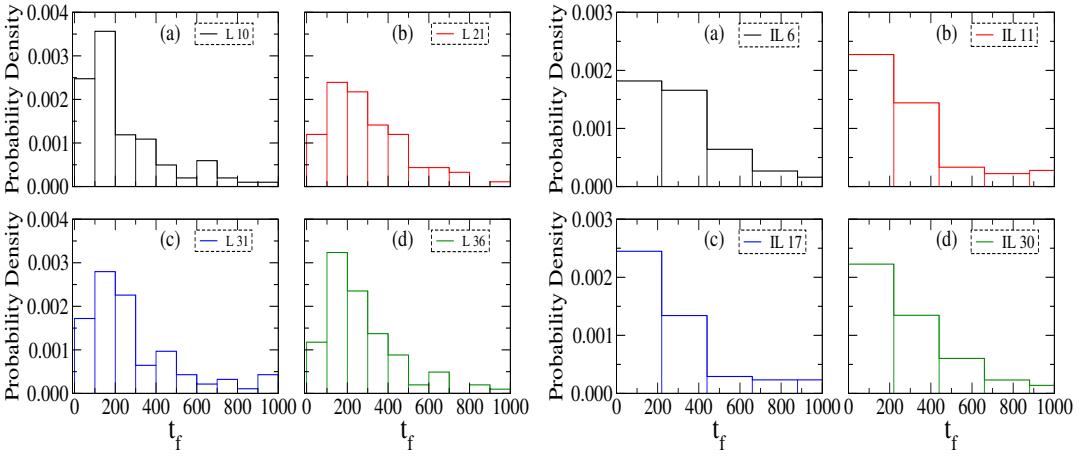

FIGURE 5.2: (I): Histograms of fixation time t_f for four sample literate subjects, show peaks. (II): Histograms of fixation time t_f for four sample illiterate subjects. The distributions do not have a peak. The legend indicates the correspondence between the symbol and the type/serial number of the subject.

The significant difference between two types appears in the distribution of fixations. The fixation times of literate subjects have skewed distributions which indicate the presence of a characteristic time scale. The typical distributions in Fig. 5.2I with peaks that occur in the range $190 - 260\ ms$, and long complex tails, typify the fixation distribution for literate subjects. This suggests the presence of a typical attention-related peak when the subjects find meaningful correlations between a target image and the spoken word. For the illiterate subjects, the distributions are less uniform. Unexpectedly some of them are rather similar to the skew 1-peaked distribution found in the literate case; most of them seem to exhibit power-laws, with no characteristic timescales, so that no fixation peaks are manifested [Fig. 5.2II]. Table 5.1 depicts the fixation times for both subjects.

Overall, we found that saccades appear to follow inverse power-law distributions [Fig. 5.3I], $P(t_s) = {t_s}^{-\beta}$, where t_s is saccadic time. The values of the exponent β lie between 1 and 2. Averaging over all the subjects, we obtained the exponent $\beta = -1.77 \pm 0.23$, for both literate and illiterate subjects, with only about four of the illiterate subjects and one of the literate subjects showing significant deviations from such behavior. We

observed however, that low literate subjects tended to spend relatively larger amounts of time on saccadic movements, even when power-law behavior was apparent overall.

TABLE 5.1: Fixation time (in ms) distributions of 32 literates and 36 illiterates. Note that all 32 literates had fixation peaks, while only 5 out of 36 literates manifested fixation peaks.

Literacy level	Serial No.	Peak value
Literates	6,9,21,22,25,29,30	194.88 ± 12.92
	10,11,19,26,28,31	221.36 ± 7.12
	1,3,4,7,8,14,24	234.29 ± 3.05
	2,15,16,18,20,23,32	243.84 ± 2.62
	5,12,13,17,27	259.67 ± 9.66
Illiterates	5,4,10,14,23	247 ± 23.57
	Others	did not fixate

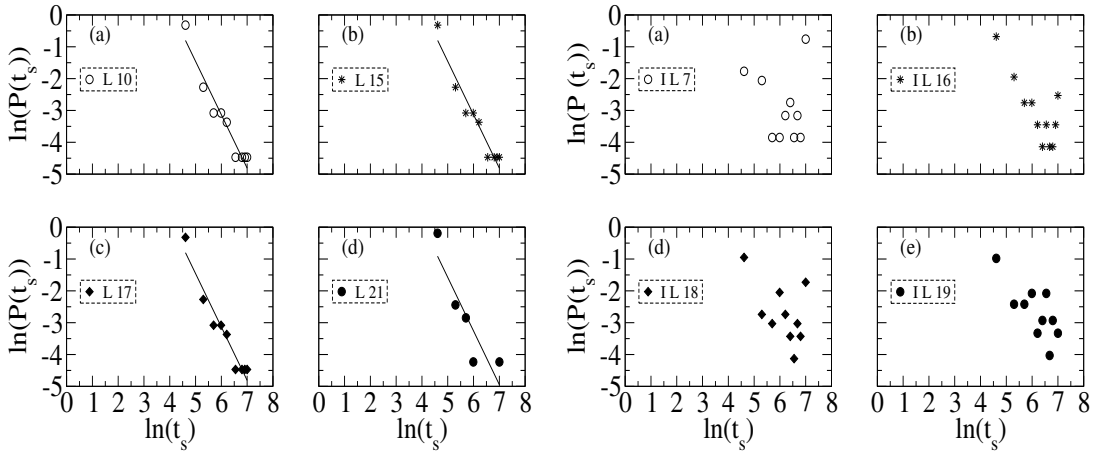

I II

FIGURE 5.3: (I): The log of the probability distribution $P(t_s)$ of saccadic time t_s vs. $\ln(t_s)$ for four literates, show power-law. (II): The log of the probability distribution $P(t_s)$ of saccadic time ts vs. $\ln(t_s)$ for four illiterates, where no power-law is discernible. No lines have been fitted to the data for this reason. The legend indicates the correspondence between the symbol and the type/serial number of the subject.

The large saccadic times of illiterate subjects imply the poorer cognitive processing, searching extensively and rarely fixating on their targets. Some of the distributions for such extreme illiterate cases are shown in Fig. 5.3II. The positions of the fixation (attentional) peak are absent, and no convincing lines are fitted to the data for the saccades either.

5.3.3 Anomalous Diffusion in Eye Movements

In this section, we discuss the diffusive properties of the time series of eye movements.

5.3.3.1 Spatial Analysis of Saccades

Our particular interest is in the construction and analysis of time series of eye movements. In this study, when subjects perform a task, the eye tracker camera records the sequences of fixation and saccade points. These alternate sequences are measured over 35 trials for 32 literate subjects and 36 illiterate subjects. Figure 5.4 shows a typical time series of Euclidean distances between saccade points spanned over total time duration. This time series is our basic unit for further investigations.

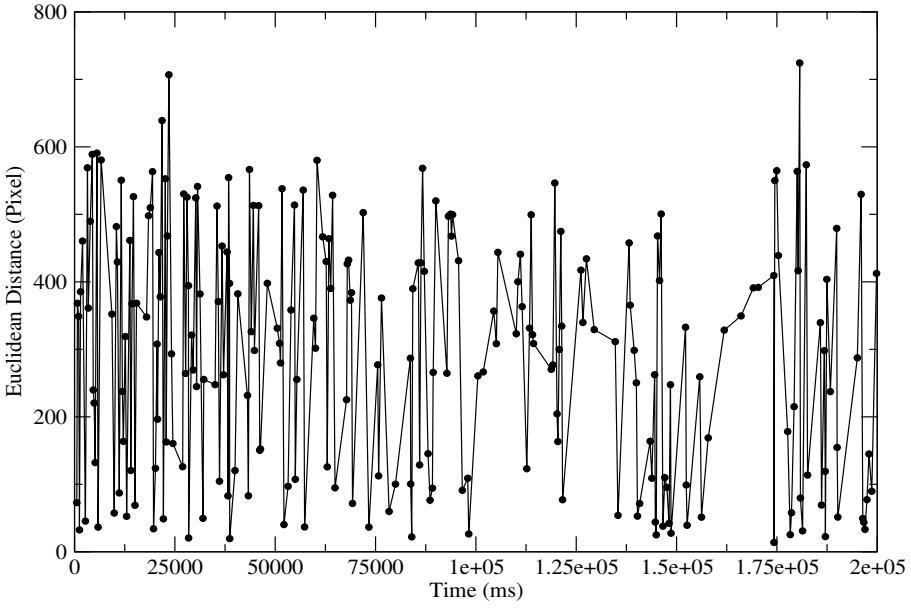

FIGURE 5.4: A typical time series of Euclidean distances of saccades.

We carefully examine the scaling property of time series of saccades. One possible way is to construct the probability distribution function of saccade, and accordingly, identify

the scaling form. Moreover, the values of the scaling exponents determine the type of the diffusion process. The ordinary and anomalous diffusion processes can be identified by the application of scaling methods to time series of saccades. Two scaling methods, standard deviation analysis (SDA) [54] and diffusion entropy analysis (DEA) [53, 62] are used to compute diffusion (δ) and Hurst H exponents. We also provide spectral analysis and distributions of Euclidean distances of saccades.

5.3.3.2 Estimation of Diffusion and Hurst Exponents

The two scaling exponents, diffusion δ and Hurst H, characterize the dynamics of saccades. We analyze the spatial positions of the gazes of eight representative subjects, spanning literate and illiterate, with an aim to determining the nature of saccadic dynamics. For each subject, time series $ds(t)$ is constructed from the Euclidean distances corresponding to the gaze coordinates at times $t = 1, 2, ..., M$ during a given saccade. Subtrajectories $Z_i(n)$ [53, 61] starting in the i^{th} time bin and spanning a time duration n are then computed using the relation,

$$Z_i(t) = \sum_{j=1}^{n} [ds(i + j - 1)]. \tag{5.21}$$

The subtrajectories $Z_i(n)$ are thus the cumulative Euclidean distances ds spanned in time windows of length $[i, i + 1]$ during saccades. These subtrajectories are the basis for both, DEA [53, 62] and SDA [54].

Scafeta *et al.*, [53, 62] have developed an analysis based on entropies of diffusion processes. This method, diffusion entropy analysis (DEA) computes Shannon entropies of trajectories of time series over variable time windows. The details of DEA are given in section 5.2.3.1. The exponent δ is estimated using the diffusion entropy analysis (DEA) [53, 62]; this involves constructing the histograms of the end points of the subtrajectories $Z_i(n)$. If $p_i(n)$ is the probability that an end point of a subtrajectory $Z(n)$ of duration n lies in the i^{th} time bin, the Shannon entropy for a time duration n is expressible as:

$$S(n) = -\sum_{i=1}^{M-m} p_i(n) \ln(p_i(n)). \tag{5.22}$$

This further reduces to,

$$S(n) = A_s + \delta \ln(n), \tag{5.23}$$

where A_s is constant. The exponent δ is obtained as:

$$\frac{S(n)}{\ln(n)} \propto \delta. \tag{5.24}$$

Figure 5.5 shows the results of DEA for eight representative literate and illiterate subjects. The fitting functions of straight lines have the form, $S(n) = A_s + \delta \ln(n)$, due to linear-log representation. The values of A_s lie between 1 and 3. The slope of the fitted lines gives the values of the diffusion exponent δ for eight representative subjects.

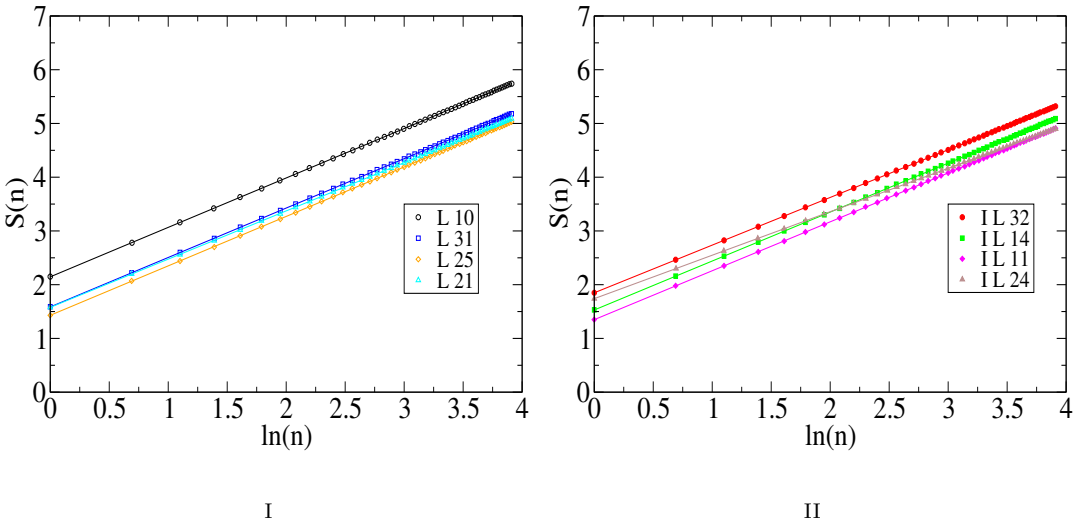

FIGURE 5.5: Plots of Shannon entropies $S(n)$ vs. $\ln(n)$ for saccade time series corresponding to eight representative literate (I) and illiterate (II) subjects. The legend indicates the correspondence between the symbol and the type/serial number of the subject. The exponent's δ is found from the slopes and tabulated in Table 5.2.

Now, we present the estimation of Hurst exponent H using SDA. The standard deviation analysis (SDA) is a traditional method used in variance estimation [54]. In our case, this method estimates the variance or the standard deviation of subtrajectories at each discrete time. We compute the standard deviation $D(n)$ of the subtrajectories $Z_i(n)$ for time $t = 1, 2, ..., M$ during a given saccade. We use following formula,

$$D(n) = \sqrt{\frac{\sum_{i=1}^{M-n}[Z_i(n) - \overline{Z(n)}]^2}{M - n - 1}}, \tag{5.25}$$

where $\overline{Z(n)}$ is the average of subtrajectories of length n. The Hurst exponent H is obtained as:

$$D(n) \sim n^H. \tag{5.26}$$

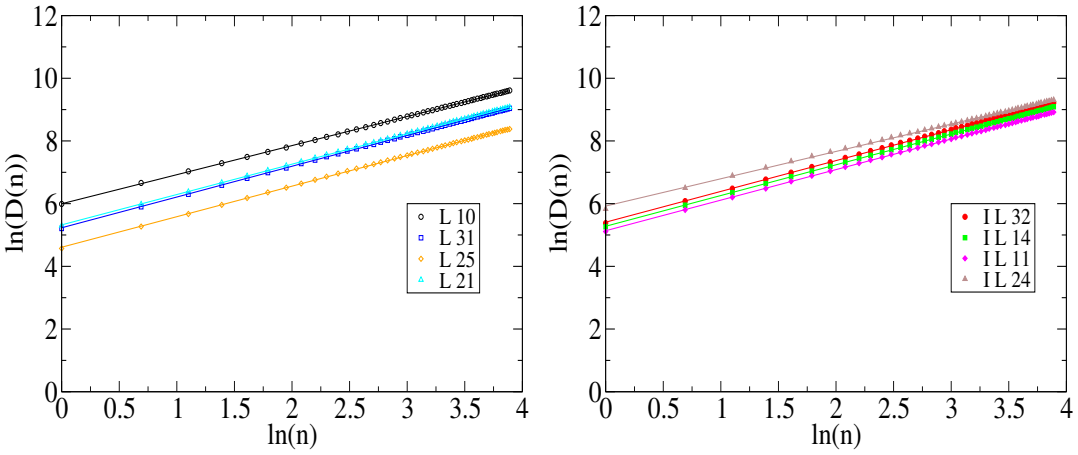

FIGURE 5.6: Plots of $\ln(D(n))$ vs. $\ln(n)$ for subtrajectories $Z(n)$ corresponding to eight literate (I) and illiterate (II) representative subjects during saccadic eye movement. The exponent's H is found from the slopes. The legend indicates the correspondence between the symbol and the type/serial number of the subject.

Figure 5.6 shows the results of SDA for eight representative literate and illiterate subjects. The slope of the line $\ln(D(n)) = C + H\ln(n)$ gives the Hurst exponent H. The values of constant C lie in the interval $4 < C < 6$.

TABLE 5.2: The values of Hurst H and diffusion δ exponents for eight sample literate and illiterate subjects whose data is plotted in Figs. 5.5 and 5.6.

Literacy Level	Serial No.	H	δ
Literates	10	0.92	0.87
	21	0.96	0.90
	25	0.97	0.92
	31	0.98	0.91
Illiterates	11	0.97	0.90
	14	0.98	0.89
	24	0.87	0.81
	32	0.98	0.92

Table 5.2 shows the values of exponents H and δ. The values of these exponents lie between 1/2 and 1. The values of H ($H > 0.5$ indicates superdiffusion) are obtained and the fact that $\delta \neq H$ across Table 5.2 both suggest that our data are consistent with Levy processes. The findings of Van Loon *et al.*, [63], who found non-Gaussian behavior for the timing of sequence for the 'later' saccades in a multiple-fixation search

like our own, buttress our conclusions. They are in contrast to the findings of Shelhamer [64], where fractional Brownian motion was observed in the predictive eye movements of saccades; this is probably because, in our case, the experimental paradigm is not predictive at all, and subjects are not aware that they are performing a task.

5.3.3.3 Spectral Analysis and Distributions of Euclidean Distances

In this section, we provide spectral analysis and probability distribution of Euclidean distances of saccade. Our aim is to identify the $1/f^{\alpha}$ behavior via power spectral density. The power spectrum of the saccade time series $ds(t)$ is obtained using discrete Fourier transform technique (DFT) [55].

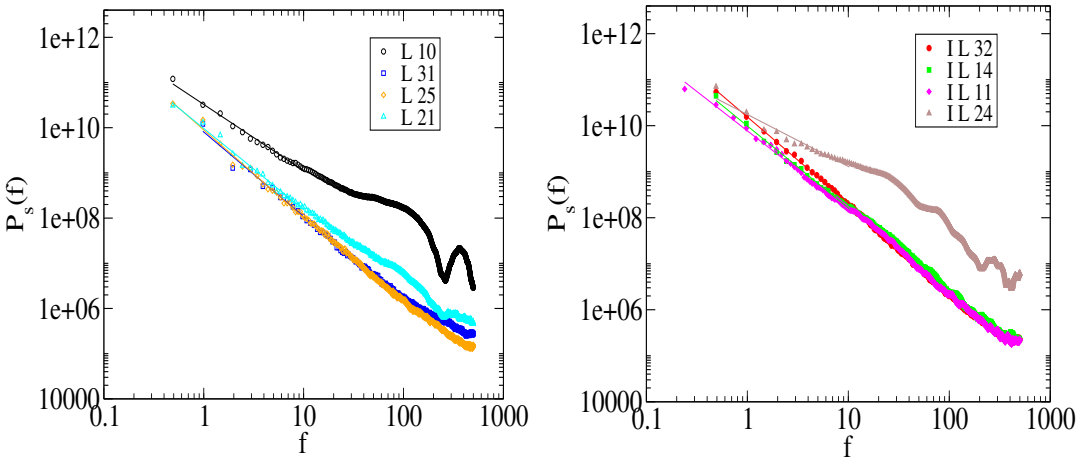

FIGURE 5.7: Plots of the power spectrum $P_s(f)$ against frequency f for eight representative literate (I) and illiterate (II) subjects. The legend indicates the correspondence between the symbol and the type/serial number of the subject. The exponent α is found from the slope of fitted line (see Table 5.3).

The power spectral density of $ds(t)$ is written as:

$$P_s(f_j) = \frac{1}{M}\left|\sum_{j=0}^{M-1} ds_j e^{2\pi i j f_j/M}\right|^2 . \tag{5.27}$$

Power spectral densities of time series for eight representative literate and illiterate subjects are shown in Fig. 5.7. The slope of the straight line in log-log representation gives value of the exponent α. The values of α lie between 1 and 2 (Table 5.3). This result indicates the nontrivial temporal correlations of anomalous diffusion.

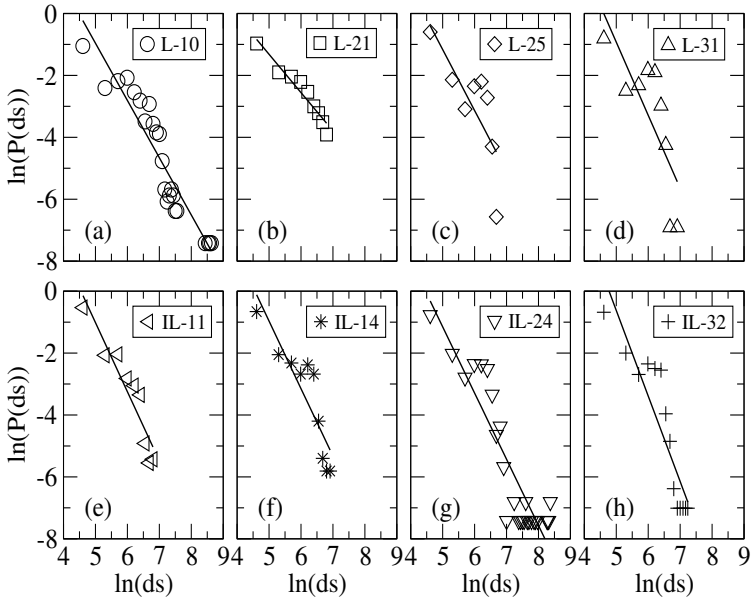

FIGURE 5.8: Plots of $\ln(P(ds(t)))$ vs. $\ln(ds(t))$ for sample literates ((a) to (d)) and illiterates ((e) to (h)) respectively. The legend indicates the correspondence between the symbol and the type/serial number of the subject. The exponent κ is obtained from slope of line (see Table 5.3).

TABLE 5.3: The values of α and κ exponents for the sample literate and illiterate subjects whose data are plotted in Fig. 5.7 and Fig. 5.8.

Literacy Level	Serial No.	α	κ
Literates	10	1.46	1.85
	21	1.79	2.75
	25	1.94	1.96
	31	1.87	2.35
Illiterates	11	1.71	2.81
	14	1.78	2.17
	24	1.13	2.14
	32	1.87	1.35

The probabilities of Euclidean distances of saccades are computed. The probability distribution $P(ds(t))$ of Euclidean distances of saccades show the inverse power-law, $P(ds(t)) = ds(t)^{-\kappa}$, where $1 < \kappa < 3$. Figure 5.8 displays the probability distributions of Euclidean distances. Our findings suggest that the Euclidean distances of saccades exhibit Levy distribution. The values of exponent κ for eight representative subjects are given in Table 5.3.

5.4 Conclusions

We have described temporal and spatial analyses of eye movements. Our most striking observation here is that there is a clear separation of behavior in visual processing, via the distributions of saccadic and fixation times; the former shows a scale-invariance, while the latter does not. In general, the effect of literacy shows up only in the fixation dynamics, where literate subjects typically show the presence of an attentional timescale of around 220 ms on an average. We have analyzed the time series of Euclidean distances of saccades. The scaling exponents, H and δ are estimated using standard deviation analysis and diffusion entropy analysis. Our results support the Levy-like dynamics of saccades, analogous to animal foraging where animals are typically unaware of where next they will find food. As expected, this is very similar to what is seen in our case: subjects are unaware of the locations of their next targets, and accordingly, the Hurst exponent H takes on values that are much greater than 0.5. Our findings would seem to suggest that saccadic eye movements probably obey fractional Levy dynamics, irrespective of the literacy level of the subject. Other possible confirmations of superdiffusive dynamics come from the plots of Fourier power spectrum $P_s(f) \sim (1/f^{\alpha})$ against f and distributions, $P(ds(t)) = ds(t)^{-\kappa}$, of Euclidean distances of saccades. The values of these two exponents α $(1 < \alpha < 2)$ and κ $(1 < \kappa < 3)$ attribute to anomalous dynamics.

Bibliography

[1] B. J. Baars and N. M. Gage, *Cognition, Brain, and Consciousness* (Academic Press), 2010.

[2] D. Reisberg, *Cognition* (W. W. Norton and Company, New York), 2009.

[3] G. T. Buswell, *How subjects Look at Pictures* (University of Chicago Press), 1935.

[4] M. I. Posner, *Quart. J. Exp. Psychol.* **32**, 3(1980).

[5] M. Carrasco, *Vis. Res.* **51**, 1484(2011).

[6] R. J. Leigh and D. S. Zee, *The Neurology of Eye Movements* (Oxford University Press), 2006.

[7] K. Rayner, *Psychol. Bull.* **124**, 372(1998).

[8] M. I. Posner and M. K. Rothbart, *Ann. Rev. Psychol.* **58**, 1(2007).

[9] J. M. Henderson, *Trends. Cogn. Sci.* **7(11)**, 498(2003).

[10] M. K. Tanenhaus *et al.*, *Science* **268**, 1632(1995).

[11] F. Huettig, R. K. Mishra, and C. N. Olivers, *Fron. in Psychol.* **2**, 394(2012).

[12] F. Huettig and N. Singh and R. Ramesh, *Fron. in Psycho.* **2**, 28(2011).

[13] M. M. Chun, J. D. Golomb, and N. B. Turk-Browne, *Ann. Rev. Psychol.* **62**, 73(2011).

[14] E. Kowler, *Vis. Res.* **51**, 1457(2011).

[15] J. W. Bisley, and M. E. Goldberg, *Ann. Rev. Neurosci.* **33** 1(2010).

[16] M. I. Posner and S. E. Petersen, *Ann. Rev. Neurosci.* **13**, 25(1990).

[17] A. T. Duchowski, *Eye Tracking Technology* (Springer, New York), 2007.

[18] R. H. S. Carpenter, *Movements of the Eyes* (Pion Ltd, London), 1988.

[19] D. E. Irwin, in *Eye movements and visual cognition : Scene perception and reading, K. Rayner (Ed.)* (Springer-Verlag,New York), 1992.

[20] W. L. Shebilske and D. F. Fisher, in *Eye Movements and Psychological Functions : International Views* (Hillsdale, NJ: Lawrence Erlbaum), 1983.

[21] D. D. Salvucci and J. H. Goldberg, *Proceedings of Eye Tracking Research and Application Symposium*, 71(2000).

[22] L. Stark and S. R. Ellis, in *Eye Movements : Cognition and Visual Perception* (Hillsdale, NJ: Lawrence Erlbaum), 1981.

[23] H. Widdel, in *Theoretical and Applied aspects of Eye Movement Research (pp. 21-29)* (Elsevier, New York), 1984.

[24] R. DenBuurman T. Boersma and J. F. Gerrisen, *Reading Research Quarterly* **16**, 227(1981).

[25] C. L. Erkelens and I. M. L. C. Vogels, in *Eye Movement Research : Mechanisms, Processes, and Applications* (Elsevier, New York), 1995.

[26] T. Sen and T. Megaw, in *in Theoretical and Applied Aspects of Eye Movement Research* (Elsevier, Amsterdam), 1984.

[27] R. K. Mishra, N. Singh, A. Pandey, and F. Huettig, *J. Eye. Mov. Res.* , **5(1): 3**, 1(2012).

[28] H. E. Stanley, *Introduction to Phase Transitions and Critical Phenomena* (Oxford University Press), 1988.

[29] J. H. Brown and G. B. West, *Scaling in Biology* (Oxford University Press), 2000.

[30] B. J. West, *Physiology, Promiscuity and Prophecy at Millenium* (World Scientific Publishing), 1999.

[31] P. Bak, *How Nature Works* (Springer-Verlag, New York), 1996.

[32] B. B. Mandelbrot, *The Fractal Geometry of Nature* (W. H. Freeman and Company, New York), 1983.

[33] J. Bertan, *Statistics for Long-Memory Processes* (CRC Press), 1994.

[34] B. C. Arnold, *Pareto Distributions* (International Cooperative Publishing House), 1983.

[35] G. K. Zipf, *Human Behaviour and The Principle of Least Effort* (Addison-Wesley Press), 1949.

[36] G. M. Viswanathan *et al.*, *Nature (London)* **381** , 413(1996).

[37] N. Chater and G. D. A. Brown, *Cognition* **69**, 17(1999).

[38] T. Rhodes and M. T. Turvey, *Physica A* **385**, 255(2007).

[39] Y. Chen *et al.*, *Phys. Rev. Lett.* **79**, 4501(1997).

[40] C. T. Kello *et al.*, *Trends. Cog. Sci.*, **14(5)**, 222(2000).

[41] M. F. Shlesinger and G. M. Zaslavsky and J. Klafter, *Nature* **363**, 31(1993).

[42] D. H. Zanette, *Phys. Rev. E* **55**, 6632(1997).

[43] J. P. Bouchaud, *Physics Reports* **195(4-5)**, 127(1990).

[44] M. F. Shlesinger and G. M. Zaslavsky and U. Frisch, *Levy Flights and Related Topics in Physics* (Springer, Berlin), 1995.

[45] M. F. Shlesinger, B. J. West and J. Klafter, *Phys. Rev. Lett.* **58**, 1100(1987).

[46] A. M. Reynolds, *J. Phys. A: Math. Theor.* **42**, 434006(2009).

[47] B. B. Mandelbrot and J. W. Van Ness, *SIAM, Review* **10**, 422(1968).

[48] P. C. Ivanov, et al., *Nature (London)* **383**, 323(1996).

[49] S. D. Campbell and F. X. Diebold *J. of the American Stat. Asso.* **100**, 469(2005).

[50] K. Gupta *et al.*, *IJIES* **1(6)**, 42(2013)

[51] R. H. Shumwa, *Applied statistical time series analysis.* (Englewood Cliffs, NJ: Prentice Hall), 1988.

[52] G. E. P. Box, G. M. Jenkins, G. C. Reinsel, *Time Series Analysis Forecasting and Gontrol* (Wiley), 2008.

[53] N. Scafetta and V. Latora, and P. Grigolini, *Phys. Rev. E.* **66**, 031906(2002).

[54] P. Allegrini and M. Barbi and P. Grigolini and B. J. West,*Phys. Rev. E.* **52**, 5281(1995).

[55] W. H. Press *et al.*, *Numerical Recipes in Fortran 77: The Art of Scientific Computing* (Cambridge University Press), 1992

[56] F. N. Hooge, *Physica A&C* **83**, 14(1976).

[57] P. Dutta and P. M. Horn, *Rev. Mod. Phys.* **53**, 497(1981).

[58] J. M. Hausdorff and C. -K. Peng, *Phys. Rev. E* **54**, 2154(1996).

[59] T. Gisiger, *Biol. Rev.* 76, 161(2001);

[60] R. F. Voss, in *Fractal Geometry and Computer Graphics* (Springer, Berlin and Heidelberg), 1992.

[61] D. G. Stephen *et al.*, *Phys. Rev. E.* **79**, 056114(2009).

[62] N. Scafetta and P. Grigolini, *Phys. Rev. E.* **66**, 036130(2002).

[63] M. Van Loon, I. Th. C. Hooge and A. V. Van den Berg, *Proc. R. Soc. Lond. B* **269**, 1571(2002).

[64] M. Shelhamer, *Biol. Cybern.* **93(1)**, 43(2005).

Chapter 6

Model Selection and Simulation of Levy Random Walk

This chapter comprises two sections. The first section focuses on the statistics of model selection and information theoretical methods. We describe the simulation of Levy random walks in second section.

6.1 Statistics of Model Selection

Data are the values of measurements of a random variable in an experiment. A meaningful empirical data analysis considers model construction and selection, estimation of parameter for the unknown population of data. To make valid inferences, a model selection is an integral part of data analysis. Moreover, information theory and statistics [1] provide methods of selection for the best approximating model for the data. The information theoretical techniques are different from those of regression analysis [2] and hypothesis testing [3]. The Akaike [4] and Bayesian [5] information criteria not only select the best approximating model but also make ranking and scaling of other models.

6.1.1 Basics of Likelihood Theory

Likelihood theory discusses model specification, estimation of parameters and precision of measurements [6]. This theory has several similarities with traditional least square theory [7]. The likelihood method begins with construction of probability models for a given data and parameters, and accordingly, selects the best approximate model. In

contrast, least square methods are simple and easily compute the fitting parameters of linear and nonlinear models by minimizing sum of the squares of the residuals [7]. The least square frameworks are viewed as an inefficient methods to estimate of second moment (variance) of models with non-Gaussian residuals [8, 9]. On the other hand, likelihood theory follows an iterative procedure to compute the parameters of linear and nonlinear models with non-Gaussian residuals [10].

Likelihood is a function of unknown parameters and denoted as: $\mathcal{L}(\theta|data, model)$. The function $\mathcal{L}$ gives the 'likelihood' of unknown parameters θ of an approximating model, for the given empirical data [11]. It constructs joint distribution of data; for example, in case of n measurements of x, the likelihood function [11] is given as: $\mathcal{L}(\theta|x, model) = \prod_{i=1}^{n} P(x_i)$. Further, likelihood theory iteratively compute the most likely one as the best estimate of unknown parameters. The function $\mathcal{L}$ attains maximum, i.e. $\frac{\partial \mathcal{L}}{\partial \theta} = 0$, at the best estimate value of parameter [11]. Moreover, the function $\mathcal{L}$ and its natural logarithm $\ln \mathcal{L}$ have maximum at same point. Alternatively, the maximum likelihood estimate (MLE) is achieved at a point where the log-likelihood function has its maximum, $\frac{\partial(\ln \mathcal{L})}{\partial \theta} = 0$ [11]. This maximization of log-likelihood function with respect to parameters gives the best fit of a probability model to the data. In case of large samples and asymptotic analysis, the MLE of probability models gives numerically optimal values of parameters [12, 13]. Furthermore, the likelihood and information theories jointly provide the basis for selection of the best probability model and its parameters. In next sections, we explain the maximum likelihood estimation of four candidate probability models and the information criterion.

6.1.2 Maximum Likelihood Estimation of Candidate Models

In this section, we present theoretical ideas of MLE of candidate probability models that are used for saccade times. This method starts with initial guesses of parameters and then it performs an iterative procedure on joint probability distribution of data [11]. The joint distribution of data x is given as,

$$F(x) = \prod_{i=1}^{n} P(x_i). \tag{6.1}$$

Here, we provide the MLE of four candidate probability models: exponential, log-normal, gamma and power-law.

- **Exponential Distribution**:

  The probability density function of exponential distribution [14] is given as:

$$P_e(x) = \lambda * \exp(-\lambda x). \tag{6.2}$$

  The likelihood function is written as:

$$\begin{aligned} \mathcal{L}_e(x|\lambda) &= \prod_{i=1}^{n} P_e(x_i), \\ &= \lambda^n \exp\left(-\lambda \sum_{i=1}^{n} x_i\right). \end{aligned} \tag{6.3}$$

  Hence, the log-likelihood becomes,

$$\ln \mathcal{L} = n \ln \lambda - \lambda \sum_{i=1}^{n} x_i. \tag{6.4}$$

  Equating $\frac{\partial \ln \mathcal{L}}{\partial \lambda}$ to zero, the maximum likelihood estimate of the parameter λ is obtained as,

$$\lambda = \frac{n}{\sum_{i=1}^{n} x_i}. \tag{6.5}$$

- **Log-normal Distribution**

  The probability density function of log-normal distribution [15] with mean υ and variance σ is written as:

$$P_l(x) = \frac{1}{x\sigma\sqrt{2\pi}} \exp\left(-\frac{(\ln x - \upsilon)^2}{\sqrt{2\sigma^2}}\right). \tag{6.6}$$

  The likelihood function becomes,

$$\begin{aligned} \mathcal{L}_l(x|\upsilon, \sigma) &= \prod_{i=1}^{n} P_l(x_i), \\ &= \frac{1}{\sqrt{(2\pi\sigma^2)^n}} \prod_{i=1}^{n} \frac{1}{x_i} \exp\left(\sum_{i=1}^{n} -\frac{(\ln x_i - \upsilon)^2}{\sqrt{2\sigma^2}}\right). \end{aligned} \tag{6.7}$$

The log-likelihood becomes,

$$\ln \mathcal{L} = -\frac{n}{2}\ln(2\pi\sigma^2) - \sum_{i=1}^{n}\ln(x_i) - \frac{\sum_{i=1}^{n}\ln(x_i)^2}{2\sigma^2} + \frac{\sum_{i=1}^{n}\upsilon\ln(x_i)}{\sigma^2} - \frac{n\upsilon^2}{2\sigma^2}. \quad (6.8)$$

Setting $\frac{\partial \ln \mathcal{L}}{\partial \upsilon} = 0$, and $\frac{\partial \ln \mathcal{L}}{\partial \sigma} = 0$, we get maximum likelihood estimate of υ and σ^2,

$$\upsilon = \frac{\sum_{i=1}^{n}\ln(x_i)}{n}, \quad (6.9)$$

$$\sigma^2 = \frac{\sum_{i=1}^{n}(\ln(x_i) - \upsilon)^2}{n}. \quad (6.10)$$

- **Gamma Distribution**

The probability density function of Gamma distribution [16] with shape parameter k and scale parameter b is given as:

$$P_g(x) = \frac{x^{k-1}\exp(\frac{-x}{b})}{b^k\Gamma(k)}. \quad (6.11)$$

The likelihood function becomes,

$$\begin{aligned}\mathcal{L}_g(x|k,b) &= \prod_{i=1}^{n} P_g(x_i) \\ &= \prod_{i=1}^{n}\frac{(x_i)^{k-1}\exp(\frac{-x_i}{b})}{b^k\Gamma(k)}. \end{aligned} \quad (6.12)$$

The log-likelihood function is written as:

$$\ln \mathcal{L} = (k-1)\sum_{i=1}^{n}\ln x_i - n\ln\Gamma(k) - nk\ln b - \frac{1}{b}\sum_{i=1}^{n}x_i \quad (6.13)$$

Setting $\frac{\partial \ln \mathcal{L}}{\partial b}$ equal to zero yields the maximum likelihood estimate of the b,

$$b = \frac{\sum_{i=1}^{n}x_i}{nk}. \quad (6.14)$$

Substituting b (Eq. 6.14) into Eq. 6.13 and setting $\frac{\partial \ln \mathcal{L}}{\partial k} = 0$, we get,

$$\ln(k) - \psi(k) = \ln\left(\frac{1}{n}\sum_{i=1}^{n} x_i\right) - \frac{1}{n}\sum_{i=1}^{n}\ln(x_i), \tag{6.15}$$

where $\psi(k) = \frac{\Gamma^{'}(k)}{\Gamma(k)}$ is the digamma function.

- **Power-law Distribution**

  Now, we consider MLE of power-law with its parameter $\beta^{'}$. The pdf of power-law distribution [17, 18] is written as:

$$P_p(t) = Cx^{-\beta^{'}} = \frac{\beta^{'}-1}{x_{min}}\left(\frac{x}{x_{min}}\right)^{-\beta^{'}}. \tag{6.16}$$

  The likelihood function for the data x becomes,

$$\begin{aligned}\mathcal{L}_p(x|\beta^{'}) &= \prod_{i=1}^{n} P_p(x_i) \\ &= \prod_{i=1}^{n}\frac{\beta^{'}-1}{x_{min}}\left(\frac{x_i}{x_{min}}\right)^{-\beta^{'}}.\end{aligned} \tag{6.17}$$

  The log-likelihood function is obtained as:

$$\ln\mathcal{L} = \sum_{i=1}^{n}\left[\ln(\beta^{'}-1) - \ln(x_{min}) - \beta^{'}\ln\left(\frac{x_i}{x_{min}}\right)\right]. \tag{6.18}$$

  Setting $\frac{\partial \ln \mathcal{L}}{\partial \beta^{'}} = 0$, yields the maximum likelihood estimate of the $\beta^{'}$,

$$\beta^{'} = 1 + n\left[\sum_{i}\ln\left(\frac{x_i}{x_{min}}\right)\right]^{-1}. \tag{6.19}$$

6.1.3 Akaike Information Criterion

This section focuses on the theoretical background of information criterion. Akaike introduced a relationship between information theory and maximum likelihood function [4]. He connected Kullback-Leibler (KL) distance to Fisher's log-likelihood function. The KL distance is the statistical distance between probability distributions. For example, for two continuous distributions h and g, the KL distance [1, 4, 11] or information

is written as:

$$I(h,g) = \int h(x) \log\left(\frac{h(x)}{g(x|\theta)}\right) dx, \tag{6.20}$$

where θ are parameters of 'g' model. The function $I(h,g)$ in Eq. (6.20) gives the information lost when model g is used to approximate h. In discrete case, the information loss can be expressible as:

$$I(h,g) = \sum_{i=1}^{n} p_i \log\left(\frac{p_i}{q_i}\right), \tag{6.21}$$

where p_i are probabilities of i^{th} outcome and q_i constitute the probabilities of approximating distribution. These probabilities satisfy the axioms, $0 \leq p_i \leq 1$, $0 \leq q_i \leq 1$ and $\sum_{i=1}^{n} p_i = \sum_{i=1}^{n} q_i = 1$.

Equation 6.20 can be written as:

$$I(h,g) = \int h(x) \log(h(x)) - \int h(x) \log(g(x|\theta)). \tag{6.22}$$

This is viewed as differences between two expectations [4, 11],

$$I(h,g) = E_h[\log(h(x))] - E_h[\log(g(x|\theta))], \tag{6.23}$$

where, E_h denotes the expectation with respect to h. The first expectation, $E_h[\log(h(x))]$ is constant and depends only on the unknown distribution h [1, 11]. Therefore, $I(h,g)$ becomes as,

$$I(h,g) = J - E_h[\log(g(x|\theta))], \tag{6.24}$$

where J is constant. Akaike [19, 20] considered the expectation $E_\theta[I(h,(g(x|\theta))]$ and simplified the Eq. (6.24) into a simple relation,

$$AIC = -2\log(L(\theta|x)) + J. \tag{6.25}$$

Here, AIC denotes the Akaike information criterion and J is number of parameters of a probability model. Numerical optimization techniques [21, 22] estimate the value of log-likelihood function $\log(L(\theta|x))$. Further, in case of a small sample size [23, 24], the AIC is further modified to,

$$AIC_c = AIC + \frac{2J(J+1)}{n-J-1}, \tag{6.26}$$

where n is sample size. The AIC difference [11, 19, 20], D_i of the i^{th} model of a given set is obtained as:

$$D_i = AIC_i - AIC_{min}, \tag{6.27}$$

where AIC_{min} is the minimum value of AIC of a model in a given set. The differences D_i are used to estimate the relative likelihood of probability models [11, 19, 20]. The relative likelihood F_i of i^{th} model in a set for the given data is given as:

$$F_i \propto \exp\left(\frac{-D_i}{2}\right). \tag{6.28}$$

The relative Akaike weight [11, 19, 20] ω_i of i^{th} model is calculated as:

$$\omega_i = \frac{\exp\left(\frac{-D_i}{2}\right)}{\sum_{i=1}^{m}\left[\exp\left(\frac{-D_m}{2}\right)\right]}, \tag{6.29}$$

where summation in the denominator taken over total m models considered.

6.2 Likelihood and Information Criteria for Saccade

In chapter 5, we have shown that saccade time follows inverse power-law distribution. We use the likelihood and information theories to prove our claim of inverse power-law. We consider four candidate probability models for saccade data: exponential, log-normal, gamma and power-law.

TABLE 6.1: The values of log-likelihood, Akaike information (AIC), and Akaike weights for exponential, log-normal, gamma and power-law distributions.

Candidate Model	No. of parameters	Log-likelihood	AIC	Akaike weight (ω)
Exponential	1	-507.263	1015.526	0
Log-normal	2	-488.456	978.912	0
Gamma	2	-505.876	1013.752	0
Power-law	1	-472.791	946.582	1

Our MATLAB algorithm comprises two steps. First, we calculate the probabilities of saccade times. Secondly, we fit the exponential, log-normal, gamma and power-law distributions to the data. The MATLAB code gives the values of the log-likelihood and parameters of four candidate models. We then calculate Akaike information criterion (AIC), differences, and Akaike weights using Eqs. 6.25, 6.27 and 6.29 respectively.

Table 6.1 shows the values of log-likelihood, AIC and Akaike weights for four candidate probability models. The low value of Akaike information in Table 6.1 indicates that the power-law fits well to the saccade data. In addition, the power-law distribution has higher values of log-likelihood and Akaike weight than the exponential, log-normal and gamma distributions. This predominance of a power-law distribution lends to support our claims of scale invariance of the saccades. The cumulative distributions of saccade time data of a sample literate subject and the four candidate models are shown in Fig. 6.1.

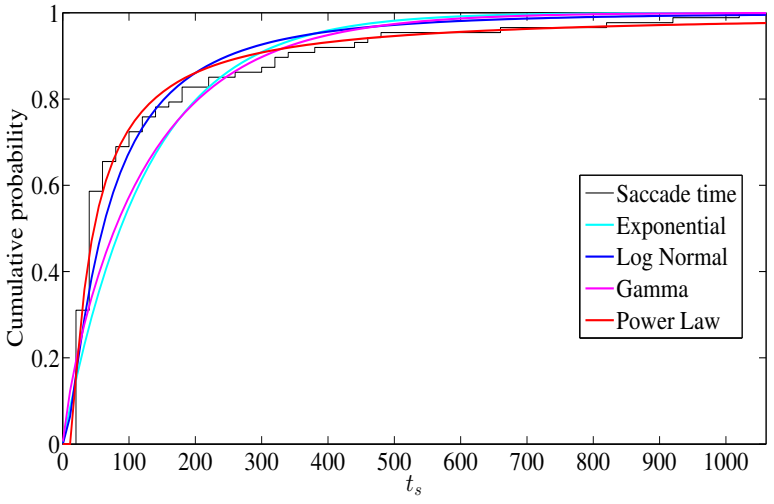

FIGURE 6.1: Cumulative distributions of saccade times (black solid line) for a sample literate subject, exponential (cyan solid line), log-normal (blue solid line), gamma (magenta solid line) and power-law (red solid line) distributions.

6.3 Levy Random Walk Model

Our time series analysis of Euclidean distances saccades confirms that their dynamics are Levy-like. Levy motions such as Levy flights and walks are found advantageous in random searching behavior of animals when searchers do not have prior knowledge of target locations [25, 26]. The advantage of Levy random walks is that they assign finite

velocity to random walker [27]. We assume that the movements of random walkers are analogous to eye movements. The subjects move their eyes rapidly in random direction on the computer screen during linguistic task. In this case, longer jumps are frequently observed in patterns of eye movements [28]. Moreover, saccade can take small and long jumps with finite velocity. Figure 6.2 shows typical patterns of gaze points of the eye movements. Note that in our study, subjects are under no instrumental control and carefully unaware that they are performing a set of task.

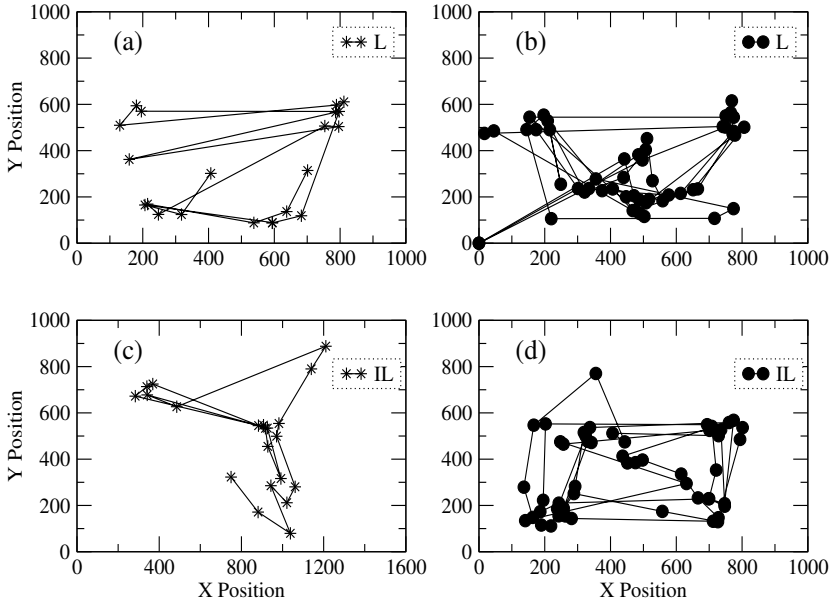

FIGURE 6.2: Plots of eye movement locations of literate and illiterate subjects for single ((a) and (c)) and double ((b) and (d)) trials. The legend indicates the correspondence between the symbol and the type/serial number of the subject.

We carry out simulation of two-dimensional Levy random walk. A walker choose direction at random and travel a distance l in XY plane, according to transformation $l = \frac{r^{-1/\mu}-1}{2^{1/\mu}-1}$, where $r \in$ [0,1] [26]. The exponent μ is the Levy index which varies from 1 to 3. We consider four cases: $\mu = 1.2, 1.4, 1.6$ and 1.8. For each case, the positions (x, y) of the random walkers are recorded over 10^5 steps. Times series of Euclidean distances of Levy walks are constructed. Figure 6.3 show a typical Levy random walk and its time series of Euclidean distances.

Our interest is to study diffusive behavior of Levy random walks. We perform diffusion entropy [28, 29, 30] and standard deviation [28, 31] analyses on the Levy walker time

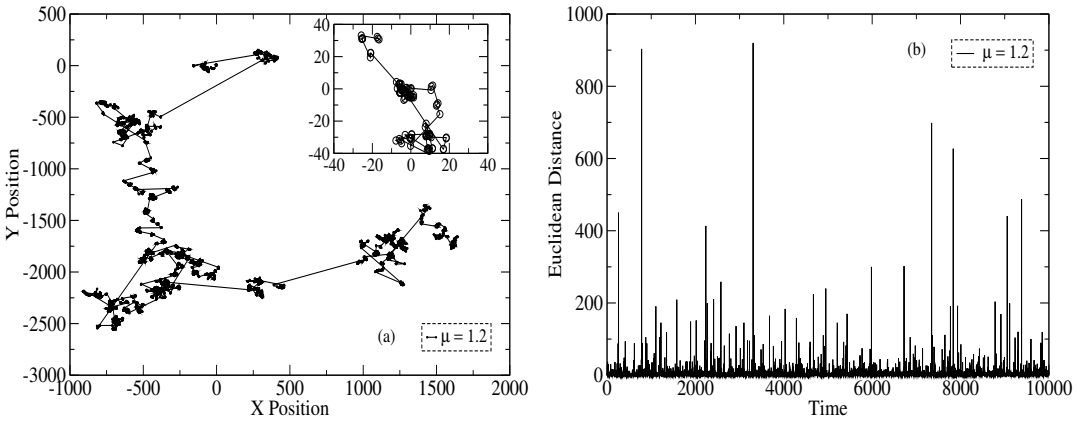

I II

FIGURE 6.3: (I): A typical Levy random walk of 10^5 steps for $\mu = 1.2$. The inset shows a walk of 100 steps (II): A typical time series of Euclidean distances of two dimensional Levy walker for 10^5 steps.

series, and accordingly, estimate Hurst (H) and diffusion (δ) exponents. The subtrajectories of time series ds_l of Levy walker are constructed as:

$$Z_i(t) = \sum_{j=1}^{n} [ds_l(i+j-1)], \tag{6.30}$$

where n is the length of subtrajectory. Though the details of SDA and DEA are explained in chapter 5, we reproduce the two main equations here :

$$S_l(n) = A_l + \delta \ln(n). \tag{6.31}$$

Thus, DEA gives diffusion exponent δ: $\frac{S_l(n)}{\ln(n)} \propto \delta$.

The standard deviations of subtrajectories of Levy walker time series is estimated as:

$$D_l(n) = \sqrt{\frac{\sum_{i=1}^{M-n}[Z_i(n) - \overline{Z(n)}]^2}{M-n-1}}. \tag{6.32}$$

The exponent H is obtained using the relation: $D_l(n) \sim n^H$. Figure 6.4 and 6.5 show the results of DEA and SDA for Levy walker time series respectively. The values of the Hurst H, and diffusion δ exponents for Levy walker time series are shown in Table 6.2. The values of H and δ suggest the superdiffusive dynamics of Levy walks.

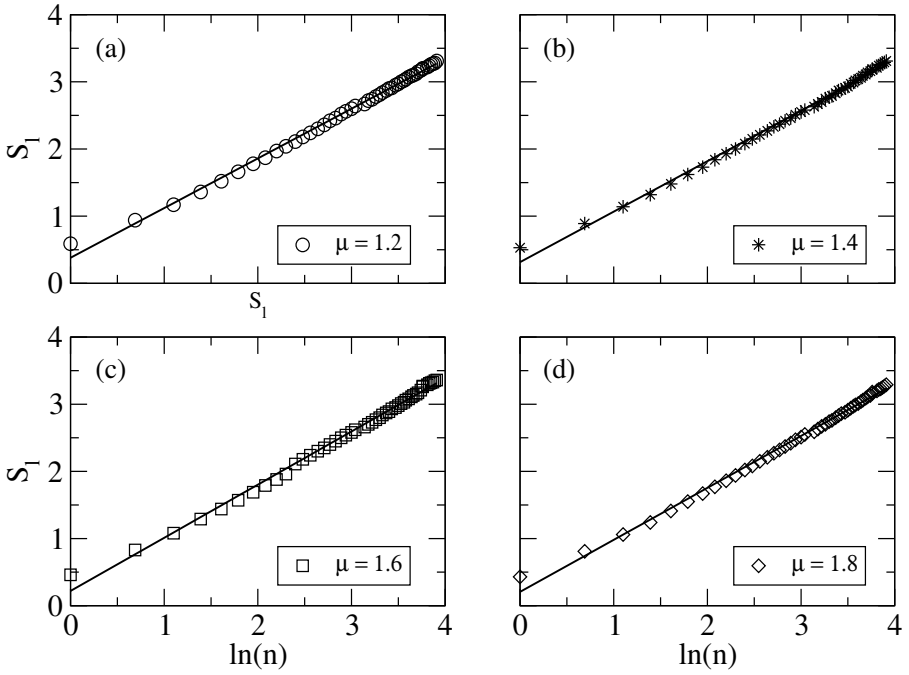

FIGURE 6.4: Plots of Shannon entropies $S(n)$ vs. $\ln(n)$ for saccades corresponding to four Levy walker time series.

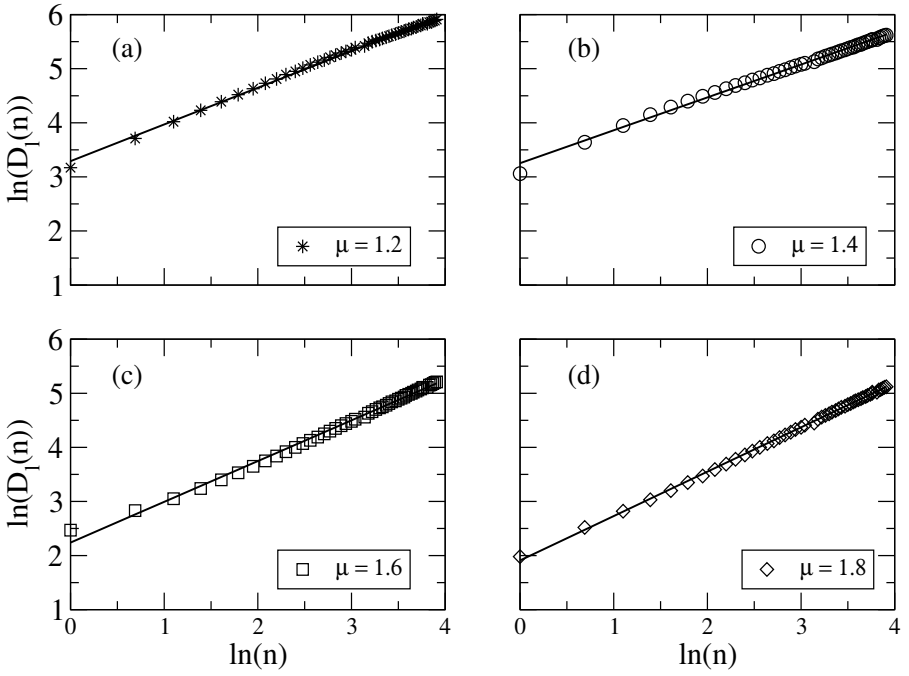

FIGURE 6.5: Plots of $\ln(D_l(n))$ vs. $\ln(n)$ for sub-trajectories $Z(n)$ corresponding to four Levy walker time series.

TABLE 6.2: The values of Levy index μ, Hurst H, and diffusion δ exponents for Levy walker time series

μ	H	δ
1.2	0.68	0.73
1.4	0.60	0.75
1.6	0.75	0.80
1.8	0.82	0.77

6.4 Conclusions

This chapter has explained the application of information theoretical methods to empirical data of saccades and simulations of Levy random walk. The power-law distribution of saccade times for literate subject has minimum Akaike information, maximum Akaike weight and log-likelihood values than other probability models. These results reveal that inverse power-law is the best approximate model for saccades. Our results of SDA and DEA for Levy walker time series substantially indicate the superdiffusive dynamics of a random walker. Our findings further ensure that ordinary Levy walks can model the visual searching behavior.

Bibliography

[1] S. Kullback, *Information Theory and Statistics* (Dover Publications), 1997.

[2] J. Fox, *Applied Regression Analysis and Generalized Linear Models* (SAGE Publications), 2008.

[3] E. L. Lehmann, J. P. Romano, *Testing Statistical Hypotheses* (Springer), 2008.

[4] H. Akaike, *IEEE Transactions on Automatic Control AC* **19**, 716(1974).

[5] G. Schwarz, *Ann. of Stat.* **6**, 461(1978).

[6] A. W. F. Edwards, *Likelihood*, (Johns Hopkins University Press), 1992.

[7] R. W. Farebrother, *Linear Least Squares Computations* (Marcel Dekker, USA), 1988.

[8] P. McCullagh and J. A. Nelder, *Generalized linear models* (Chapman and Hall), 1989.

[9] C. C. Heyde, *Quasi-likelihood and its application: a general approach to optimal parameter estimation.* (Springer-Verlag), 1997.

[10] B. Jorgesen, *Biometrika* **70(1)**, 19(1983).

[11] K. P. Burnham, D. R. Anderson, *Model Selection and Multimodel Inference* (Springer-Verlag New York, 2002).

[12] L. Fahrmeir and H. Kaufmann, *Ann. Statist.* **13(1)**, 1(1985)

[13] R. Douc, É. Moulines, and T. Rydén, *Ann. Statist.* **32(5)**, 1781(2004)

[14] M. Taboga, *Lectures on probability theory and mathematical statistics* (Independent Publishing Platform), 2012.

[15] R. L. Prentice, *Biometrika* **61(3)**, 539(1974).

[16] V. Kumar and G. Shukla *J. of Reliability and Statistical Studies* **3(1)**, 43(2010).

[17] A. Clauset, C. R. Shalizi and M. E. J. Newman *SIAM Review* **51(4)**, 661(2009).

[18] E. M. Edwards *et al.*, *Nature (London)* **449**, 1044-8(2007).

[19] H. Akaike, *Ann. of the Inst. Stat. Mathematics* **30**, 9(1978).

[20] H. Akaike, *The Statistician* **27**, 217(1978).

[21] J. A. Nelder and R. Mead, *Computer Journal* **7**, 308(1965).

[22] K. Lange, *Numerical Analysis for Statisticians* (Springer), 2010.

[23] C. M. Hurvich, and C. -L. Tsai, *Biometrika* **76**, 297(1989).

[24] H. Bozdogan, *Psychometrika* **52**, 345(1987).

[25] G. M. Viswanathan *et al.*, *Nature (London)* **381** , 413-5(1996).

[26] A. M. Reynolds, *J. Phys. A: Math. Theor* **42**, 434006(2009).

[27] M. F. Shlesinger, G. M. Zaslavsky and U. Frisch, *Levy Flights and Related Topics in Physics* (Springer, Berlin, 1995).

[28] D. G. Stephen *et al.*, *Phys. Rev. E* **79**, 056114(2009).

[29] N. Scafetta and V. Latora, and P. Grigolini, *Phys. Rev. E.* **66**, 031906(2002).

[30] N. Scafetta and P. Grigolini, *Phys. Rev. E.* **66**, 036130(2002).

[31] P. Allegrini, M. Barbi, P. Grigolini and B. J. West, *Phys. Rev. E.* **52**, 5281(1995).

Chapter 7

Summary and Future Perspectives

This thesis has presented the studies of spontaneous crystallization of granular spheres and spatio-temporal dynamics of human eye movements. Many new results have been obtained on both studies. In the following, first, I summarize all the major results of both studies, and then discuss perspectives of the future work.

7.1 Summary

Chapter 1 starts with a general introduction and describe the aims and outline of the thesis.

Chapter 2 provides a survey of the literature on statics and dynamics of granular materials, and human cognition through eye movements.

Chapter 3 comprises the first part of thesis, study of the spontaneous crystallization of granular spheres. We have given details of the hybrid Monte Carlo simulation of monodisperse spheres. This algorithm presents a realistic view of cooperative dynamics of granular spheres under shaking. In addition, it also provides a coherent picture of the development of crystalline structures. We have described systematic way of characterization of spontaneous crystalline transitions of spheres for nine shaking amplitudes. It has been shown that radial distribution function and global bond orientational order

parameter are useful techniques to identify the spatial orders at global level for all packing densities. The local order analysis gives insight into the developments of fcc and hcp sphere-clusters at various densities. Both the global and local order metrics change at packing densities of 0.62, 0.64, and 0.68. Importantly, the results of both analyses imply that shaking plays a vital role in the development of crystalline orders. Taken together, the ordering is incomplete at low shaking amplitudes; it leads to single fcc cluster for intermediate amplitudes and the coexistence of fcc and hcp is seen for higher shaking amplitudes.

Chapter 4 gives an introduction and application of Delaunay tessellations. Delaunay tessellation, a geometric method, has been applied to sphere packings of different densities. This method successfully computes the geometrical parameters such as volume, dihedral angle and length of Delaunay simplex. The volumes of tetrahedra follow two parameter gamma distributions. We have applied statistical mechanical methods to sphere packings, and accordingly, estimated the fluctuations and entropies of volumes. The volume fluctuations and entropies show drastic change at packing densities of 0.62, 0.64 and 0.68. We have calculated dihedral angles, length measures and the percentage of Delaunay tetrahedra. The results of dihedral angle, tetrahedricity, and quartoctahedricity distributions indicate that growth of regular or quasiregular tetrahedra increases with density. In case of intermediate and higher amplitudes, at maximum density of $\phi \sim 0.72$, the percentage of quasiregular tetrahedra reaches to a maximum of 31% and the peak of distributions of dihedral angle appears at 70°. Similarly, at maximum density of $\phi \sim 0.72$, the minima's of tetrahedricity T and quartoctahedricity Q are seen at 0.018 and 0.013 respectively, for intermediate and higher amplitudes.

Chapter 5 provides the spatio-temporal analysis of human eye movements. We explain the methodology of eye movements and experimental paradigm of linguistic study. We have analyzed temporal and spatial data of eye movements. The probability distributions of saccade and fixation times show a clear separation between these movements. We have found that saccades follow a power-law distribution whereas fixations show a characteristic timescale of 220 ms on an average for literate subjects. Interestingly, the temporal distributions of few illiterate subjects also exhibit similar behavior to those of the literate subjects. To examine the spatial dynamics of saccade, we have applied the scaling methods of standard deviation and entropy to the time series of Euclidean distances of saccades. The scaling exponents, H and δ, are computed using SDA and DEA

respectively. The values of Hurst and diffusion exponent in the interval $1/2 < H, \delta < 1$ indicate the Levy like anomalous diffusion of saccades. Also, the probabilities of Euclidean distances and power spectral density of saccade times series are computed. These results also attribute to anomalous diffusion of Levy type.

In Chapter 6, we have presented a basis for model selection and simulation of two-dimensional Levy random walk. The statistical techniques of maximum likelihood and Akaike information are found useful to select the best approximate model for saccade times. We have calculated the log-likelihood, Akaike information and weights for four candidate probability models. Our findings suggest that the power-law distribution shows the best fit to saccade data. We have presented the simulation of two-dimensional Levy random walks. The results of standard deviation, and diffusion entropy analyses of the time series of Levy walk show the superdiffusive dynamics of walker.

7.2 Future Perspectives

A careful investigation on the emergence of single fcc structure should be done. We would like to study the development of simple cubic, body-centered cubic structures along with fcc and hcp. The angular and length measures of simplices should be used for the identification of different crystalline structures. The bond order parameters and geometrical quantities change at packing densities of 0.64 and 0.68, which deserves further investigation.

The spatio-temporal analysis of eye movement data and the simulation of Levy random walk have been given in chapter 5 and 6 respecively. It is important to compute the velocity correlation function of saccades. This may provide clear understanding of saccade dynamics. It is well known that fractional Brownian and fractional Levy motions are also efficient techniques for the modelling of superdiffusive behavior. We would like extend the simulation from ordinary Levy walk to fractional Levy motion.

List of Publications

- D. P. Shinde, Anita Mehta, and R. K. Mishra, "Searching and fixating: Scale-invariance vs. characteristic timescales in attentional processes", *Europhys. Lett*, **94**, 68001(2011)..
- D. P. Shinde, Anita Mehta, and G. C. Barker, "Shaking-induced crystallization of dense sphere packings" *Phys. Rev. E.*, **89**, 022204(2014)..
- D. P. Shinde, "Delaunay tessellations of ordered dense sphere packings" (in preparation).
- D. P. Shinde, "Anomalous diffusion in eye movements during visual search" (in preparation).